NASA CR-120827

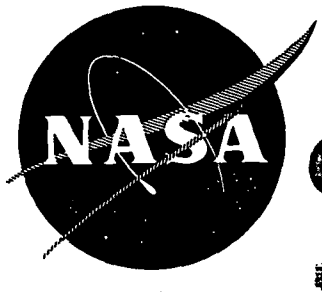

IGNITION OF FUEL VAPORS BENEATH TITANIUM AIRCRAFT SKINS EXPOSED TO LIGHTNING

by

T.C. Kosvic, N.L. Helgeson, and M. Gerstein

DYNAMIC SCIENCE
A Division of Marshall Industries

prepared for

NATIONAL AERONAUTICS AND SPACE ADMINISTRATION

NASA Lewis Research Center
Contract NAS 3-12009
Paul T. Hacker, Program Manager

NOTICE

This report was prepared as an account of Government-sponsored work. Neither the United States, nor the National Aeronautics and Space Administration (NASA), nor any person acting on behalf of NASA:

A.) Makes any warranty or representation, expressed or implied, with respect to the accuracy, completeness or usefulness of the information contained in this report, or that the use of any information, apparatus, method, or process disclosed in this report may not infringe privately-owned rights; or

B.) Assumes any liabilities with respect to the use of, or for damages resulting from the use of, any information, apparatus, method or process disclosed in this report.

As used above, "person acting on behalf of NASA" includes any employee or contractor of NASA, or employee of such contractor, to the extent that such employee or contractor of NASA or employee of such contractor prepares, disseminates, or provides access to any information pursuant to his employment or contract with NASA, or his employment with such contractor.

Requests for copies of this report should be referred to

National Aeronautics and Space Administration
Scientific and Technical Information Facility
P. O. Box 33
College Park, Maryland 20740

NASA CR-120827

FINAL REPORT

IGNITION OF FUEL VAPORS BENEATH TITANIUM AIRCRAFT SKINS EXPOSED TO LIGHTNING

by

T. C. Kosvic, N. L. Helgeson, and M. Gerstein

DYNAMIC SCIENCE
A Division of Marshall Industries
2400 Michelson Drive
Irvine, California 92664

prepared for

NATIONAL AERONAUTICS AND SPACE ADMINISTRATION

September 1971

CONTRACT NAS 3-12009

NASA Lewis Research Center
Cleveland, Ohio
Paul T. Hacker, Program Manager
Aerospace Safety Research and Data Institute

FOREWORD

The research described herein was conducted by the Dynamic Science Division of Marshall Industries under NASA Contract NAS3-12009, with the supervision of the NASA Project Manager, Mr. Paul Hacker, of the NASA Lewis Research Center. Testing was performed at the Lightning Simulation Facility of the Boeing Company.

The work was performed under the direction of Mr. Thomas C. Kosvic and Mr. Norman L. Helgeson. Dr. Melvin Gerstein supported the analytical efforts and contributed to the understanding of lightning strike processes. The authors thank Dr. R. P. Wilson, Jr., for his editing assistance in the preparation of the report. The authors gratefully wish to acknowledge the assistance of Messrs. R. O. Brick, S. Schneider, and the Boeing Project Engineer, Mr. Steve Kuo. In addition, recognition must be paid to the efforts of Mr. W. R. Irwin of Dynamic Science for test assistance.

TABLE OF CONTENTS

LIST OF TABLES

LIST OF FIGURES

ABSTRACT

Hot-spot and puncture ignition of fuel vapors by simulated lightning discharges was studied experimentally. The influences of skin coating, skin structure, discharge polarity, skin thickness, discharge current level, and current duration were measured and interpreted. Ignition thresholds are reported for titanium alloy constructed as sheets, sheets coated with sealants, and sandwich skins. An analytical model was developed to provide insight into the mechanism controlling ignition of fuel tank ullage vapors. In addition, a moving electrode experiment was conducted to obtain a measure of typical arc dwell times.

Results indicated that the ignition threshold charge transfer for coated sheets, honeycomb, and truss skins is respectively about 200%, 400%, 800% that of bare alloy sheet of .102 cm (.040 in.)-thickness. It was found that hot-spot ignition can occur well after termination of the arc, and that sandwich materials allow ignition only if punctured.

SUMMARY

In order to determine the strength of natural lightning strikes required to ignite fuel tank vapors beneath various aircraft skins, two-stage arc discharges (40-kamp surge tapering to residual level of 75-200 amp) were applied to titanium alloy (Ti 8-Al 1-Mo 1 V) in the following four configurations:

(i) Bare sheets (.102 cm (.040 in.) and .127 cm (.050 in.) thickness)
(ii) Sealant-coated sheets
(iii) Truss sandwich skins
(iv) Honeycomb sandwich skin

Discharge polarity (+ or -), residual current level and discharge duration (50-5000 msec) were controlled parameters. Measurements included ignition thresholds, charge transfer required for puncture, and undersurface history of the radial temperature distributions during the arc discharge.

The capacity of the skin structure for storing or dissipating heat without passing it on to the flammable vapors adjacent to the undersurface is crucial to whether or not ignition will occur. Thus, it is not surprising that experiments showed the truss sandwich to be most protective, followed by the honeycomb sandwich, the coated sheet, and finally the bare sheet, with charge threshold ratios approximately 8:4:2:1, respectively. Ignition thresholds for bare titanium sheet are considerably higher than earlier measurements would indicate, and are moderately dependent on current level. Measurements of the underside temperature indicate that ignition of titanium always occurs by hot spot rather than by puncture, although at high current levels the two occur nearly simultaneously. Ignition or puncture of titanium by thermal soak-back is common after the termination of a strong arc.

A mathematical model was developed to explain the thermal response trends indicated by the experimental data. By comparing these predicted thermal histories with well known fuel/air ignition delays, discharge conditions sufficient for ignition were approximately delineated.

The experiment was modified to simulate the "swept stroke" which occurs when an aircraft traverses a lightning discharge channel. This was done by means of a rotating-disc "swept stroke" apparatus. Initial evaluation included photographic measurement of the stepping and dwell time between steps, using a high voltage, low current arc discharge.

INTRODUCTION

Lightning as a Fuel Vapor Ignition Stimulus

The effect of a lightning discharge on an aircraft in flight has long been a problem of serious concern. It has been estimated that the typical aircraft is struck by lightning up to once for each 2400 flying hours (Ref. 1). When a lightning leader does attach to an aircraft in flight, there can be direct damage to the structure, or injury to the passengers and crew. But perhaps most hazardous is the indirect effect of lightning, should it stimulate an energy release of much greater magnitude--namely, ignition of combustible fuel-tank vapors. This disastrous phenomenon can occur by three different mechanisms as follows:

(1) ignition outside the fuel tank by direct contact of the lightning plasma with vented vapors;

(2) ignition within the fuel tank by electrical arcing between surfaces at discontinuities;

(3) ignition within the fuel tank by lightning penetration or heating of the fuel tank skin material (wing skin).

It is the third mechanism that is the subject of this report. Approximately 10% of lightning strikes occur in aircraft fuel-system areas, of which 70% cause a puncture or severe hot spot where they hit. One recent accident involving a Boeing 707 near Elkton, Maryland, generally has been attributed to ignition of fuel-tank vapors by natural lightning (Ref. 2).

Role of Current Program in Minimizing Ignition Hazard

In order to minimize ignition hazards by proper design of fuel tanks, it is essential to understand the role of the aircraft skin in the ignition mechanism. Several studies have been conducted to this end (Refs. 3, 4 and 5), and it may be useful to place these materials-response studies in perspective. In order to redesign fuel tanks so that ignition hazards are minimized, several contributing links in the ignition chain must be examined and quantified, as

follows:

(i) Nature and variations of natural lightning - What thermal flux is the skin exposed to when lightning strikes?

(ii) Response of various aircraft skins to a given stroke - To what extent is the discharge heating carried over to the combustible gas underneath the skin?

(iii) Ignitability of ullage gases - How readily do various fuel/air mixtures ignite, and what fuel/air mixtures are to be expected in the fuel-tank ullage?

The present study addresses itself squarely to item (ii), the thermal response of aircraft skins.

The objective is not a comprehensive design recommendation, but rather a definitive study of the thermal response of selected aircraft skins to simulated lightning discharges.

Ignition Mechanisms: Hot-Spot vs Puncture

Aluminum skins must suffer puncture in order to ignite underlying fuel-tank vapors (Refs. 3 and 4). The ignition mechanism in this case is reported to involve direct exposure of fuel vapors to the arc plasma, where the temperature can be as high as 15,300°K (27,000°F) (Ref. 6). Since the melting temperature of aluminum (930°K (1214°F)) is near the lower ignition limit of fuel/air mixtures (Ref. 7), it is not surprising that ignition is not observed until the undersurface temperature exceeds the melting point, leading to puncture. That is, solid aluminum is too cold to ignite ullage combustibles.

However, some of the newer aircraft materials, such as titanium and metallic and nonmetallic composites, may allow ignition without puncture because of their higher melting points. For example, the melting point of titanium (2033°K (3200°F)) far exceeds ignition temperatures reported for hydrocarbon-air mixtures (Ref. 7).

Previous work (Ref. 3) has demonstrated the possibility of ignition of vapors within a fuel tank by a hot spot on a tank skin consisting of bare titanium sheet. It was the purpose of the work reported herein to quantify these preliminary tests. Using several fuel tank skin materials and

construction techniques, we determined the threshold current levels and durations needed to produce ignition by either hot-spot or burn-through, using simulated lightning discharges.

Key Features of the Current Approach

A controlled arc discharge was used to simulate natural lightning. In order to simulate the fuel tank ullage composition, fuel gas and air were precisely metered to known concentrations in a test volume, one panel of which consisted of the candidate aircraft skin.

Certain features of the arc discharge bear mention: Although accurate simulation of lightning involves both an initial current spike and a continuing current "plateau", the energy deposition due to the initial spike is negligible. Only the level and duration of the post-spike plateau affect hot-spot and puncture ignition, and it was these two independent variables that were adjusted for each test. Brick (Ref. 8) and others have confirmed that ignition threshold depends both on the total charge transferred and upon the rate of transfer. Thus current and duration must be varied independently (rather than, say, in inverse proportion).

Perhaps the most distinguishing feature of the current study is the interpretation of data based on a mathematical model of thermal skin response. Such a model not only provides a rational framework for contemplating the data with order and convenience, but also can be used to predict the protective ability of new skins. In this way, the most promising configurations can be screened out for confirmative testing.

To provide some indication of the applicability of these results to "zone 2" (FAA designation for inboard region) of a moving aircraft, a preliminary experimental study of the swept stroke was executed. Photographs of the arc as it jumped along the edge of a spinning disc were obtained. Such measurements of dwell time complement the stationary discharge studies which make up the bulk of the report.

Guide to the Report

After depicting the experimental techniques, the complete results are documented, both for ignition tests and for other tests which were purely thermal (puncture thresholds, temperature profiles). Following their presentation, the results are interpreted in terms of the thermal behavior expected for a metal skin exposed to surface heat flux. For a more ambitious analytical treatment, including gas-phase chemical effects, the reader is directed to Appendix B.

The report concludes with a concise list of key conclusions, with recommendations for further activity.

EXPERIMENTAL METHODS

This study required the measurement of several parameters. Of primary interest was the time to ignition of a known fuel/air mixture by simulated lightning strokes of varying strength and duration. In order to evaluate these data on a meaningful basis, it was necessary that the following parameters be accurately controlled: the current history and polarity, the fuel/air mixture ratio, and the thickness and construction of the specimen. Uncontrolled but closely observed were the time to ignition and the undersurface temperature.

Test Materials

Aircraft Skin Specimens. - The essence of this study was to provide data to compare the effectiveness of several candidate aircraft fuel-tank skins in protecting against ignition of fuel/air vapor mixtures by lightning discharge. Test panels included the following:

1. Bare titanium alloy sheet (Ti-8 Al-1 Mo-IV) in thicknesses of .102 cm (.040 in.), and .127 cm (.050 in.). A previous program (Ref. 3) obtained results for .051 cm (.020 in.), .102 cm (.040 in.), and .153 cm (.060 in.) sheet. Thicknesses of .102 cm (.040 in.) and .127 cm (.050 in.) were tested to supplement the previous results.

2. Titanium alloy sheet coated with two different fuel-tank sealant materials, Dow Corning (DC) 94-003 and Minnesota Mining and Manufacturing (MMM) EC 1981. The first material is a high strength, fuel resistant, two-component fluoroscilicone rubber. The second is a one part, flexible, heat and fuel resistant coating with synthetic resin base. Both materials have passed fuel compatibility tests and are being considered as fuel tank sealants. Both sealant materials were applied to .102 cm (.040 in.) Ti sheet to an approximate thickness of .076 cm (.030 in.) by the Boeing Company Materials Laboratory. No attempt was made to rate the two as sealants or protective coatings for lightning. They were used as examples of typical sealants to provide data on effects of sealants on fuel vapor ignition time.

3. Titanium sandwich materials.

   Three sandwich materials were tested, as shown in Figure 1. The first and second were titanium truss skins; one lighter in construction (designated LTS) than the second (designated HTS). The third sandwich material was a titanium honeycomb (designated HC), the top and bottom sheets, of .0292 cm (.0115 in.) thickness, enclosing

a 1.27 cm (0.5 in.) titanium honeycomb (.013 cm (.005 in.) Ti in hexagon matrix of 1.18 cells/cm (3 cells/inch))

In short, thickness, coating, and structure were varied to determine their influences on ignition time, burn through, and undersurface temperature history.

Test Chamber. - The test panels were used as one side of a cubical volume into which a combustible mixture could be introduced. This test chamber was the same as that utilized in the previous work (Ref. 3) and is shown in Figure 3. It consisted of a 61-cm (2-ft) cube made of an angle iron frame. Three sides were permanently covered by aluminum sheets. Two sides, which were used for observation of ignition, were sealed with transparent material (plexiglass or mylar film) to contain the combustible mixture prior to the initiation of a test. The remaining surface consisted of the test material panel which was clamped in place by a set of toggle clamps. These allowed test panels to be easily installed and removed (Figure 3) between tests.

Fuel/Air Mixture Preparation. A device was built to provide an accurate and reproducible propane/air mixture in the cubical test chamber. All tests were run at fuel/air mixture corresponding to 1.5 times stoichiometric. Figure 2 shows a schematic of the fuel/air mixture apparatus. The test mixture was prepared in the following manner. The Volumetric Measuring Bomb was filled with propane to a specified pressure at a measured temperature. The mass of gas in the cylinder was determined from the equation of state for a perfect gas. The propane was then transferred to the test chamber through a transfer tube consisting of a plastic insulating tube and a copper tube with pin holes to assist in distributing the fuel within the chamber. Since the volume of the test chamber was constant, a known mass of propane (calculated from the pressure and temperature of the propane in the Volumetric Measuring Bomb) could be added to provide the desired fuel/air mixture in the test chamber.

Lightning Simulator

The basic lightning facility used in this study is located at the Boeing Aircraft Company in Seattle, Washington, and is portrayed in photographic and schematic form in Figures 3 and 4, respectively. A two stage discharge was provided by a battery bank and a one microfarad capacitor with high voltage power supply. Upon discharge of the capacitor, an initial 40-kamp pulse of rise time 10 μ-sec, decaying to one half strength at 20 μ-sec, was followed by a constant direct current continuing for 50-5000 msec, adjustable from 40 to 600 amps. This residual current was drawn from the batteries and controlled by a variable resistor and a timed circuit breaker. In order to discharge the one microfarad capacitor through the gap between the tungsten electrode and the test specimen, the mechanical flap switch was released to complete the circuit. The desired shape of the initial current spike could be established by selecting the resistance and inductance of this portion of the circuit.

The knife switch in the continuing current portion of the circuit closed mechanically when the flap switch was closed. The current-time profile from the battery bank was controlled by an air inductor to provide a smooth transition between the current spike and the long duration current at the preselected level of the continuing current.

Measurement Techniques

Arc Monitor. - The current-time traces for the current spike and long duration current were recorded on separate oscilloscopes as the voltage drop across calibrated shunt resistors and was measured with a precision of about one percent. Both scopes were triggered by the closure of the flap switch. Typical examples of current discharge oscillograms are presented in Figure 5. Figure 5a shows the high current portion (40 kamp) that was used for the entire test series. Figure 5b shows an example of a continuing current (165 amp) which was varied from test to test.

Ignition Measurement. - Accurate measurement of the time to ignition was an essential part of this study. For this reason a rather extensive effort was devoted to this measurement. Three basic techniques were considered: (1) photocell, (2) motion pictures and (3) microphone.

A Clairex (CL 603) photocell was used for ignition time measurement. This photocell has a time response less than 10^{-8} seconds and spectral response from 3000 Å - 10,000 Å. This range includes ultraviolet, visible, and near infrared wavelength bands.

Preliminary tests with one photocell (PC_1) aimed directly at the undersurface of the test panel showed the light emitted by the hot spot (area above approximately 810°K (1000°F) to saturate the photocell and obscure the faint combustion wave. This was solved by employing an additional light sensor (PC_2) mounted as shown in Figure 6. Photocell PC_1 was aimed directly at the inside surface of the test panel and recorded the time to hot-spot light emission, while PC_2 was oriented parallel to the test panel and enclosed in a narrow tube for collimation to measure the propagation of the combustion wave out from the test panel. The sensitivity of PC_2 was adjusted to be compatible with the faint emission of the combustion wave while PC_1 was adjusted to respond to the high light emission from the hot spot.

High speed motion pictures were taken during preliminary testing. The movies showed the time of hot spot formation and the time of formation of the initial combustion wave. This wave was observed as being a faintly luminescent blue flame propagating at a few feet per second from the point source hot spot. When the waves filled the test chamber, the increased pressure burst the plastic (mylar) film and secondary orange colored combustion was observed. The movies provided a direct observation of the ignition, but in practice were a costly and time consuming measurement procedure. For this reason the emphasis was placed on the photocell with the movies as a backup for calibration purposes.

During check out tests, comparison was made between ignition times measured with motion pictures and with the photocell. In general, agreement between ignition times on the motion picture and the photocell was within 10 msec. Once the correlation between the two techniques was established the motion picture coverage was only used on selected tests.

The microphone used during screening work on the previous study (Ref. 3) was discarded after the series of preliminary runs when little correspondence with either motion pictures or photocells could be established. The microphone measured the pressure waves associated with the bursting of the plastic diaphragm and not the true ignition time.

Temperature Measurement. - Thermocouples were selected as the temperature measurement technique most applicable to provide a transient temperature distribution at radial positions from the skin hot spot. Preliminary testing with both high current/low voltage (arc welder) and high voltage/low current (transformer coil) sources and work reported in Reference 4 showed that the major problem with the use of thermocouples was the electrical isolation of the thermocouple circuit from direct and induced voltages caused by the discharge. The configuration selected and used is illustrated schematically in Figure 7. A doubly shielded cable with an extra shield to carry to ground heavy current spikes was used for the thermocouple circuit. In addition, the circuit was further protected by a high frequency L-C filter that eliminated any initial currents caused by the high current discharge.

The thermocouple signal was measured on an oscilloscope and permanently recorded by an oscilloscope* camera. An example of a typical thermocouple trace is shown in Figure 8 for a test conducted at 213 amps for 150 msec. The output of a thermocouple located .60-cm (.24 in.) from the center of the hot spot (Figure 8b) is compared with the current/photocell trace (Figure 8a). It is seen that the thermocouple reaches its peak temperature after the photocell records maximum light emission. This indicates radial dissipation of thermal energy (increase in diameter of heated undersurface area).

*An oscillograph was used initially; but when electrical influences destroyed several galvonometers, the oscilloscope was substituted.

Chromel-alumel thermocouples spot-welded to the test panel were used to measure undersurface temperature. Chromel-alumel thermocouples are useful up to 1644°K (2500°F). The three-mil wire had a response time below 5 msec for 99% attainment of steady state.

Procedures

Procedure for Ignition Tests. - The test panel was clamped in place and the electrode positioned at the desired location. The plastic film was taped in place. Pressure of propane within the pressure vessel was adjusted to provide the required fuel volume. The propane was then introduced into the test chamber.

The capacitor of the lightning simulator was charged and the required current-time history set up by selecting the continuing-current resistor for desired current and the circuit breaker to give the duration. The lightning simulater was then discharged through a .64 cm (.25 in.) diameter tungsten electrode to the test panel, triggering the recording oscilloscopes. Oscilloscope traces were taken of photocell outputs and current histories. After a period of time to relieve the test box of product gases, new plastic was installed and another test initiated.

Procedure for Hot Spot and Puncture Tests. - Two types of tests were run in the absence of combustible gas, focusing on thermal aspects: (1) tests to determine the transient temperature distribution on the underside of the test panel, and (2) tests to define threshold charge transfer for puncture of the various test panels. For temperature measurement tests, the procedure involved installing the test panel with thermocouples attached, discharging the lightning simulator, and recording the thermocouple outputs. The tests for puncture threshold involved discharging the lightning simulator and observing whether or not puncture had occurred. Current histories were selected to bracket the threshold point to be determined, allowing rapid convergence to the limiting value.

EXPERIMENTAL RESULTS

Ignition Threshold

One of the major objectives of the work reported herein was to determine the ignition delay and the minimum charge transfer ($\int I\,dt$) for ignition of a flammable mixture beneath a tank skin which is exposed to the discharge. The charge transfer represents total deposited energy, whereas the current level (or arc duration for given total charge transfer) is associated with the rate of energy deposition. It is well known from ignition theory that both of these factors must be considered in order to explain ignition thresholds.

Results of the ignition threshold tests are presented in Tables I-IX and are also presented graphically as current vs. ignition delay in Figures 9-17, as listed below. Test numbers are given in the tables to facilitate discussion

Thickness, cm (in.)	Polarity of Test Panel	Coating	Configuration	Table	Figure
.102 (0.040)	+	None	Sheet	I	9
.102 (0.040)	-	None	Sheet	II	10
.127 (0.050)	+	None	Sheet	III	11
.127 (0.050)	-	None	Sheet	IV	12
.102 (0.040)	+	MMM EC1981	Sheet	V	13
.102 (0.040)	+	DC94-003	Sheet	VI	14
See Figure 1	+	None	Honeycomb	VII	15
See Figure 1	+	None	Light truss	VIII	16, 17
See Figure 1	+	None	Heavy truss	IX	-

and to be consistent with the numbers used in recording the data.

We report two times as follows: (1) τ_I, the ignition delay before the first emission from a combustion wave detectable by PC_2 and (2) τ_H, the time elapsed before a noticeable hot spot formed on undersurface (approximately 810°K (1000°F). Obviously $\tau_I \geq \tau_H$; an ignition wave cannot form before the underside heats up. A third characteristic time is the total discharge duration, τ_D. One might expect $\tau_D \geq \tau_I \geq \tau_H$, and indeed in the majority of cases this was true (provided

ignition occurred at all). However, ignition also occurred in many runs after the termination of the discharge ($\tau_D \leq \tau_I$), presumably because the under skin temperature continued to rise after the end of discharge (due to thermal equilibration).

Two types of ignition, each giving distinct photocell traces, as shown in Figure 18, are specified in the tabulated results:

(i) Hot spot ignition: Ignition resulting from prolonged exposure of the flammable mixture to a hot spot on the tank skin. The surface photocell (PC_1) showed a smooth peak and upon ignition the gas-oriented photocell (PC_2) showed relatively slow signal growth. (Figure 18a)

(ii) Puncture ignition: Ignition by direct exposure of a flammable mixture to the arc plasma following puncture of the tank skin. Here, PC_1 showed a jagged irregular trace and PC_2 responded with an abrupt increase at ignition. (Figure 18b). This type of oscillogram was only seen when ignition occurred in the presence of the arc, so that particles were highly illuminated through the resulting hole.

In several tests, photocell PC_2 gave no response yet a puncture was observed* in the test panel during set up for the next test. Thus puncture can occur without causing ignition. Presumably this occurs after termination of the arc discharge during thermal equilibration.

Note that the current vs. τ_I graphs describe a smooth curve which separates the ignition regime from the regime of nonignition. These curves essentially define the ignition threshold. The fact that ignition threshold is defined as a curved line rather than as a single point reflects the dual ignition criteria noted earlier; both rate of energy deposition and pulse duration influence ignition behavior.

The ignition threshold results presented in Figures 9-17 and Tables I-IX can also be transformed into charge transfer threshold curves, by integrating current over time. Selected results have been analyzed in this way and are presented in Figures 31 and 32.

*Such tests are indicated by an asterisk in the Tables.

Puncture Threshold for Sandwich Materials

A second area of investigation was the minimum charge ($\int I\,dt$) to puncture sandwich-type fuel tank skins. Puncture thresholds for titanium sheet have been determined in earlier studies[8], but there is a need for threshold data on skins of the sandwich-type.

For simplicity, these tests were carried out in the absence of a flammable mixture. Since current level was constant in any given series of tests, the threshold charge is directly proportional to the discharge duration.

The results for honeycomb sandwich and light truss sandwich are presented in Tables X and XI, respectively. This puncture data has been combined with ignition threshold tests (Table VII and Table VIII) and both appear graphically in Figures 19-21, where the puncture (or ignition) delay for each current level is plotted. In addition, the results are replotted in Figure 22 to show the quantity of charge required for puncture. Results for heavy truss sandwich can be taken from the ignition threshold tests of Table IX, where the upper sheet exhibited puncture after 2100 msec.

The honeycomb sandwich has the lowest puncture threshold of all materials tested, followed by the light truss sandwich. Puncture of the entire heavy truss sandwich was not observed.

As expected, puncture of the top sheet of the light truss sandwich required considerably greater charge transfer if the strike was directed at a peak (double thickness, Figure 21) rather than at a valley (single thickness, Figure 20)*. However, the threshold for puncture of the complete sandwich appeared to be independent of the orientation of the interior corrugation relative to the arc (Figure 22).

Observed puncture thresholds are more reproducible than the ignition thresholds for corresponding sandwich materials. At a given current level, the puncture delay for a given skin corresponds roughly to the ignition delay

*For a random lightning strike, the probability of contacting a peak can be estimated as the fraction of surface area which is double thickness. For the truss skins employed here this fraction is about 1/4.

reported earlier, with the ignition data scattered around the more reproducible puncture data. Presumably, the additional scatter observed in ignition delay is directly traceable to variations in chemical processes which occur in the flammable mixture as a combustion wave is generated.

Undersurface Temperature Profiles

The third measurement was the transient radial temperature profile at the hot spot on the undersurface of the titanium skin. Whereas threshold measurements are directed at whether the flammable mixture reaches a certain end point (namely, ignition), temperature histories trace the path by which that end point is reached.

Undersurface temperature was found to depend on four variables: $T = f(r,t, I, \text{polarity})$, where I is the current level of the discharge. The results are presented in Figures 23-26 as $T(r)$ for three times following exposure to the discharge. Three current levels and both polarities were studied and are presented according to the following classification:

Figure	Current Level (amps)	Polarity
23	213	-
24	100	+
25	164	+
26	213	+

The central axis of the discharge is accurate to $\pm$ .05 cm (.02 in.). Factors contributing to scatter included lack of fine adjustment of the position of the arc and slight instabilities that may have occurred. Some of the data that are shown on each figure were obtained on successive runs and overlayed.

It is clear from Figures 23-26 that the discharge creates a hot spot which after 150 msec has grown in width to about 0.80-cm (.32-in.) diameter*. This size corresponds to the width of the holes observed when puncture occurred, and also corresponds roughly to the electrode size. At a radial distance of 1.20 cm (.47 in.) the thermocouple response was negligible.

The effect of increased current level includes faster rise of the hot spot to the 1090°K (1500°F) level, and therefore higher peak temperature reached at the end of the discharge. These trends are shown in Figure 27, where selected data has been replotted to show T(r) for various I at fixed time (t). Note that outside the 0.20-cm (.08-in.) disk a current increase from 100 to 164 amperes appears to have a much greater thermal acceleration effect than a jump from 164 to 213 amperes.

In Figure 28, the temperature responses for positive and negative discharge polarity are compared by replotting the data obtained at fixed current I = 213 amps. The temperature responds about twice as fast with the test panel as the anode (negative discharge). Presumably the thermal response of a material exposed to an electron beam is more localized than the response of a metal sheet forced to yield electrons.

Perhaps the most revealing result was the rise in undersurface temperature after the discharge ceased. This "soak-back" effect is real and not due to inadequate thermocouple response. Nor is this effect due to chemical heat release upon ignition, for the tests were executed without a flammable mixture. As shown in Figure 8, the temperature rise .60 cm (.24 in.) from the axis starts at about the same time as PC_1 detects a hot spot. The temperature continues to rise for a rather extended period after current shutdown, indicative of thermal equilibration. Apparently there is a sizeable backlog of thermal energy stored in the neighborhood of the impact point on the upper surface.

*Width taken at half peak temperature.

INTERPRETATION OF RESULTS

Scope of Explanation

The data which has been collected falls into two classes -- thermal data (puncture and temperature profiles) and ignition data. Ignition involves not only the thermal response of the skin material but also chemical processes in the flammable gas mixture, and is therefore more ambitious to explain on a rigorous quantitative level. At the outset of the present section it should be clearly understood that we seek to characterize the thermal-response link in the ignition chain, without a quantitative assessment of the ignition hazard as a whole. One approach to solving the broader problem of ignition is outlined in Appendix B, where a quantitative ignition model is presented with a sample calculation for a single pulse shape and skin configuration.

The present section begins with a qualitative description of thermal response to energy deposition by lightning, followed by some rough estimates of selected thermal behavior parameters for titanium and aluminum sheets. It is shown that these rough estimates explain several observed trends. In particular, the discussion focuses on the following five features:

(i) Relation between hot-spot and puncture ignition.
(ii) Why puncture and ignition can occur after shutdown.
(iii) The response of titanium vis-a-vis aluminum.
(iv) Why negative polarity induces a stronger thermal response.
(v) Effects of skin thickness and construction on thresholds.

Thermal Response of Materials Exposed to Lightning

Whether a flammable mixture enclosed in a fuel tank will be heated to ignition by external discharge depends primarily on how the heat flux is dissipated by the tank skin material. This thermal response is controlled by the energy deposition at the top surface exposed to the arc, the thermal transport properties of the skin material, and the latent capacity of the material to store or absorb heat in various phases. The primary source of thermal energy is the electron excitation created in the surface of the skin* by the

*Estimates of the effective depth of penetration fall in the range 10^{-5}-10^{-6} cm.

arc processes, which deposit 10^4-10^5 watt/cm^2. According to Cobine[6], Joule or resistance heating throughout the depth of the material is of secondary importance in generating a hot spot. The power dissipated in Joule heating may be estimated for a spherically spreading current path from the relation

$$P = I^2 \rho_e \int_{r_o}^{\infty} \frac{dr}{2\pi r^2} ,$$

where r_o is the initial radius of the exposed spot and ρ_e the electrical resistivity (ohm-cm). For maximum current (500 amps) and minimum spot size (.05 cm (.02 in.)) the power dissipated in titanium is still only 1400 watt/cm^2 (1230 Btu/ft^2 sec), which is twenty times less than the surface heating flux. Joule heating is even less significant for aluminum because the resistivity drops a factor of 30.

The response of the material to surface deposition of energy is depicted in Figure 29. A portion of the thermal energy injected into the skin material by these two sources is transported both longitudinally and radially to other portions of the skin by conduction, which serves to heat up the under side of the skin and also to dissipate the thermal energy deposited at the electrode spot. At representative current levels, however, conduction is secondary and the power input from the arc is balanced primarily by evaporating skin material. The latent heat of vaporization of the metal serves to control the rate of vaporization of the metal and thus the resulting erosion rate. The erosion rate has been shown to be a function of the current level. The thermal transport properties of the material determines the rate of penetration of the heated zone relative to the eroding surface and also whether or not a heated zone will significantly lead the eroding surface.

The time between the heating of the undersurface to a particular temperature and the arrival of the eroding surface (puncture) is, then, controlled primarily by the current level (erosion rate), the latent heat of vaporization, and thermal transport properties of the skin material. If the arc is withdrawn before puncture, the temperature history of the undersurface

is controlled by equilibration of the heat stored in the portion of material near the arc. This heat can be in the form of sensible heat and latent heat contained in the superheated liquid layer beneath the electrode spot. The equilibration of this heat is affected by both surface boundary conditions* and three dimensional diffusion (heat soak-back).

Estimation of Key Thermal Response Parameters

In order to explain the measured trends in thermal data, the above description of thermal response must be quantified. Gross estimates of selected response parameters will be obtained for titanium and aluminum sheets exposed to surface heating, a problem which has been analyzed in the general case[24,25] and in connection with welding, laser drilling[28], and electron-beam interactions[29]. We can borrow from these earlier analyses in order to estimate the thermal response of tank skins to lightning.

At the outset, we will test for and prove one dimensionality for the assumed conditions. Then the remaining response parameters are simply obtained from the one-dimensional, semi-infinite model[24,25,28,29]. It is shown that the elapsed time before the exposed surface begins to vaporize is very brief, and that as further heating occurs the surface regression accelerates toward an asymptotic speed on the order of 1 cm/sec (.4 in/sec). The puncture delay (τ_p) is estimated as the time before the steadily regressing surface reaches a depth equal to given skin thickness**. Assuming that the onset of melting at the undersurface closely corresponds to a detectable "hot spot," the elapsed time between hot spot and puncture can be estimated as the time it takes the molten layer to vaporize. Finally, we estimate the maximum temperature difference which can be sustained across the plate.

*Heat loss by convection to the air stream over the upper surface is expected to modulate the heat soak-back for an aircraft in flight.

**Errors arising from the following two approximations tend to compensate one another: the semi-infinite approximation and the assumption of stationary (maximum) regression speed.

For these calculations the surface heat flux is taken equal to 3×10^4 watt/cm^2 (2.64×10^4 Btu/ft^2 sec) over a .60-cm (.24 in.) disk* of .10-cm (.04 in.) thickness, and the relevant properties of titanium and aluminum listed in Table XII. The expressions used and the results for titanium and aluminum are shown in Table XIII.

TABLE XII

THERMOPHYSICAL PROPERTIES OF AIRCRAFT SKIN MATERIALS[11,26,27]

Property	Titanium	Aluminum
Density ρ (g/cm^3)	4.5	2.7
Thermal conductivity k (cal/sec cm$^\circ$K)	.040	.37
Specific heat C_p (cal/g $^\circ$K)	.13	.23
Thermal diffusivity α (cm^2/sec) $\equiv k/\rho C_p$	.07	.60
Electrical Resistivity (μ ohm-cm)	199	6.3
Fusion point ($^\circ$K)	1950	930
Heat of fusion (cal/g)	77	93
Vaporization point ($^\circ$K)	3550	2750
Heat of vaporization ΔH_{vap} (cal/g)	2140	2580

*The diameter of the thermally affected spot is taken equal to observed puncture-diameter. In reality, an arc column of .10-cm (.04 in.) diameter and flux near 10^6 watt/cm^2 may jitter randomly across the .60-cm (.24 in.) spot, but the averaged effect is likely to be as assumed above.

TABLE XIII

COMPARATIVE THERMAL RESPONSES OF TITANIUM AND ALUMINUM
(Assume $\dot{q} = 3 \times 10^4$ watt/cm^2 over disk of diameter, d = .60 cm (.24 in.) and thickness, z_o = .10 cm (.04 in.)

Characteristic	Crude Expression	Effect of I	Ref.	Titanium	Aluminum	Comments
One-dimensionality	1st Criterion $d^2/\alpha\tau >> 1$ 2nd Criterion $d/z_o >> 1$	Indep.	24	$d^2/\alpha\tau = 28$ $d/z_o \approx 6$	$d^2/\alpha\tau \approx 3.3$ $d/z_o \equiv 6$	Radial dissipation important only at long τ (e.g., after pulse) 1-D assumption valid for titanium, marginal for aluminum.
Elapsed time before top surface reaches vaporization T	$\tau_V = \frac{\pi}{\alpha}\left(\frac{k\Delta T_{vap}}{2\dot{q}}\right)^2$	$\tau_V \sim I^{-2}$	25	4 msec	13 msec	Surface begins to vaporize very quickly
Elapsed time before thermal wave reaches undersurface*	$\tau_T = z_o^2/4\alpha$	Indep.	25	35 msec	4 msec	Rarely are Al skins this thin. For long discharges, titanium may be considered isothermal
Elapsed time to set up steady regression	$\tau_s \leq \alpha\left(\frac{\rho\ \Delta H_{vap}}{\dot{q}}\right)^2$	$\tau_s \sim I^{-2}$	25	140 msec	600 msec	During typical 200-msec pulse, regression wave cannot keep pace with thermal wave
Steady regression speed	$V = \left(\frac{\dot{q}}{\rho\ \Delta H_{vap}}\right)$	$V \sim I$	25	.74 cm/sec (.29 in/sec)	1.00 cm/sec (.39 in/sec)	This assumes $\Delta H_{vap} >> C_p \Delta T_{vap}$ which is true for aluminum and titanium
Elapsed time before puncture	$\tau_p = z_o/V$	$\tau_p \sim I^{-1}$	-	130 msec	100 msec	Agrees roughly with puncture data

*Not time to reach a given temperature, or time to form "hot spot". Rather, this is the time elapsed before the undersurface reaches a given fraction of the surface temperature.

TABLE XIII (Continued)

COMPARATIVE THERMAL RESPONSES OF TITANIUM AND ALUMINUM

(Assume $\dot{q} = 3 \times 10^4$ watt/cm^2 over .6 cm disk, .1 cm thick)

Characteristic	Crude Expression	Effect of I	Ref.	Titanium	Aluminum	Comments
Depth of molten zone below regressing surface	$z_m = \frac{\alpha}{V} \ell_n \left(\frac{T_{vap} - T_o}{T_{melt} - T_o} \right)$	$z_m \sim I^{-1}$	25	.066 cm (.026 in.)	(1 cm)** (.39 in)**	As vaporization begins, aluminum is molten throughout, but titanium .127-cm (.050 in.) thick is half solid.
Elapsed time between hot spot and puncture	$\tau_p - \tau_H = z_m/V$	$\Delta\tau \sim I^{-2}$	-	89 msec	(1000 msec)**	Puncture and ignition do not occur simultaneously
Maximum temperature difference sustained across plate	$\frac{T(z_o)}{T_{vap}} = \exp\left(-\frac{Vz_o}{\alpha}\right)$	$\frac{T(z_o)}{T_{vap}} \sim e^{-I}$	25	$\frac{T(z_o)}{T_{vap}} \approx \frac{1}{3}$	$\frac{T(z_o)}{T_{vap}} \approx .85$	Steeper gradient with titanium
Maximum overshoot after shutdown	--	See above	-	100%	7.5%	Relatively high probability of soak back with titanium

**Values applicable only to aluminum skins much thicker than 1 cm; presented for comparison with titanium.

Discussion of Experimental Results

As they apply to the experimental data, certain illuminating results in Table XIII bear emphasis and clarification. First, it is clear that radial heat conduction is completely negligible for titanium during the first 500 msec of the discharge. Only well after current shutdown has the heat wave penetrated noticeably outside the specified spot diameter.

Therefore, the thermal analysis can be carried out in one-dimension. Furthermore, the rise time of the upper surface is so brief that vaporization begins almost immediately. The remaining parameters are calculated from Dulnev's model[25] for an eroding surface preceded by a thermal wave. Because this model is for heat penetration into a semi-infinite body, the calculated thermal delays and penetration depths are presumably greater than corresponding values in a skin of finite thickness (where the heat is trapped). Nevertheless, the basic trends are of interest, as well as the magnitude of these conservatively-calculated parameters.

Apparently the undersurface of a .102-cm (.040-in.) titanium skin feels the effect of the discharge less than 40 msec after the upper surface. For long pulse duration (of the order of 400 msec or longer if puncture has not occurred), the profile beneath the spot can be assumed to be isothermal, with the applied energy going into vaporization of metal. Calculations of regression rate show that puncture will occur at around 130 msec for the current flux assumed here. This puncture delay corresponds to typical observed values.

In previous work (Ref. 3) on the ignition of fuel tank vapors by lightning strikes, two ignition mechanisms were identified. These are ignition by puncture (direct exposure of combustible gases to the arc plasma) and ignition by hot spot (heating of vapors adjacent to skin to ignition point by thermal conduction from a hot spot). The results of the present study show that the two mechanisms are not distinctly different and that transition from one to the other may be made by varying current level and current duration. The ignition delay is the same whether or not puncture has occurred.

It is inevitable that the undersurface will reach an "ignition" condition (in excess of 1400°K (~ 2050°F)) before the regressing top surface can reach the bottom, causing puncture. This is true regardless of current level, as shown in Figure 34. If chemical ignition of adjacent gases were instantaneous at 1400°K (≈ 2050°F), then all ignitions would be due to the hot-spot mechanism (with puncture irrelevant). However, ignition is not instantaneous, and if the heating precursor is too late, puncture may occur before the gas thermal incubation period is complete. The next few calculations in Table XIII show that there is adequate thermal "warning" (89 msec) before the regressing surface arrives. Apparently ignition by puncture does not occur, although ignition is often followed by puncture. For other conditions, the plate can be eroded so fast that the regressing surface reaches the bottom nearly simultaneously with the thermal wave.

The observed post-discharge ignition and/or puncture can also be rationalized by means of this one-dimensional model. From the last two calculations in Table XIII, it is seen that during the first 100 msec of the pulse a sizeable axial temperature gradient can be supported across the .102 cm (.040 in.) skin, due to the low conductivity of titanium. When the discharge is abruptly cut off, the temperature equilibration processes begin. Geometric considerations dictate that axial equilibration leads radial conduction, so that the undersurface temperature rises to the axial mean. Since the temperature variation across the skin can be as high as a factor of 3, this post-discharge rise is expected to be significant. As a result, ignition frequently occurs after current shutdown, as shown in Figure 30.

Examination of the experimental data shows the relationship of current on-time to measured time-to-ignition. In Figure 30, data from Table II at currents around 100 amps are plotted as time to ignition against time current was on. The minimum ignition delay was seen to be about 140 msec. As current-on time was decreased further, ignition delay increased to up to 600 msec. That portion of the test data where ignition occurred after current shutdown (heat soak-back ignition) is indicated as those above and to the left of the equal time line.

Aluminum behaves quite differently. Due to its high conductivity, the axial gradient in temperature is quite low and radial conduction is dominant at current shutdown. Thus post-discharge ignition or puncture is rare. Like-

wise, the melting point is so low that the heated metal core must be entirely liquid with substantial erosion before the undersurface can reach the spontaneous ignition temperature ($\sim 1400^{o}K$ ($\sim 2050^{o}F$)). For this reason, ignition beneath aluminum skins is often associated with puncture.

In the present program, at fixed high current levels and short discharge times where the negative discharge produced puncture ignition, the positive discharge did not (see, for example, tests 197-201 and 125-128). At low current levels and long pulse duration the hot-spot thresholds were within $\pm$ 15% regardless of polarity. Our hypothesis is that a wider area was heated by the arc under positive polarity (cathode spot). In terms of Table XIII, the heat flux $\dot{q}$ would be reduced in proportion to r_o^{-2}, reducing the temperature rise, the erosion rate, etc.

The data has shown that thicker plates provide greater protection than thin plates against ignition by lightning strikes (Figures 31 and 32), and that the amount of protection increases for the coating and sandwich materials, with heavy truss skin, the ultimate of all materials tested (Figure 33). These trends are explained in terms of the crude Table XIII model: Greater thickness and lower effective conductivity increase both the puncture delay ($\tau_P \sim z_o$) and the thermal response time ($\tau_T \sim z_o^2/\alpha$) for hot spot formation on the undersurface.

CONCLUSIONS AND RECOMMENDATIONS

Several features of the potential hazard which exists when a lightning strike becomes attached to the skin of an aircraft fuel tank have been investigated. The tank materials tested included titanium alloy sheet, coated Ti sheet, and Ti sandwich configurations. The principal conclusions are as follows:

(i) Ignition Thresholds: Empirical ignition thresholds are given as charge vs. delay $(Q, \tau)^*$; see Figures 31 and 33. The thresholds for bare sheet are about a factor of three higher than those reported by Brick[8], and have positive slope at large τ.

(ii) Puncture Thresholds: Measured puncture thresholds $(Q, \tau)^*$ are reported for sandwich materials never before tested (Figure 22). The threshold levels are relatively large ($Q \sim 200$ coulombs) and the threshold curve is relatively level up to $\tau \approx 1$ sec (indicating negligible radial heat conduction).

(iii) Effects of Skin Thickness and Construction: The capacity for storing or dissipating heat without passing it on to the flammable vapors adjacent to the undersurface is crucial. Thus it is not surprising that experiments showed the truss sandwich to be most protective, followed by the honeycomb sandwich, the coated sheet, and finally the bare sheet. Figure 33 shows the threshold ratios are respectively 8:4:2:1. If bare sheet must be used, the thicker the skin the better (Figure 32).

(iv) Ignition by Hot Spot and Puncture: Theoretical considerations and thermocouple measurements of the underside temperature indicate that ignition of titanium always occurs by hot spot rather than by puncture and direct contact of the arc with the flammable fuel vapors. Puncture of course occurs, but only after ignition has already been generated by a hot spot. The only exceptions to this rule would be an extremely thin skin ($\sim .025$ cm (.010 in.) or an extremely large current (500 amps). Ignition was most often accompanied by puncture at high current levels and for skins of low effective conductivity (coated sheets, sandwich materials). The two mechanisms become indistinguishable as the sheet thickness is reduced and as the current is increased.

(v) Post-Discharge Effects: Ignition or puncture of titanium by thermal soak-back is very common after the termination of a strong arc, because the axial temperature gradient is quite steep and radial dissipation is of little help during thermal equilibration. Ignition occurred up to 1/2 sec after current shutdown.

(vi) Effects of Polarity: The ignition thresholds are lower for a negative discharge than for a positive. Furthermore, the measured temperature of the undersurface rises much faster for a negative discharge, indicating faster erosion rate.

These results leave several key questions to be answered by studies recommended for the near future: Are these ignition thresholds applicable to the swept stroke hazard, and if so what are the typical dwell times for a stepping arc? Initial evaluation of a rotating disc "swept stroke" experiment shows that the dwell time appears to be about 2 msec when measured photographically at 55-m/sec (125-mph) relative velocity (Appendix A). Further swept-stroke studies are recommended.

How can this thermal response data be synthesized into a quantitative model for predicting ignition thresholds? Such a model could be applied to new tank materials in order to assess protective ability and specify the optimum tank skin. The first steps toward a comprehensive ignition model have been taken in Appendix B, and a trial solution for titanium sheet has been generated. In order to develop this model into a powerful predictive tool, future experiments should make provision to account for the complete energy balance over the affected portion of the tank skin. It is also recommended that a rigorous description of the gas-phase ignition process be developed, using the undersurface temperature profile as a boundary condition.

APPENDIX A
PRELIMINARY STUDY OF SWEPT STROKE

In order to simulate the effects of aircraft motion through an electrical discharge, a moving electrode apparatus was constructed, as shown in Figure 35. Swept strokes are known to occur across inboard regions of aircraft (e.g., wing tops, called "Zone 2" by FAA), and rarely cause severe damage other than burn spots. LTRI[30] has also investigated the swept stroke (1) by applying a discharge to a rotating disk and (2) by blowing the discharge across the skin with an air blower.

The experiments involving the moving electrode were conducted primarily to obtain some indication of the behavior of the arc near the surface and a rough estimate of arc dwell times.

Apparatus

Basically, it consisted of an electric motor with a belt drive to a rotating disc (61 cm (2 ft) in diameter), whose outer edge moved nominally at 55 m/sec (125 mph). In order to provide sufficient length in the arc for stepping to be observable, a rather high voltage drop is required. The Boeing Lightning Simulator did not develop high enough voltage for this purpose. Therefore, a high voltage, low amperage power supply (50 kV, .01 amps) was used for this test series. This power supply gave an arc length of about 1.2 cm (0.5 in.), compared to .60 cm (.25 in.) with the Boeing Apparatus.

A Red Lake Hycam camera was set up to observe the edge of the rotating disc. Best results were obtained at 2000 pictures per second with f/2.8 setting. High-speed recording film (Kodak RAR 2475, ASA 1000) was required because of the low light emission and short exposure time.

The apparatus, albeit simple, is felt to give some measure of control over the factors influencing "sweeping" of the arc. One important aspect was not simulated entirely. The discharge did not appear to occur in the stagnant region outside the flow field generated by the disc. The current level was lower than that used in the high current stroke simulations but was still sufficient to vaporize the aluminum disc, as evidenced by pit marks noted

after testing.

Results

Figure 36 shows results from a motion picture of the arc sweep experiment. The disc (not visible but represented by the white line) is traveling at 55 m/sec (125 mph). In the top frame, the arc attaches to the disc from the electrode. The arc is stretched in the second and third frames (0.5 msec apart), until, in the fourth frame, it reattaches at a new point. A dimness in the light emission can be noted during the stretching period; the time period between attachments is 2 msec. It is of note that the entire arc length appears to be within the flow field (boundary layer) of the rotating disc; there is no arc section normal to the disc.

The arc length increased from 1.2 to 2.5 cm (0.5 to 1.0 in.) as it stepped, decreasing the voltage drop per unit length from 40 Kv/cm to 20 Kv/cm. This range of field strength brackets that reported by Cobine (Ref. 6) as the minimum field required for breakdown (30 Kv/cm).

The dwell time measured for the above conditions was .002 seconds. This compares favorably with that reported in Reference 8 for flow through an arc channel (high current).

Discussion

The mechanism of the swept stroke is not completely understood, but several effects are known. The arc discharge originates in the atmosphere, and is simply a column of ionized air which is relatively stagnant. When the aircraft forms a part of the circuit, the attachment portion is in a region of high velocity gradients (the boundary layer over the aircraft). Thus the airplane accelerates that portion of the ionized gas that is within the aircraft flow field. The arc attachment point is then traveling at the velocity of the airplane (zero slip condition) and the velocity of the gases within the arc decreases to nearly zero at the free stream. By picturing the flow in a coordinate system within the moving aircraft the arc appears to be blown across the aircraft skin.

The arc reattachment can be pictured as shown in Figure 37. The arc is, in effect, "stretched" by the air flow until the resistance through the arc channel (R_a) is greater than that of the nonionized air (R_c) whereupon this gap is broken down and the arc reattached at the new point. Causes for this phenomena are severalfold: first, the convection of large quantities of cold air into the arc zone will have the effect of increasing the electrical resistance through the channel; second, increasing the distance between the electrodes (because of aircraft motion) will decrease the voltage drop per unit length (electron driving force); and third, increased convective heat losses from the electrode spot will tend to reduce evaporation and ionization of the metal, thereby further increasing the resistance through the channel. Additional phenomena associated with arc motion are surface skin conditions and asymmetric magnetic fields causing the arc to move.

APPENDIX B

OUTLINE OF A HOT-SPOT IGNITION MODEL FOR FUEL TANK VAPORS

Basic Approach

As the outer surface ot a fuel tank is exposed to arc heating, the flammable gas underneath feels only the underside. Therefore, the prediction of ignition rests on two phenomena: the temperature history of the underside, $T(r, z_o, t)$, and the ignition processes for a flammable gas adjacent to a hot wall. Fortunately the two phenomena can be analyzed separately; the thermal response of the aircraft skin is independent of gas phase processes because of the extremely low conductivity of the gas.

Determination of the Underside Temperature History

An arc discharge of 50-500 amps from a .63-cm (.25-in.) electrode deposits heat on the surface of the tank material at a rate of 10^4-10^5 watt/cm^2, with negligible Joule heating of the interior [6]. Titanium, like most metals, responds to moderate heat flux ($\sim 10^3$ watt/cm^2) by simple conduction, but must turn to erosion if the heat flux rises to the 10^4-10^7 watt/cm^2 range. These concepts are sketched in Figure 38. If the heat flux is even higher, ionization of titanium begins to absorb a tremendous amount of heat and, at extreme flux levels ($\dot{q} > 10^8$ watt/cm^2), dominates the dissipation mechanism. The regime to be analyzed is singled out on Figure 38; the primary thermal response to lightning involves a vaporizing surface preceded by a heat diffusion wave. Calculations show that the surface begins to vaporize in a time ($\sim$ 1 msec) quite short compared to the pulse duration (see Table XIII). It is this balance between input power and evaporation and heat transfer through the electrode material that controls the electrode erosion (regression) rate and the subsequent heating of the interior surface exposed to fuel vapors.

A second primary assumption is that the thermal response can be considered one-dimensional, along the axis of the arc (normal to the skin surface). The justification for this assumption lies in the inequalities $d^2/\alpha\tau >> 1$ and $d/z_o >> 1$, which are shown in Table XIII to hold for the case under consideration. A third assumption is that the heat escaping into the fuel vapors is

negligible compared to the total heat flux; the control volume is essentially insulated and adiabatic except for vaporized titanium.

Once the source of heat that results from a lightning strike has been specified, and the geometry assumed to be one-dimensional, the heat diffusion equation can be used to calculate the temperature history of the side of the skin material opposite to the arc, using the assumed boundary conditions for the outer and inner surfaces. Let us consider a metal panel of thickness z_o as shown in Figure 39. Using cylindrical coordinates and denoting r and z as the radial and axial coordinates, we can describe the molten metal as confined within a small cylindrical volume with radius $r \leq R$ and thickness $z \leq z_o$ shown in Figure 39. The governing equation describing the heat transfer within the metal panel is

$$\frac{1}{\alpha}\frac{\partial T}{\partial t} = \frac{1}{r}\frac{\partial}{\partial r}\left(r\frac{\partial T}{\partial r}\right) + \frac{\partial^2 T}{\partial z^2} + f'(r,z) \qquad (1)$$

(0 over $\frac{1}{r}\frac{\partial}{\partial r}\left(r\frac{\partial T}{\partial r}\right)$: Assume one-dimensional; 0 over $f'(r,z)$: Assume negligible Joule heating)

where

T = temperature
α = thermal diffusivity, $k/\rho c_p$
r = radial distance
z = axial distance
f' = strength of thermal energy source (energy/volume-time)

We seek a solution for a finite plate where one boundary is allowed to move at a finite velocity toward the other. Situations such as this involving an eroding surface are often handled by employing the Landau transformation (Refs. 13 or 14). This technique was originally developed and used on semi-infinite bodies but it has been applied to the solution of finite bodies for several special cases[15,16]. Using a moving coordinate system such that the surface s = 0 is moving with a velocity U_s, Eq. (1) becomes

$$\frac{1}{\alpha}\frac{\partial T}{\partial t} = \frac{\partial^2 T}{\partial s^2} + \frac{U_s}{\alpha}\frac{\partial T}{\partial s} \quad , \tag{2}$$

where distance is measured relative to the moving surface.

This equation is solved for T(s,t) subject to boundary conditions of the second kind:

$$T(o,t) = T_{vap} \tag{3}$$

$$\frac{\partial T}{\partial s}(z_o,t) = 0 \quad \text{(insulated surface)} \tag{4}$$

$$T(s,o) = T_o \tag{5}$$

$$-k\frac{\partial T(o,t)}{\partial s} = \dot{q} - U_s(t)\ \rho\Delta H_{vap} \tag{6}$$

Since Eq. (2) is second order in s , first order in t, and includes an unknown eigenvalue $U_s(t)$, the four conditions (3)-(6) are enough to make the problem well set.

A numerical computation procedure based on use of a Thermal Analyzer Computer Program was used to solve Equation (2) for T(s,t). The automated model permits the input of a prescribed power density $\dot{q}(t)$ (current level), and calculates both the surface erosion rate U_s and the temperature distribution T(s,t) through the plate.

Figure 40 shows numerically calculated temperature profiles through a .102 cm (.040-in.) sheet for a 100-amp current level. The position of the surface is denoted by the 2033°K (3200°F) position at the top of the figure. It can be seen that the erosion rate is not constant during the run, increasing from 0.2 to 0.5 cm/sec (in rough agreement with Table XIII). Initially it is low, as the heat transfer to the cold metal is high. As the average temperature is raised, however, the erosion rate increases. For the conditions of this test the hot spot of 1090°K (1500°F) was calculated to form at about 50 msec, and a temperature of 1480°K (2200°F) was reached at a time of 75 msec following initiation of the discharge. These delays are briefer than those observed in the experiment (see, for

example, Tests 69-71, in Table II). This disagreement is not unexpected as radial heat transfer, tending to lower heat flow to the interior surface, is not considered.

A feature of this approach is that the rise in under-surface temperature due to heat soak-back from the molten layer can be estimated by specifying a truncated form of $\dot{q}$ (t) to simulate the power input from the electric arc being turned off at any time during the run.

Figure 41 shows the effect on calculated under-surface temperatures of shutting off the current at 50 and 25 msec. The effect of heat soak-back is clear; the temperature of the lower surface continues to increase even after current shutdown. This demonstrates the possibilities of extended ignition delays at short current on-times. This effect becomes important at short arc dwell times, or in our case, short current durations. Whether ignition occurs in these cases is determined by extent to which radial dissipation ameliorates the rise of lower surface temperature. The problem of radial dissipation has been approached previously[18], and the solution is presented graphically in Figure 42 for an initial step-function distribution of temperature. The spot diameter is taken at .10 cm (.04 in.) instead of the more realistic .60 cm (.25 in.) in order to emphasize radial dissipation. When radial heat dissipation is included, a maximum temperature of around 500 ^{o}K (450^{o}F) is reached at the lower side of the skin and at t = ∞ the temperature returns to ambient conditions 311^{o}K (100^{o}F). These trends are clear in Figure 43. The temperature transient dies out quite rapidly: at t = 200 msec following current shut down the temperature is down to about 400^{o}K ($\sim$ 250^{o}F). When radial heat dissipation is included it appears that the hazard is much reduced.

For a given thickness, as the diameter of the exposed spot increases the importance of radial conduction decreases. Thus, the hazard reduction for a hot spot of more realistic diameter (.60 cm (.25 in.)) would not necessarily be as marked as that shown in Figure 43.

Chemical Delay Time

In a rigorous approach, our calculated profiles $T(z_o,t)$ would be used as boundary conditions in the solution of the conservation equations describing the temperature and species profiles in the gas phase. These equations would include not only convection and diffusion terms for gas movement but also source terms representing species conversion with corresponding heat evolution.

An ignition criterion would be arbitrarily but reasonably assumed (for example, that ignition occurs when the gas temperature reaches 1000°K (1340°F)). In practice, the nonlinearity of the source terms and the role of natural convection terms make the solution of these equations extremely challenging.

For the purposes of showing a complete ignition model, we here assume that if the inner surface stays at T* longer than $\tau_c(T^*)$, you get ignition. Here we define T* as the minimum spontaneous ignition temperature, which has been determined for many hydrocarbons as summarized by Gerstein (Ref. 7). Studies have shown that the least wall temperature that will ignite an adjacent hydrocarbon/air mixture is around 750-920°K (890-1196°F). Therefore, it would be desirable to have ignition data starting at approximately 750°K (890°F) and extending to the higher temperatures, measured experimentally on the interior surface of plates.

The results of several investigations on the ignition delay (τ_c) for hydrocarbon/air mixtures are available in the literature. But often they are not directly comparable to each other, nor to the conditions of the current program. Adomeit (Ref. 20) reported experimental measurements from which chemical ignition delay times are available and the data appear to be applicable, with some adjustment, to the present problem. Among the data reported are results for ignition of a homogeneous gas-phase mixture of pentane and air. The source of ignition was a cylindrically-shaped chromium-nickel rod .35 cm (.14 in.) in diameter. The rod was heated to a prescribed temperature by an electrical discharge in a time period that was small compared to the ignition delay. The growth of the thermal boundary layer, by conduction, about the hot wire, and the time of the thermal ignition were observed and recorded on interferrograms. Ignition occurred within a time interval such that free convection had not yet set in.

To permit the use of this data in the present case it must be reevaluated in terms of the planar geometry of the fuel tank wall. The effect of geometry is basically a difference in heat flux ($\dot{q}$). In cylindrical coordinates $\dot{q}$ may be evaluated for large times graphically (Ref. 21) and for small times either

graphically or from the following:

$$\dot{q} = \frac{k\Delta T}{a} \left\{ \left(\frac{a^2}{\pi\alpha t}\right)^{1/2} + \frac{1}{2} - \frac{1}{4}\left(\frac{\alpha t}{a^2\pi}\right) + \frac{\alpha t}{8a^2} \quad \ldots\ldots \right\} , \qquad (7)$$

where a is the radius of the hot body. For planar geometry

$$\dot{q} = \frac{k\Delta T}{\sqrt{\pi\alpha t}}$$

which is the first term of the expansion in equation (7). Once $(\dot{q})_{planar}$ is specified, τ_c (planar) can be calculated from τ_c (cylindrical) using the $(\dot{q}, \tau_{ign})$ correlation of Ref. 20. Results of calculations for the planar geometry are shown in Figure 44, along with the results for cylindrical geometry.

Other ignition delay data for propane/air mixtures have also been reported in the literature. Brokaw and Jackson (Ref. 22) preheated the fuel and air streams separately and, after rapidly mixing the reactants, measured the ignition delay as the time to ignition following the mixing operation. A typical result indicated that the ignition delay at a temperature of 1000°K (1340°F) was about 1 second. Chang (Ref. 23) preheated the air stream and fed a cold stream of fuel into it. A typical result from his measurements showed the ignition delay to be about 0.1 second at 1000°K (1340°F). The correlation given above, if extrapolated to 1000°K (1340°F), would indicate an ignition delay time of about 0.1 second. This agreement is satisfactory.

Ignition Threshold

The ignition criterion is arbitrarily stated as follows: If the lower surface remains above a temperature T* for a period exceeding the chemical delay τ_c corresponding to T*, then ignition occurs. In symbols,

$$T(z_o, t) \geq T^* \text{ for } \Delta t \geq \tau_c(T^*)$$

$$\downarrow$$

ignition,

where $\tau_c(T^*)$ is defined in Figure 44. It is apparent that the existence of a finite chemical response time (τ_c) can prevent ignition for intermediate temperatures in the range 1000-1400°K (1340-2060°F). If the underside of the skin reaches a temperature of 1500°K (2240°F) even momentarily, ignition is essentially unavoidable. However, at lower temperatures (say 1150°K (1585°F), the chemical ignition delay is of the order of 100 msec and whether ignition occurs clearly could depend upon the length of time which a hot spot persists. We have seen in a previous section that the peak temperature of the underside of the skin may not occur until after the lightning stroke has ceased to flow and that the temperature of the skin may persist at relatively high temperatures. This becomes important, then, in determining the minimum dwell time of a lightning strike that could initiate a thermal ignition. For although an arc may be attached at a particular spot for only several milliseconds, a significant amount of thermal energy may have accumulated in the skin material to cause a delayed ignition.

In order to illustrate the use of this ignition criterion, estimated temperature histories at the inner surface of the fuel tank are presented in Figure 45. On this same plot is superimposed a chemical ignition delay curve taken from Figure 44, but referenced to the time at which the underside reaches peak temperature. Any temperature history breaking above the no-ignition envelope will cause ignition, according to the model. Particular cases are discussed below:

Curve A (Low current, short duration)

The ignition delay is essentially infinite at 560°K (550°F), the maximum temperature reached by the inner surface. No ignition.

Curve B (Low current, moderate duration)

The underside spends 100 msec above 800°K (982°F), but this is not enough for ignition.

Curve C (Moderate current, moderate duration)

The underside remains above 1100°K (1520°F) for over 2000 msec. Ignition in this case is guaranteed.

Curve D (High current)

Ignition and puncture occur in quick succession around 75 msec.

This discussion has outlined how the calculated results can be used to evaluate the hazard associated with lightning strikes to various sheet skin materials. The model for predicting undersurface temperatures appears to be essentially developed, but to achieve realistic results a more rigorous treatment is recommended for thermal transport and gas-phase ignition processes.

REFERENCES

1. Perry, B. L., "British Researches and Protective Recommendations of the British Air Registration Board," AFAL-TR-68-290 Part II, May 1969.

2. Civil Aeronautics Board, "Aircraft Accident Report," File No. 1-0015, adopted February 25, 1965.

3. Kester, F. L., M. Gerstein, and J. A. Plumer, "A Study of Aircraft Fire Hazards Related to Natural Electrical Phenomena," NASA CR-1076, June 1968.

4. Robb, J. D., E. L. Hill, M. M. Newman, and J. R. Stahmann, "Lightning Hazards to Aircraft Fuel Tanks," NACA TN 4326, Sept. 1958.

5. Kofoid, M. J., "Lightning Discharge Heating of Titanium Aircraft Skins," Boeing Scientific Research Laboratories Document 01-82-0752, Sept. 1968.

6. Cobine, J. D., and E. E. Burger, "Analysis of Electrode Phenomena in the High-Current Arc," J. of Applied Physics, 26, 1955, p. 895.

7. Gerstein, M., and R. D. Allen, "Fire Protection Research Program for Supersonic Transport," APL-TDE-64-105, October, 1964, p. 87.

8. Brick, R. O., "A Method for Establishing Lightning-Resistance/Skin Thickness Requirements for Aircraft," AFAL-TR-68-290, May 1969.

9. Bird, R. B., W. E. Stewart, and E. N. Lightfoot, Transport Phenomena, Wiley, 1960, p. 372.

10. Carslaw, H. S., and J. C. Jaeger, Conduction of Heat in Solids, 2nd Edition, Oxford Univ. Press, London, 1959, p. 485.

11. Touloukian, Y. S., editor, Thermophysical Properties of High Temperature Solid Materials, Vol. 2, Nonferrous Alloys, the McMillan Company, New York, 1967.

12. Carslaw, H. S., and J. C. Jaeger, Op. Cit, p. 100.

13. Landau, H. G., Quarterly of Applied Mathematics, 8, 81, 1950.

14. Drew, T. B., editor, Advances in Chemical Engineering, Vol. 5, 1964, Academic Press, p. 94.

15. Sanders, R. W., "Transient Heat Conduction in a Melting Finite Slab: An Exact Solution," ARS Journal, 30, 1960, p. 1030.

16. Masters, J. I., "Problem of Intense Surface Heating of a Slab Accompanied by Change of Phase," Journal of Applied Physics, 27, 1956, p. 477.

17. Carslaw, H. S., and J. C. Jaeger, Op. Cit., p. 55.

18. Carslaw, H. S., and J. C. Jaeger, Op. Cit., p. 101.

19. Adomeit, G., "Ignition of Gases at Hot Surfaces Under Nonsteady State Conditions," Tenth Symposium (International) on Combustion, pp. 237-43.

20. Adomeit, G., "Proceedings of the 1963 Heat Transfer and Fluid Mechanics Institute, "Standard University Press, 1963, p. 160.

21. Carslaw, H. S., and J. C. Jaeger, Op. Cit., p. 334.

22. Brokaw, R. S., and J. L. Jackson, "Effect of Temperature, Pressure, and Composition on Ignition Delays for Propane Flames," Fifth Symposium (International) on Combustion, Rhienhold, 1955, p. 563.

23. Chang, C. J., "Ignition Delay of Propane in Air Between 725-880°C Under Isothermal Conditions," Seventh Symposium (International) on Combustion, Butterworth, 1959, p. 431.

24. Anisimov, S. I., "Evaporation of a Light-Absorbing Metal," High Temp. 6, 110 (1968).

25. Dulnev, G. N., and Yarysev, N. A., "Investigation of the Heat and Mass Transfer Taking Place During the Interaction Between an Energy Pulse and a Material Medium," High Temp. 5, 322 (1967).

26. JANNAF Thermochemical Tables. Compiled by the Dow Chemical Company, Midland, Mich., Dec. 1961.

27. "Handbook of Chemistry and Physics," R. C. Weast, editor, The Chemical Rubber Company, Cleveland, 1964.

28. Panzer, V. S., "Laser Application in the Field of Treating Materials," ZAMP, 16, 138 (1965).

29. Lin, T. P., "Estimation of Temperature Rise in Electron Beam Heating of Thin Films," IBM J. 11, 527 (1967).

30. Lightning and Transients Research Institute, "Laboratory Study of Swept Lightning Discharge Current Effects on Titanium and Aluminum," Rept. No. 486, June 1968.

31. Kosvic, T. C., Helgeson, N. L., Breen, B. P., "Flight Vibration and Environmental Effects on Formation of Combustible Mixtures Within Aircraft Fuel Tanks," Dynamic Science Final Report, USAAVLABS Tech. Rept. 70-43, Sept. 1970.

TABLE I

IGNITION TESTS WITH BARE ALLOY SHEET (.102 cm (.040 in.), POSITIVE CHARGE)

Test No.	Discharge Current		τ_D	τ_H	τ_I	Puncture
	Spike kA	Continuing Amp	Discharge Duration, ms	Time to reach 800°K, ms	Time to Ignition, ms	
40	40	313	110	36	36	No
41	40	319	115	38	40	No
42	40	214	115	38	44	No
43	40	206	116	No data	80	No
44	40	246	118	38	42	No
45	40	246	118	48	60	No
46	40	246	118	No data	No data	No
47	40	246	118	70	80	No
48	40	230	65	320	No data	No
49	40	230	90	80	No data	No
50	40	230	105	88	No data	No
51	40	230	110	91	140	*
52	40	200	120	63	73	No
53	40	200	120	87	No data	No
54	40	200	120	35	No data	No
55	40	256	125	No data	No data	No
56	40	278	150	44	No data	No
57	40	272	150	44	90	No
58	40	270	150	68	90	No
59	40	270	150	No data	No data	No
60	40	270	150	48	120	No
61	40	270	150	No data	No data	No
62	40	270	150	48	170	No
63	40	270	150	50	300	No
64	40	None	.020	Battery Bank did not discharge-No ignition		
65	40	107	200	No data	No data	No
66	40	107	200	110	150	No
67	40	107	210	140	190	No
68	40	107	210	130	200	No

*Puncture following current shutdown.

TABLE I (Continued)

IGNITION TESTS WITH BARE ALLOY SHEET (.102 cm (.040 in.), POSITIVE CHARGE

Test No.	Discharge Current		τ_D	τ_H	τ_I	Puncture
	Spike kA	Continuing Amp	Discharge Duration, ms	Time to reach 800°K, ms	Time to Ignition, ms	
72	40	106	300	145	290	No
73	40	106	300	130	240	No
74	40	106	300	130	220	No
75	40	101	300	140	225	No
76	40	95	410	170	290	No
77	40	95	400	160	310	Yes
78	40	103	390	130	230	No
79	40	74	400	620	640	*
80	40	74	400	110	460	*
81	40	74	400	170	340	Yes
82	40	74	190	125	560	No
83	40	74	190	No data	880	No
84	40	74	190	780	880	No
85	40	96	200	135	530	No
86	40	46	200	200	680	No
87	40	46	100	No Ignition	No	No
88	40	46	160	620	700	No
164	40	130	225	90	150	No
165	40	130	225	120	220	No
166	40	197	185	90	170	No
167	40	197	185	60	170	No
168	40	140	230	140	240	Yes
169	40	187	195	60	175	Yes
170	40	164	190	90	170	No
171	40	214	190	60	140	No
172	40	164	190	110	210	*
178	40	140	190	115	180	*
179	40	140	190	110	175	No

*Puncture occurred following current shutdown.

TABLE II

IGNITION TESTS WITH BARE ALLOY SHEET (.102 cm (.040 in.), NEGATIVE CHARGE)

Test No.	Discharge Current		τ_D	τ_H	τ_I	Puncture
	Spike kA	Continuing Amp	Discharge Duration, ms	Time to reach 800°K, ms	Time to Ignition, ms	
69	40	103	200	95	150	No
70	40	103	210	90	145	No
71	40	103	210	70	145	No
89	40	46	160	No Ignition		No
90	40	46	200	200	750	No
91	40	82	200	130	230	No
92	40	82	200	110	200	*
93	40	82	200	110	380	No
94	40	82	200	110	170	No
95	40	82	200	110	200	*
96	40	126	200	60	105	*
97	40	103	200	115	170	*
98	40	1000	200	40	42	Yes (40)
99	40	100	200	120	430	No
100	40	100	200	100	220	No
101	40	102	145	105	175	No
102	40	102	85	105	570	No
103	40	103	64	170	205	No
104	40	103	65	250	310	No
105	40	99	94	75	285	No
106	40	99	104	75	320	No
107	40	96	100	80	340	No
108	40	96	200+	80	140	*
109	40	141	100	40	80	No
110	40	141	100	55	95	No
111	40	141	100	60	130	No
112	40	141	100	55	120	No
113	40	164	100	56	96	No
114	40	171	100	52	84	No
115	40	189	100	70	108	No
116	40	189	105	64	126	No

*Puncture occurred following current shutdown.

TABLE II (Continued)

IGNITION TESTS WITH BARE ALLOY SHEET (.102 cm (.040 in.), NEGATIVE CHARGE

Test No.	Discharge Current		τ_D	τ_H	τ_I	Puncture
	Spike kA	Continuing Amp	Discharge Duration, ms	Time to reach 800°K, ms	Time to Ignition, ms	
117	40	189	104	46	78	No
118	40	214	105	36	80	Yes (80)
119	40	246	74	16	22	Yes (22)
120	40	246	48	26	34	Yes (34)
121	40	246	52	32	42	Yes (42)
122	40	445	52	20	22	Yes (22)
123	40	330	48	25	27	Yes (27)
124	40	330	52	25	27	Yes (27)

TABLE III

IGNITION TESTS WITH BARE ALLOY SHEET (.127 cm (.050 in.) POSITIVE CHARGE

Test No.	Discharge Current		τ_D	τ_H	τ_I	Puncture
	Spike kA	Continuing Amp	Discharge Duration, ms	Time to reach 800°K, ms	Time to Ignition, ms	
145	40	89	300	210	620	No
146	40	91	300	180	400	No
147	40	87	300	260	700	No
148	40	93	300	220	660	No
149	40	36	410	900	No data	No
150	40	44	520	440	800	No
151	40	83	310	200	440	No
152	40	83	300	230	780	No
153	40	108	300	160	380	No
154	40	108	300	130	240	*
155	40	109	260	165	260	*
156	40	104	240	160	260	*
157	40	106	275	100	270	*
158	40	164	225	100	230	*
159	40	144	225	90	No data	*
160	40	122	225	85	240	*
161	40	130	225	90	210	*
162	40	130	225	90	210	*
163	40	130	225	90	180	*
173	40	205	190	105	170	*
174	40	197	190	75	190	*
175	40	132	190	70	170	No
176	40	150	190	55	160	No
177	40	150	190	65	170	No
180	40	142	190	180	460	No
181	40	142	230	95	180	*
182	40	161	200	65	140	*
183	40	156	200	90	170	*
184	40	156	160	70	300	No
185	40	158	180	80	160	*

*Puncture occurred following current shutdown.

TABLE III (Continued)

IGNITION TESTS WITH BARE ALLOY SHEET (.127 cm (.050 in.), POSITIVE CHARGE

Test No.	Discharge Current		τ_D	τ_H	τ_I	Puncture
	Spike kA	Continuing Amp	Discharge Duration, ms	Time to reach 800°K, ms	Time to Ignition, ms	
186	40	197	150	60	110	*
187	40	197	120	65	120	*
188	40	197	85	50	500+	No
189	40	197	110	90	390	No
190	40	197	130	90	140	No
191	40	230	110	70	140	No
192	40	230	130	64	116	*
193	40	230	130	64	106	No
194	40	280	130	48	80	No
195	40	280	130	136	Bad data	No
196	40	280	130	136	Bad data	No
197	40	280	130	85	135	No
198	40	410	100	82	Bad data	No
199	40	370	100	140	Bad data	No
200	40	321	200	95	160	*
201	40	312	205	70	135	*

*Puncture occurred following current shutdown.

TABLE IV

IGNITION TESTS WITH BARE ALLOY SHEET (.127 cm (.050 in.), NEGATIVE CHARGE

Test No.	Discharge Current		τ_D Discharge Duration	τ_H Time to reach 800°K, ms	τ_I Time to Ignition, ms	Puncture
	Spike kA	Continuing Amp				
125	40	345	58	29	31	Yes (31)
126	40	345	58	43	No data	No
127	40	330	120	29	32	Yes (32)
128	40	355	58	29	32	Yes (32)
129	40	200	57	No data	No data	No
130	40	200	100	No data	No data	No
131	40	200	205	110	170	No
132	40	200	205	100	180	No
133	40	140	205	130	225	No
134	40	140	205	110	180	No
135	40	140	205	115	285	No
136	40	150	205	105	170	No
137	40	56	310	220	530	No
138	40	56	410	200	400	No
139	40	62	410	190	340	No
140	40	62	370	200	380	No
141	40	98	250	160	270	No
142	40	98	200	160	280	No
143	40	98	330	150	260	No
144	40	98	280	130	230	*

*Puncture occurred following current shutdown.

TABLE V

IGNITION TESTS WITH EC 1981 - COATED SHEETS

Test No.	Discharge Current		τ_D	τ_H	τ_I	Puncture
	Spike kA	Continuing Amp	Discharge Duration, ms	Time to reach 800°K, ms	Time to Ignition, ms	
265	40	213	225	30	200	Yes
266	40	213	170	30	No	No
267	40	203	225	40	No	No
268	40	203	390	40	270	Yes
269	40	203	410	30	1000+	Yes
270	40	142	450	50	No	Yes
271	40	143	740	50	200	Yes
272	40	143	740	50	320	Yes
273	40	143	510	50	No	Yes
274	40	335	340	50	230	Yes
275	40	230	450	50	230	Yes
276	40	230	450	50	200	Yes
277	40	92	1080	600	900	No
278	40	92	1080	760	No	No
279	40	92	1200	630	1700	No
280	40	92	1200	610	1400	No
304	40	276	320	70	100	Yes
305	40	276	165	70	No	No
306	40	276	230	80	120	Yes
307	40	131	230	150	No	No
308	40	131	560	275	No	No
309	40	131	660	170	No	No
310	40	131	760	150	560	Yes
311	40	494	220	10	180	Yes
312	40	510	160	20	115	Yes

TABLE VI

IGNITION TESTS WITH 94-003 - COATED SHEETS

Test No.	Discharge Current		τ_D	τ_H	τ_I	Puncture
	Spike kA	Continuing Amp	Discharge Duration, ms	Time to reach 800°K, ms	Time to Ignition, ms	
281	40	92	1200	610	800	Yes
282	40	92	1000	800	900	Yes
283	40	128	630	200	440	Yes
284	40	128	740	100	No	No
285	40	136	1180	100	490	Yes
286	40	136	840	120	570	Yes
287	40	136	840	80	690	Yes
288	40	156	380	80	No	No
289	40	164	625	80	300	Yes
290	40	164	500	80	340	Yes
291	40	164	500	80	320	Yes
292	40	213	390	70	290	Yes
293	40	193	450	90	260	Yes
294	40	193	420	60	320	Yes
295	40	193	140	60	No	No
296	40	197	385	80	210	Yes
297	40	197	260	70	500	No
298	40	197	230	75	350	Yes
299	40	196	225	70	No	No
300	40	280	170	30	135	Yes
301	40	280	147	70	No	No
302	40	280	172	95	140	No
303	40	280	184	90	140	Yes
313	40	494	90	30	70	Yes
314	40	494	165	25	120	Yes
315	40	100	840	330	No	No
316	40	100	910	320	1200	Yes

TABLE VI (Continued)

IGNITION TESTS WITH 94-003 - COATED SHEETS

Test No.	Discharge Current		τ_D	τ_H	τ_I	Puncture
	Spike kA	Continuing Amp	Discharge Duration, ms	Time to reach 800°K, ms	Time to Ignition, ms	
317	40	100	1100	400	940	Yes
318	40	100	1100	280	No	No
319	40	100	1120	250	1000	Yes

TABLE VII

IGNITION TESTS WITH HONEYCOMB SANDWICH

Test No.	Discharge Current		τ_D Discharge Duration, ms	τ_H Time to Reach 800°K, ms	τ_I Time to Ignition, ms	Puncture	
	Spike kA	Continuing Amp				Top	Bottom
320	40	97	2950	1200	1450	Yes	Yes
321	40	97	1720	530	1880	Yes	No
322	40	97	2040	750	1440	Yes	Yes
323	40	36	1500	-	No	Yes	No
324	40	131	1520	500	755	Yes	Yes
325	40	131	1200	710	910	Yes	Yes
326	40	131	1300	800	970	Yes	Yes
327	40	141	820	530	730	Yes	No
328	40	161	820	480	550	Yes	Yes
329	40	161	740	-	-	Yes	No
330	40	161	820	480	600	Yes	Yes
331	40	161	720	490	630	Yes	Yes
332	40	206	630	430	450	Yes	Yes
333	40	206	630	350	540	Yes	Yes
334	40	206	330	300	620	Yes	No
335	40	213	800	320	530	Yes	Yes
336	40	271	680	200	300	Yes	Yes
337	40	296	525	480	650	Yes	Yes
338	40	274	525	290	360	Yes	Yes
339	40	274	525	180	320	Yes	Yes
340	40	328	415	200	275	Yes	Yes
341	40	328	360	200	275	Yes	Yes
377	40	660	310	100	160	Yes	Yes
378	40	80	4700	1500	1700	Yes	Yes
379	40	138	1520	500	860	Yes	Yes
380	40	138	1520	600	860	Yes	Yes
384	40	72	4200	No data	3170	Yes	Yes
385	40	72	4200	1700	2150	Yes	Yes

TABLE VIII

IGNITION TESTS WITH LIGHT-TRUSS SANDWICH

Test No.	Discharge Current			τ_D Discharge Duration, ms	τ_H Time to Reach 800°K, ms	τ_I Time to Ignition, ms	Puncture	
	Spike kA	Cont. Amp.	Stroke Point*				Top	Bottom
344	40	305	V	1770	600	650	Yes	Yes
345	40	300	V	820	570	740	Yes	Yes
346	40	300	V	820	640	930	Yes	Yes
347	40	300	V	850	520	680	Yes	Yes
348	40	131	V	2500	1720	2000	Yes	Yes
349	40	131	P	2220	No data	1750	Yes	Yes
350	40	131	P	2220	No data	1450	Yes	No
351	40	131	P	2220	-	No	Yes	No
352	40	131	P	2220	-	No	Yes	No
353	40	131	P	2650	-	No	Yes	No
354	40	131	P	3400	2150	2200	Yes	Yes
355	40	200	P	1380	800	880	Yes	Yes
356	40	200	P	1160	-	No	Yes	No
357	40	200	P	1160	800	1060	Yes	Yes
358	40	300	P	1000	No data	560	Yes	Yes
359	40	114	P	4100	3700	3800	Yes	No
360	40	114	P	4300	-	No	Yes	No
361	40	114	P	4900	2800	2950	Yes	Yes
362	40	114	P	4750	3600	3850	Yes	No
363	40	114	P	5000	4000	4100	Yes	No
364	40	122	V	5000	1750	2050	Yes	Yes
365	40	131	V	5000	3350	3750	Yes	Yes
366	40	122	V	5000	3200	3450	Yes	Yes
367	40	101	V	5000	-	No	Yes	No
368	40	108	V	5000	No data	6000	Yes	No
369	40	120	V	5000	3750	3900	Yes	Yes
370	40	192	V	1480	-	No	Yes	No
371	40	195	V	1480	800	1010	Yes	Yes
372	40	195	V	1480	-	2000+	Yes	No

*Location - Peak (P) - Double Thickness at Top
Valley (V) - Single Thickness at Top

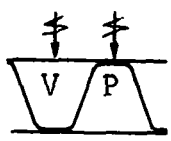

TABLE VIII (Continued)

IGNITION TESTS WITH LIGHT-TRUSS SANDWICH

Test No.	Discharge Current			τ_D Discharge Duration, ms	τ_H Time to Reach 800°K, ms	τ_I Time to Ignition, ms	Puncture	
	Spike kA	Cont. Amp.	Stroke Point*				Top	Bottom
373	40	195	V	1480	1040	1220	Yes	Yes
374	40	362	V	600	480	560	Yes	Yes
375	40	360	V	520	520	No	Yes	No
376	40	660	V	460	120	300	Yes	Yes

*Location - Peak (P) - Double Thickness at Top
Valley (V) - Single Thickness at Top

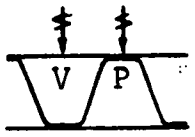

TABLE IX

IGNITION TESTS WITH HEAVY-TRUSS SANDWICH

Test No.	Discharge Current			τ_D Discharge Duration, ms	τ_H Time to Reach 800°K, ms	τ_I Time to Ignition, ms	Puncture	
	Spike kA	Cont. Amp.	Stroke Point*				Top	Bottom
342	40	311	P	2100	-	No	Yes	No
343	40	311	V	2100	-	No	Yes	No

*Location - Peak (P) - Double Thickness at Top
Valley (V) - Single Thickness at Top

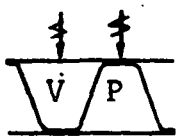

TABLE X

PUNCTURE TESTS WITH HONEYCOMB SANDWICH

Test No.	Discharge Current		Discharge Duration, ms	Puncture	
	Spike kA	Continuing Amp		Top	Bottom
381	40	95	140	Yes	No
382	40	95	64	Yes	No
383	40	95	54	No	No
386	40	72	57	No	No
387	40	72	115	Yes	No
388	40	72	74	No	No
389	40	72	78	No	No
390	40	72	86	Yes	No

TABLE XI

PUNCTURE TESTS WITH LIGHT-TRUSS SANDWICH

Test No.	Discharge Current			Discharge Duration, ms	Puncture	
	Spike kA	Cont. Amp	Stroke Point*		Top	Bottom
391	40	72	V	85	No	No
392	40	72	V	100	No	No
393	40	72	V	136	No	No
394	40	72	V	170	No	No
395	40	72	V	250	No	No
396	40	72	V	320	No	No
397	40	72	V	490	No	No
398	40	72	V	500	No	No
399	40	72	V	525	Yes	No
400	40	82	P	730	No	No
401	40	82	P	1140	No	No
402	40	82	P	1480	Yes	No
403	40	149	P	590	No	No
404	40	149	P	700	No	No
405	40	149	P	800	Yes	No
406	40	149	P	760	No	No
407	40	149	P	785	No	No
408	40	149	P	800	No	No
409	40	149	P	810	Yes	No
410	40	150	V	525	Yes	No
411	40	150	V	430	Yes	No
412	40	150	V	390	Yes	No
413	40	150	V	320	No	No
414	40	150	V	380	No	No

*Location - Peak (P) - Double Thickness at Top
Valley (V) - Single Thickness at Top

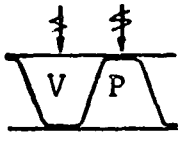

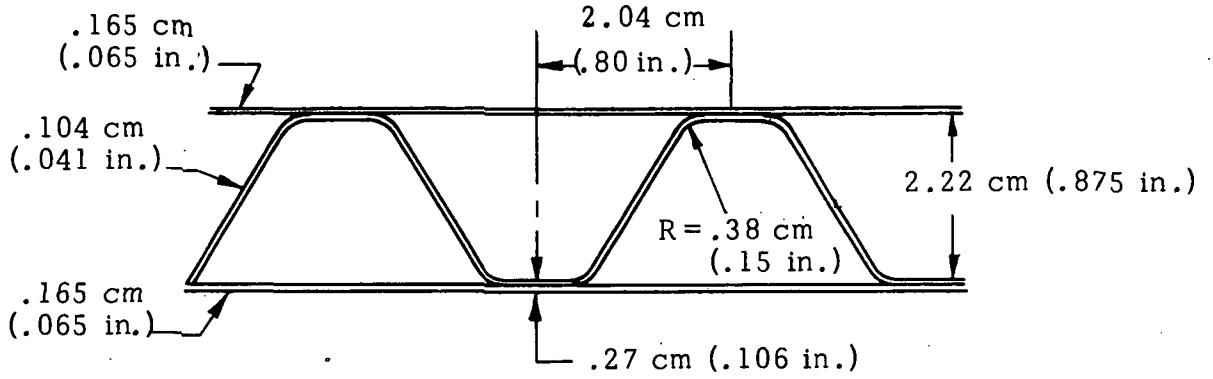

(a) Heavy Truss Sandwich (HTS)

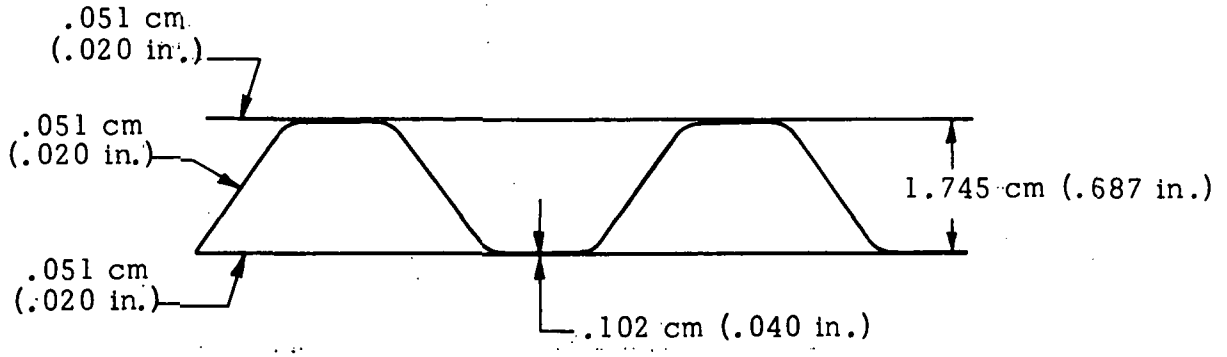

(b) Light Truss Sandwich (LTS)

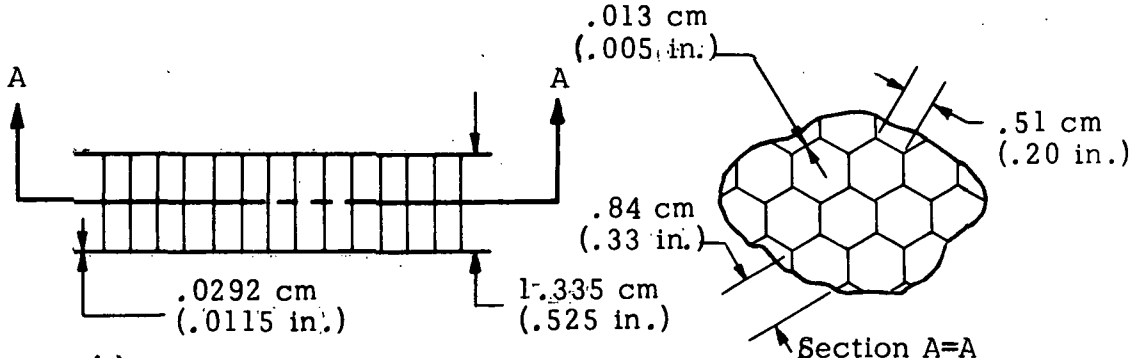

(c) Honeycomb Sandwich

Figure 1. Construction of Candidate Sandwich Materials

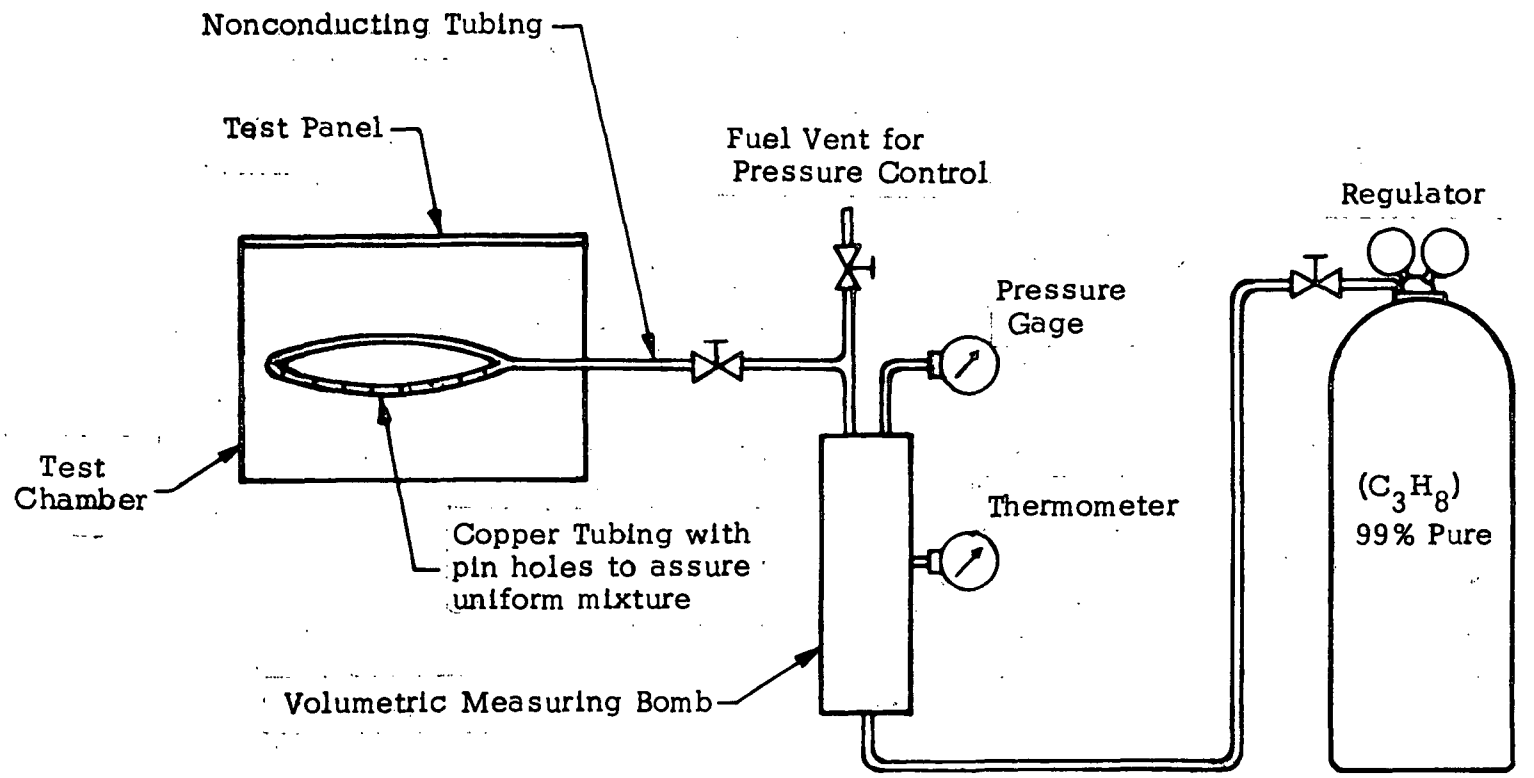

Figure 2. Provision for Fuel/Air Mixture of Known Composition

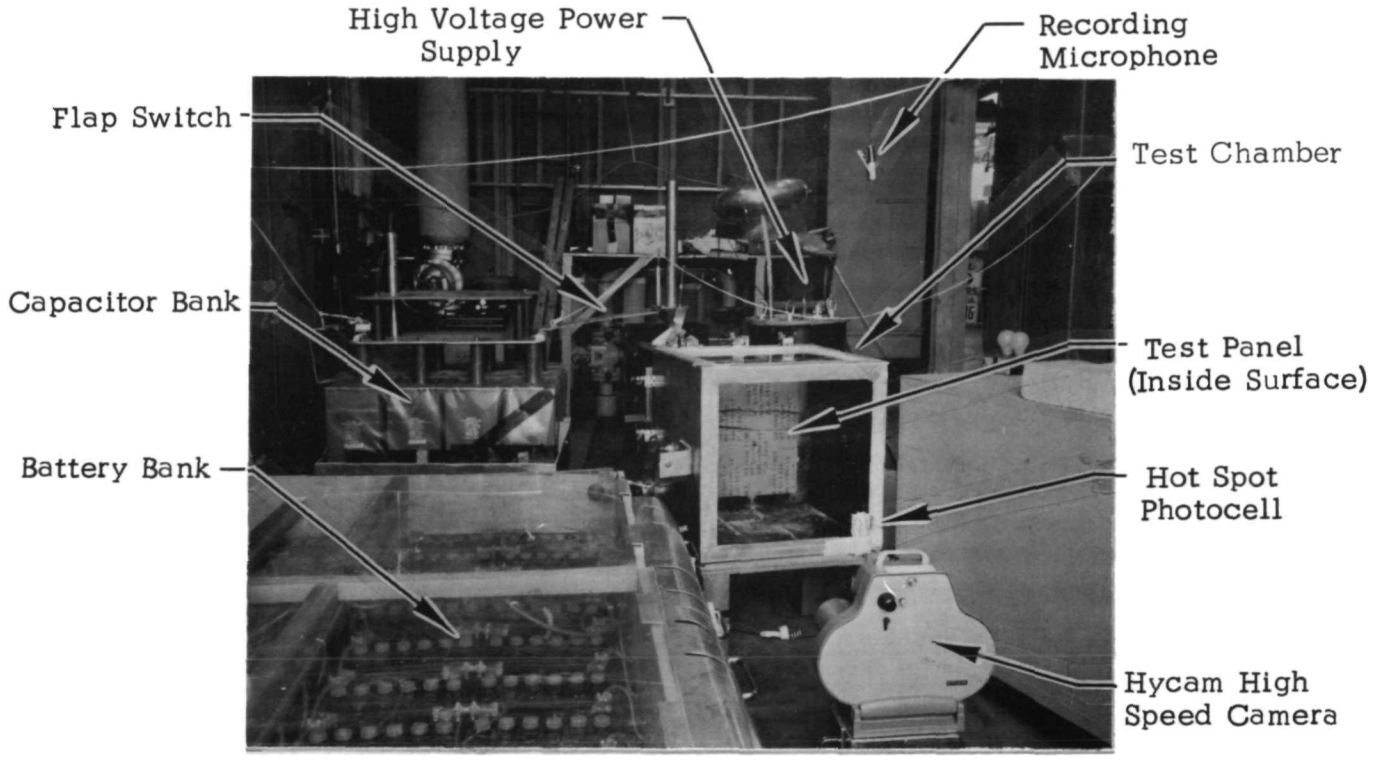

Lightning Simulator

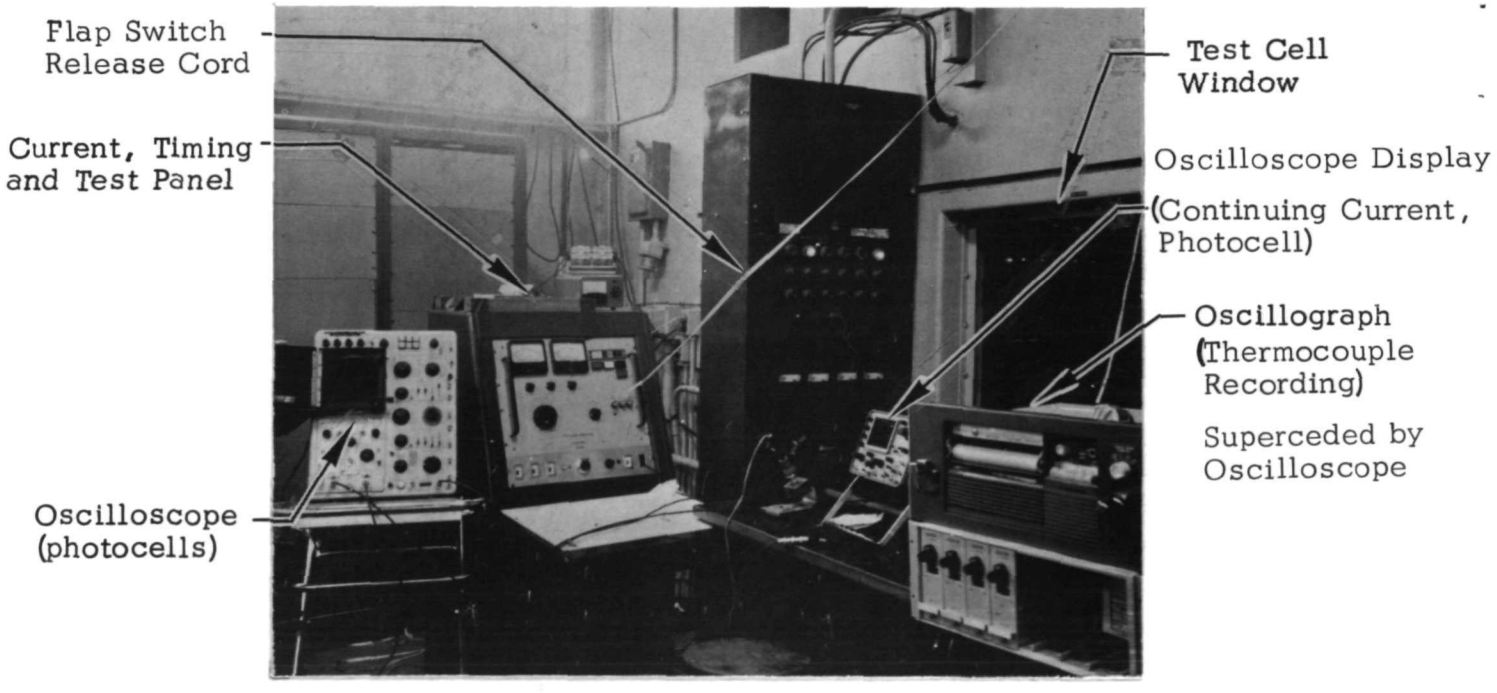

Test Control Console

Figure 3. Photograph of Lightning Simulator

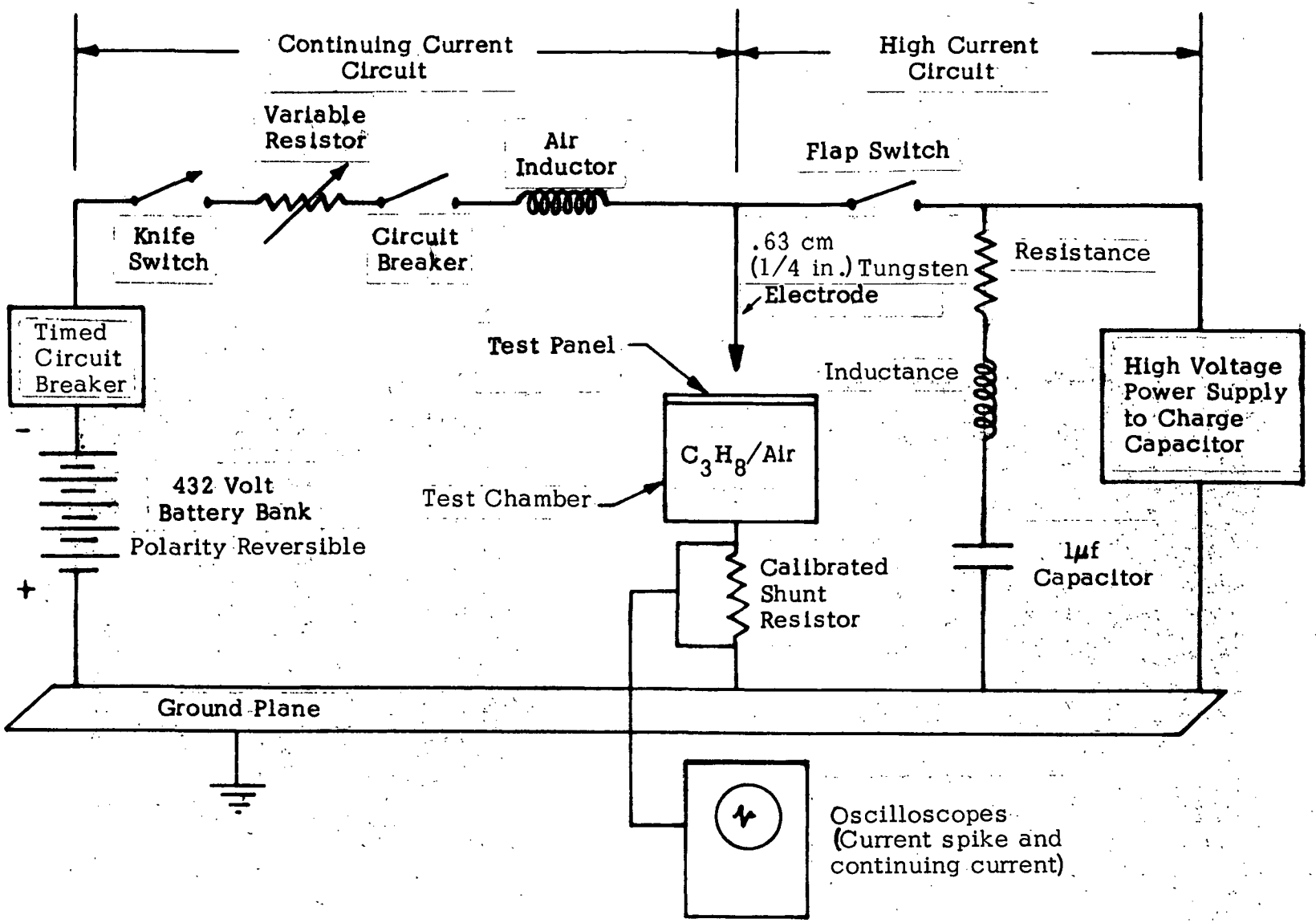

Figure 4. Schematic Description of Lightning Simulator

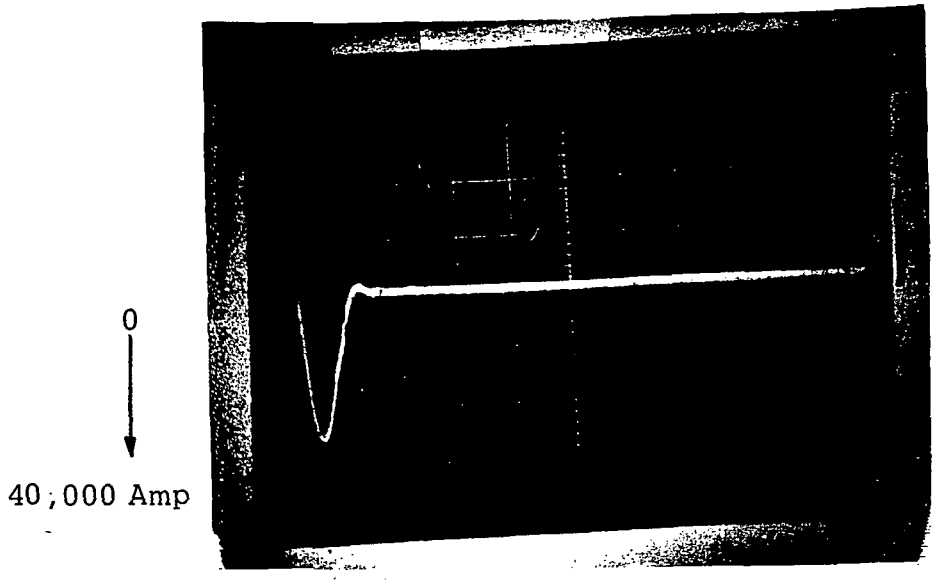

Scale Factors
Vertical - 16,000 amp/cm
Horizontal - 20 μsec/cm

Shunt Calibration
1600 amp/volt

(a) High Current Portion (40 K Amp)

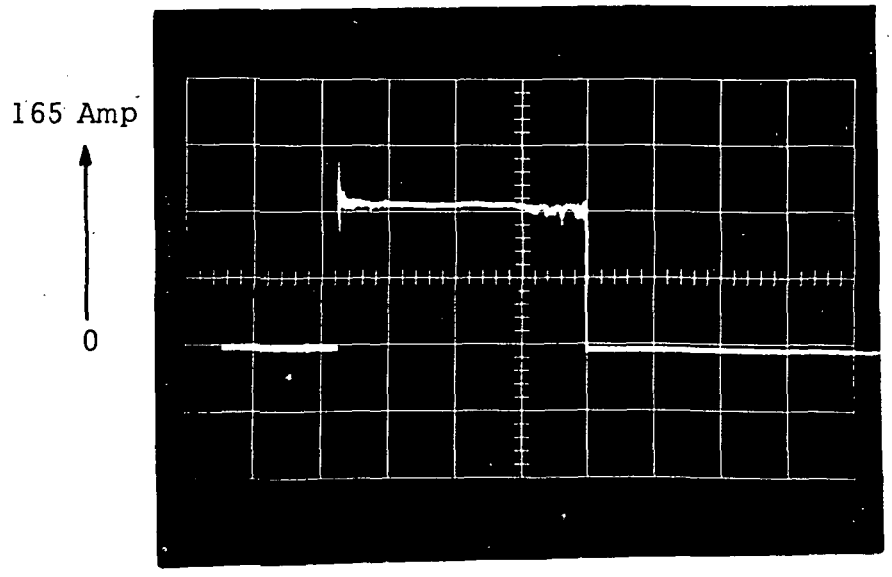

Scale Factors
Vertical - 75 amp/cm
Horizontal - 50 msec/cm

Shunt Calibration
1600 amp/volt

(b) Continuing Current Wave (varied)

Figure 5. Typical Current Discharge History

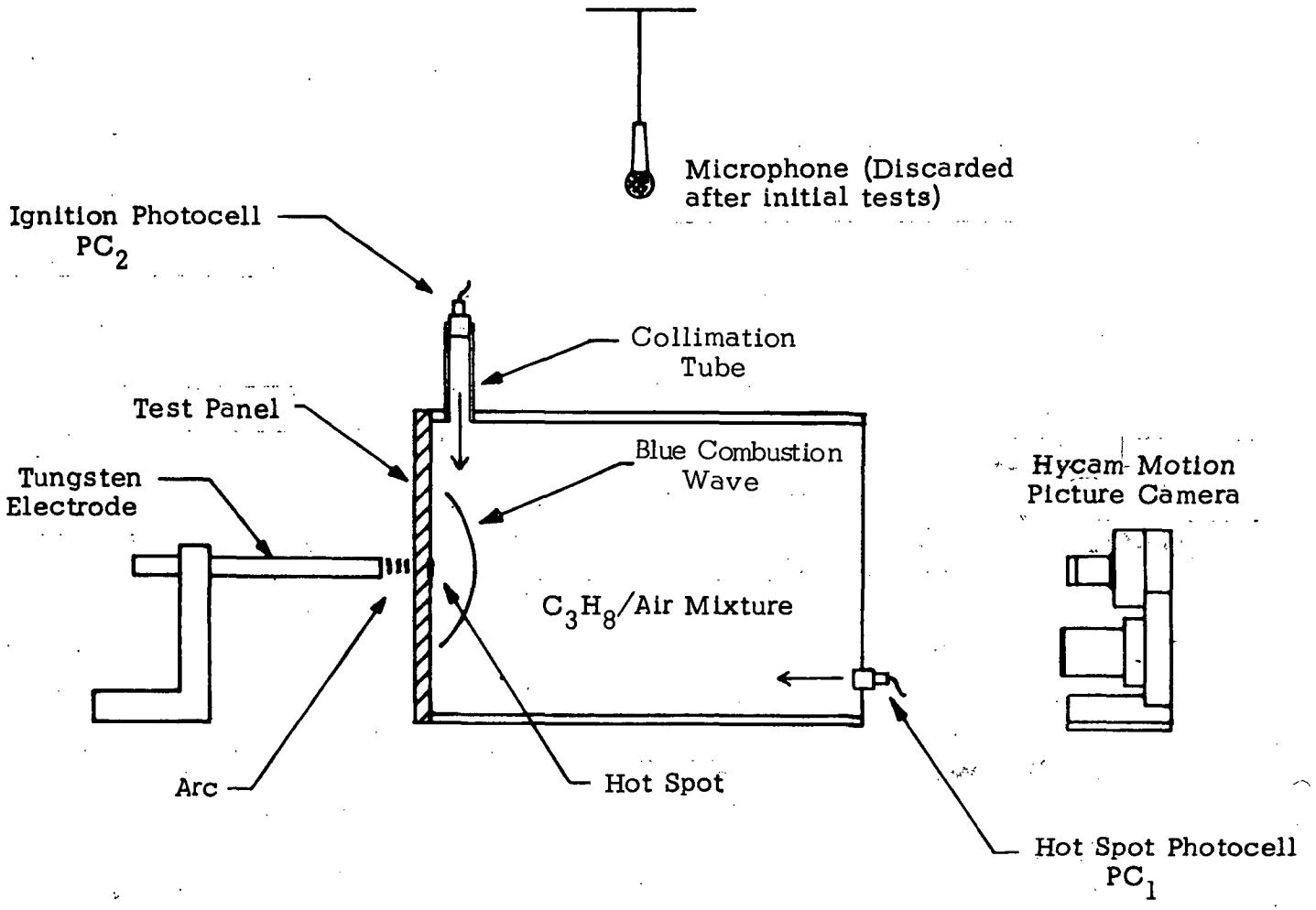

Figure 6. Apparatus for Detecting Ignition

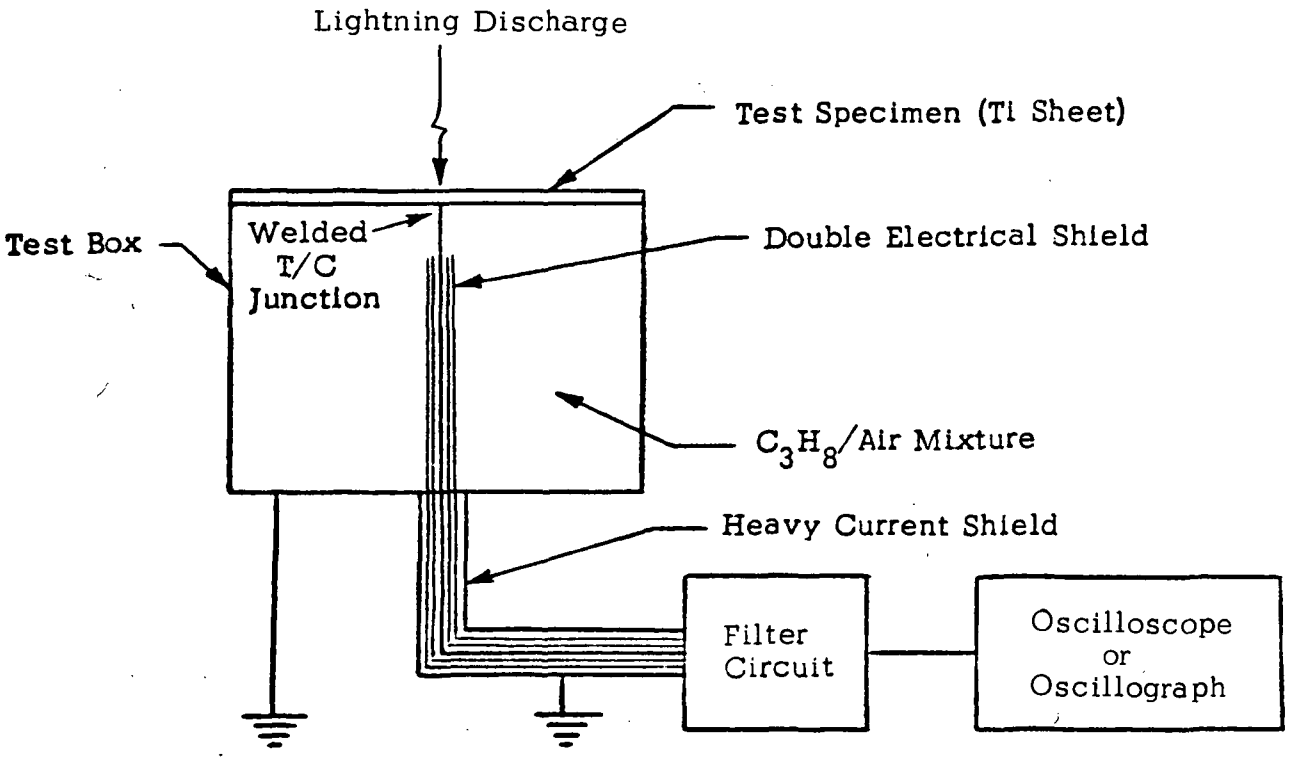

Figure 7. Temperature-Measurement Apparatus

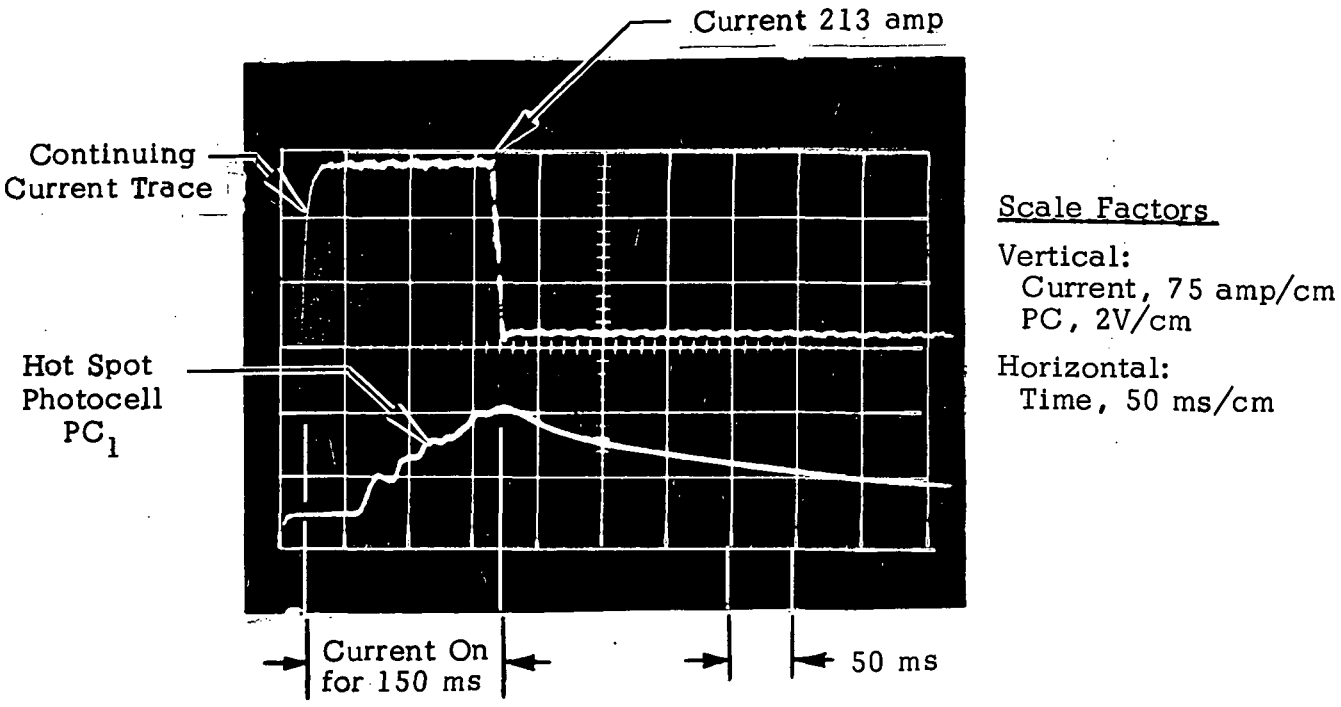

(a) Current/Photocell Trace

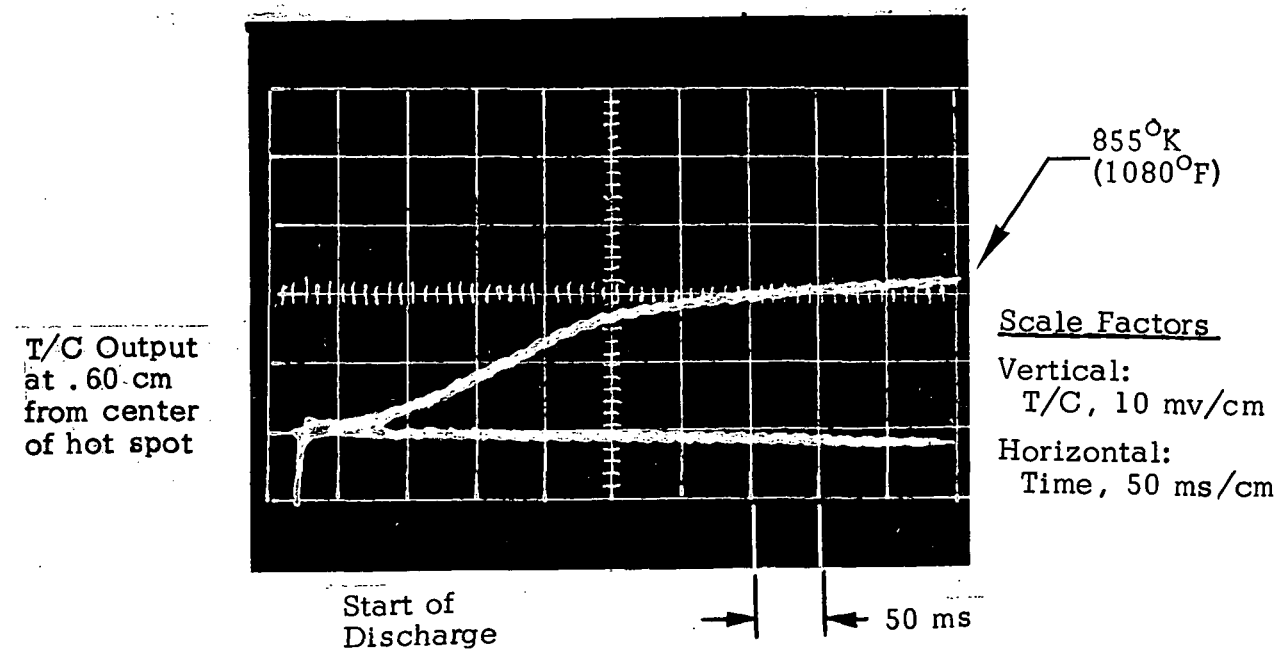

(b) Thermocouple Output

Figure 8. Typical Photocell Transient and Temperature History

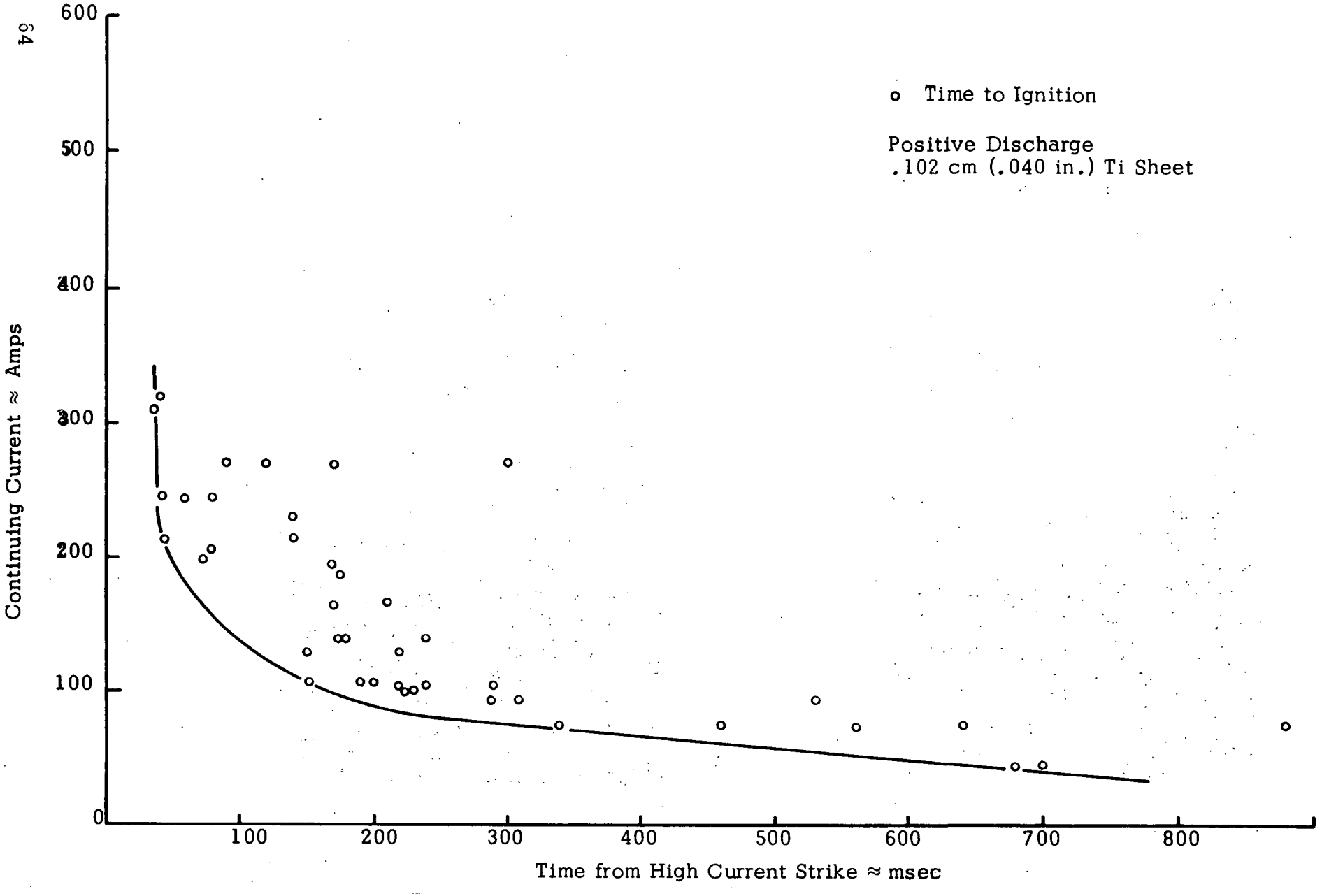

Figure 9. Ignition Tests With Bare Alloy Sheet (.102 cm (.040 in.), Positive Charge

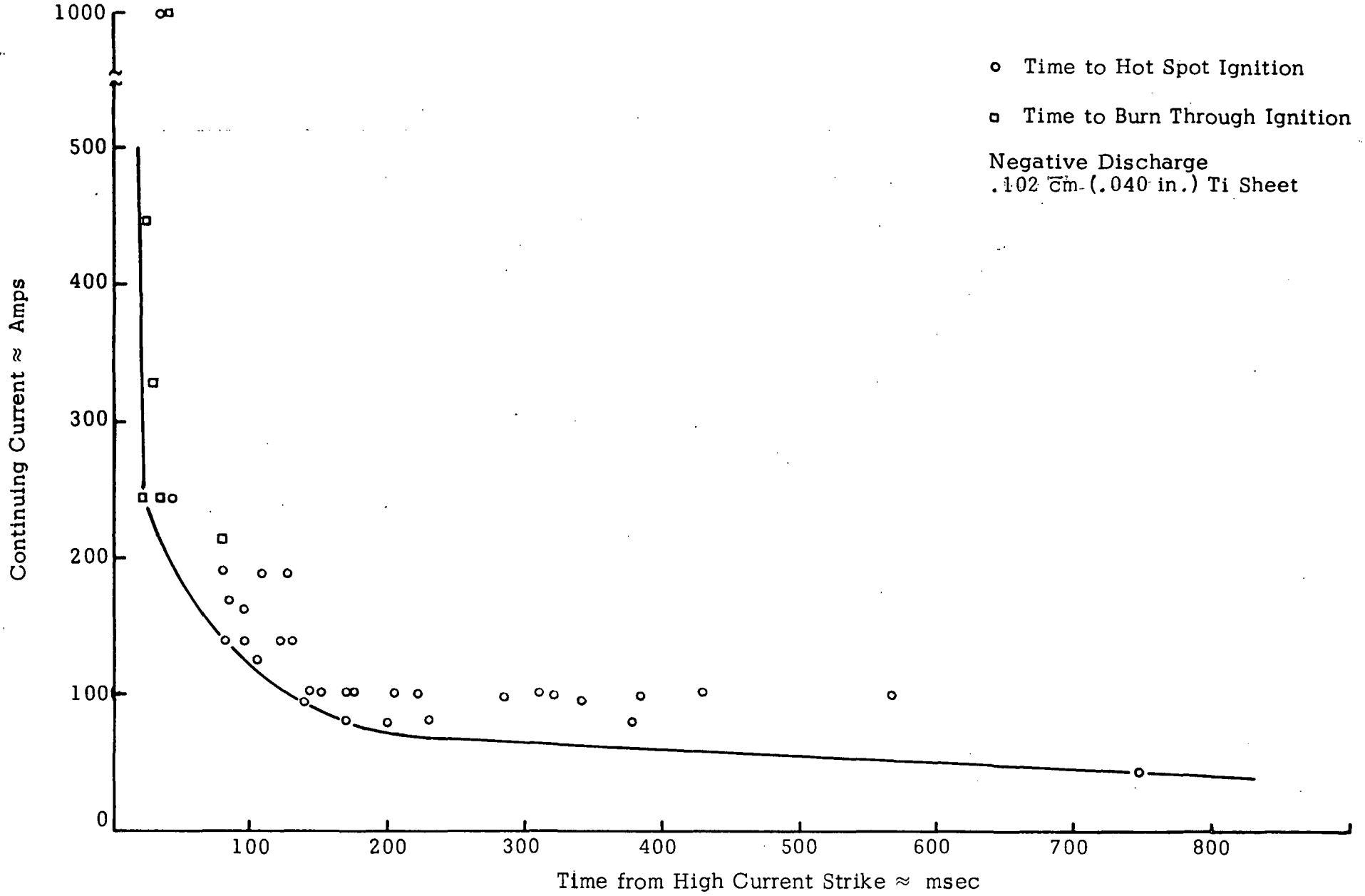

Figure 10. Ignition Tests With Bare Alloy Sheet (.102 cm (.040 in.), Negative Charge

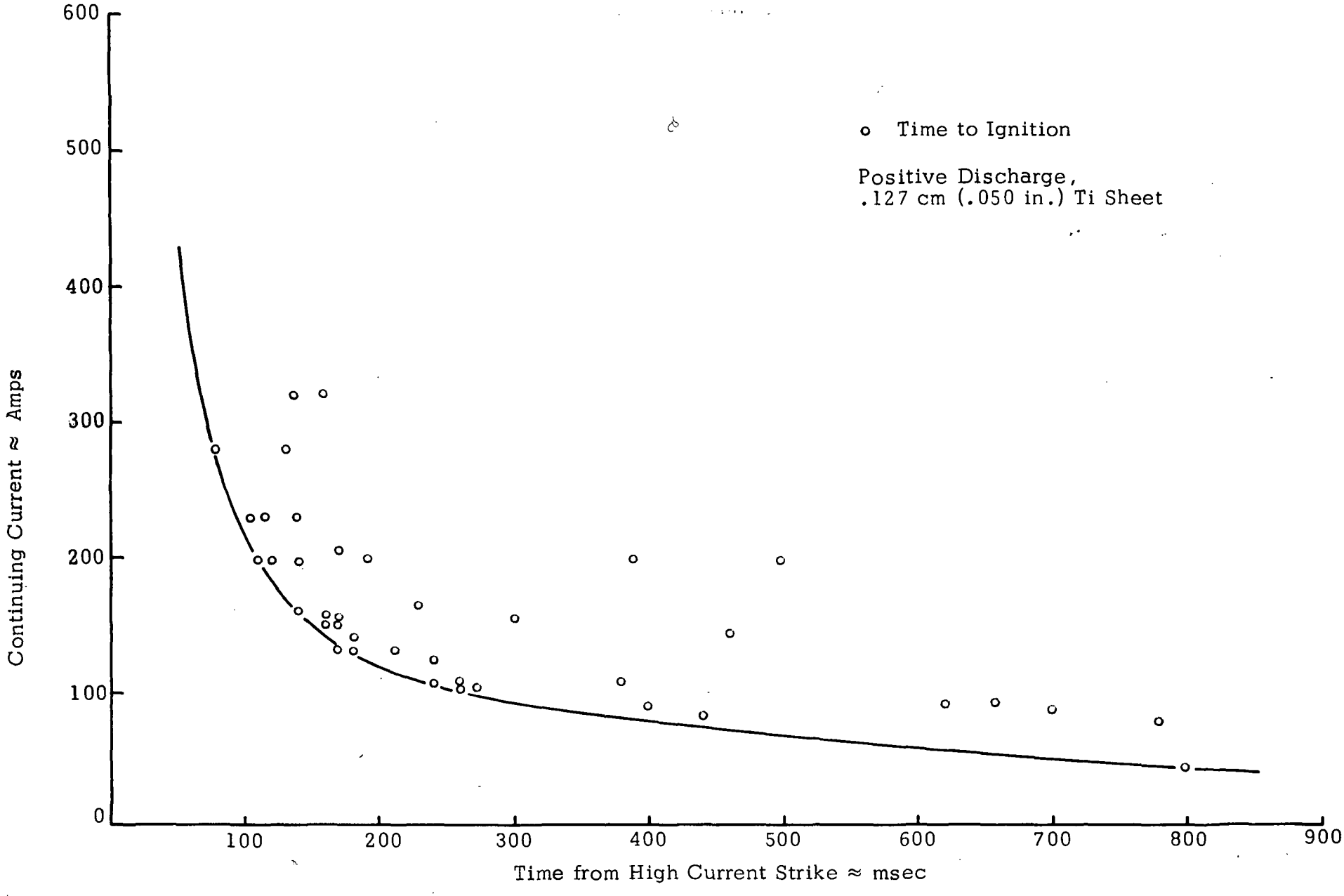

Figure 11. Ignition Tests With Bare Alloy Sheet (.127 cm (.050 in.), Positive Charge

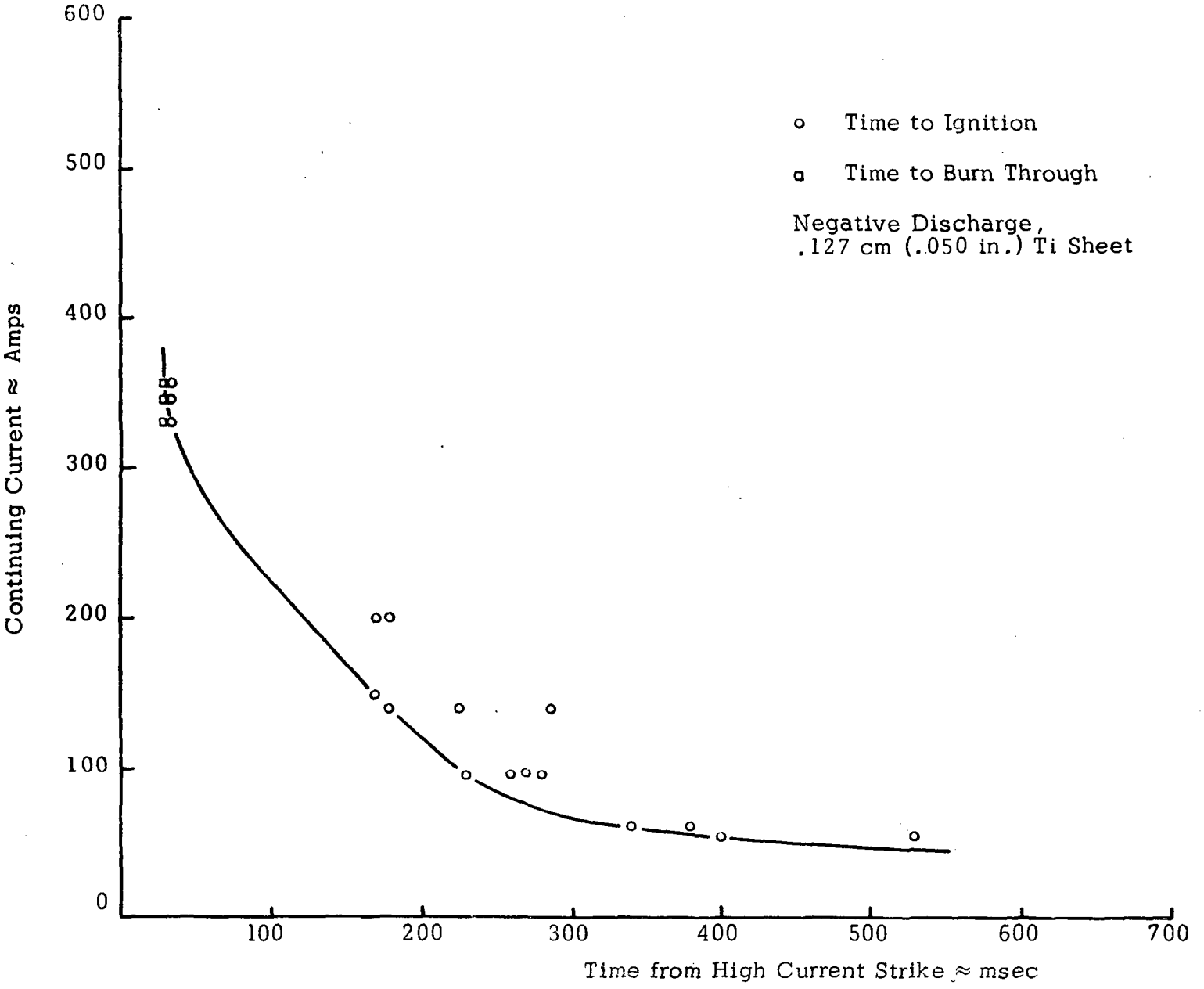

Figure 12. Ignition Tests With Bare Alloy Sheet (.127 cm (.050 in.), Negative Charge

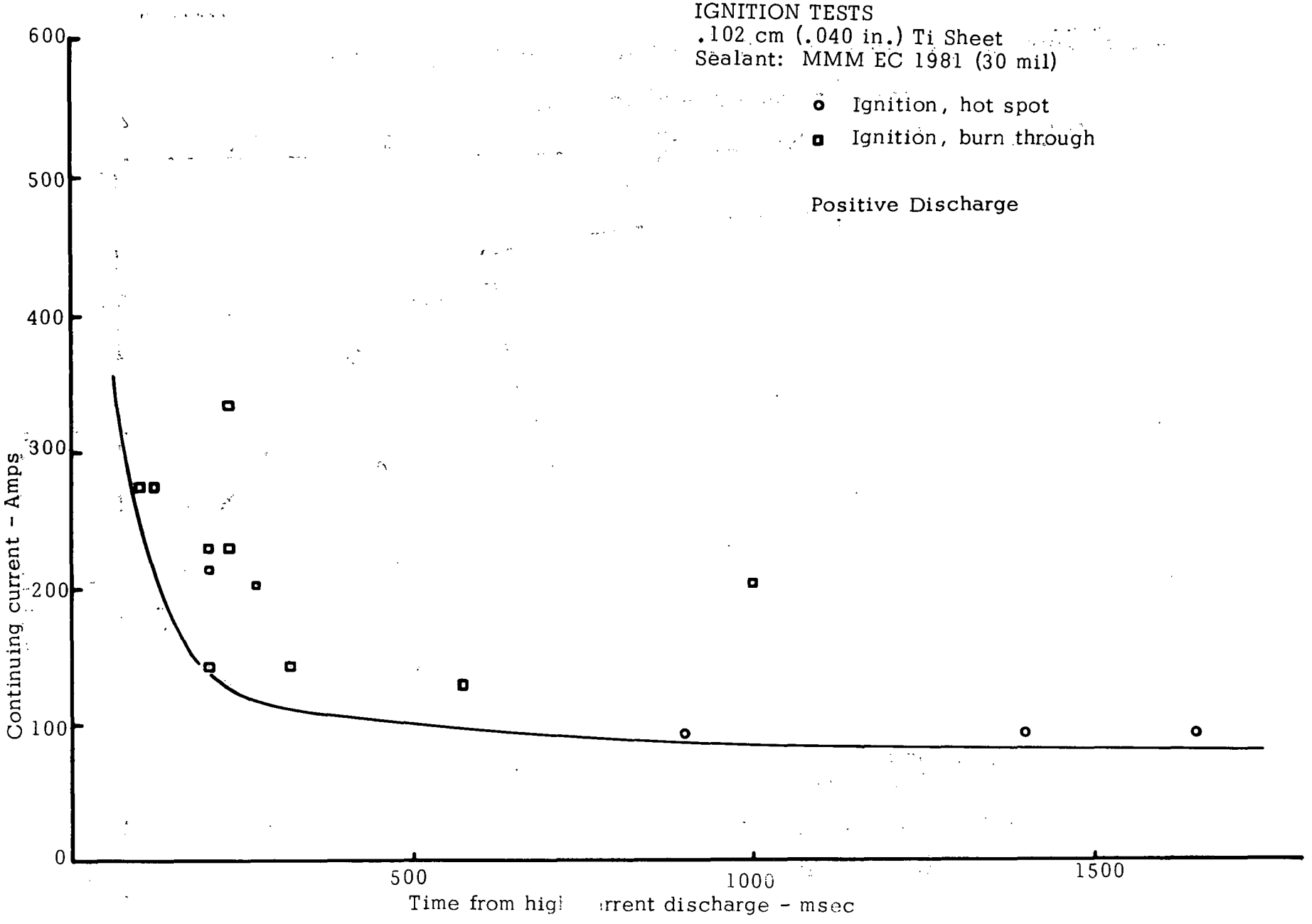

Figure 13. Ignition Tests With EC 1981 - Coated Alloy Sheet

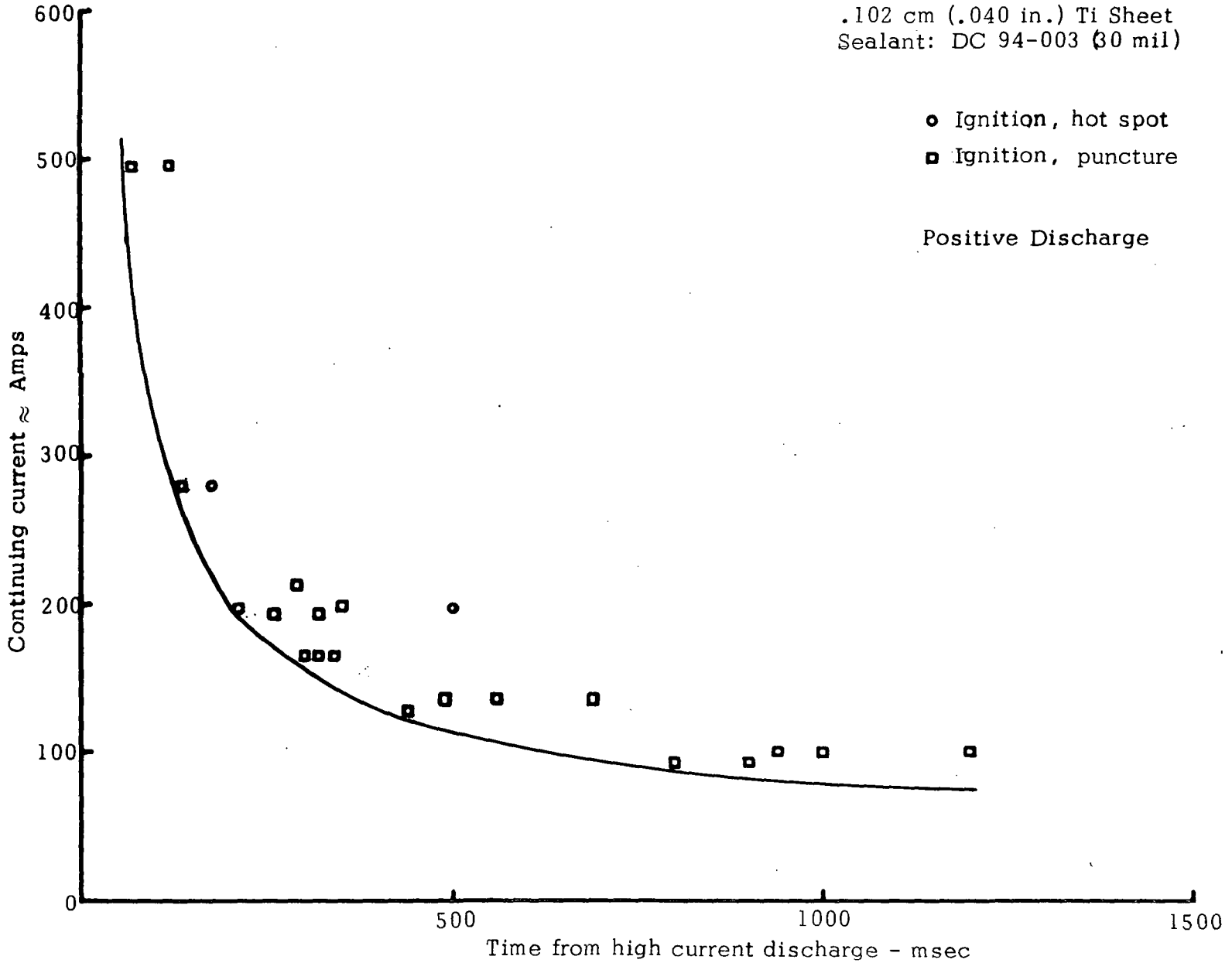

Figure 14. Ignition Tests With 94-003 - Coated Alloy Sheet

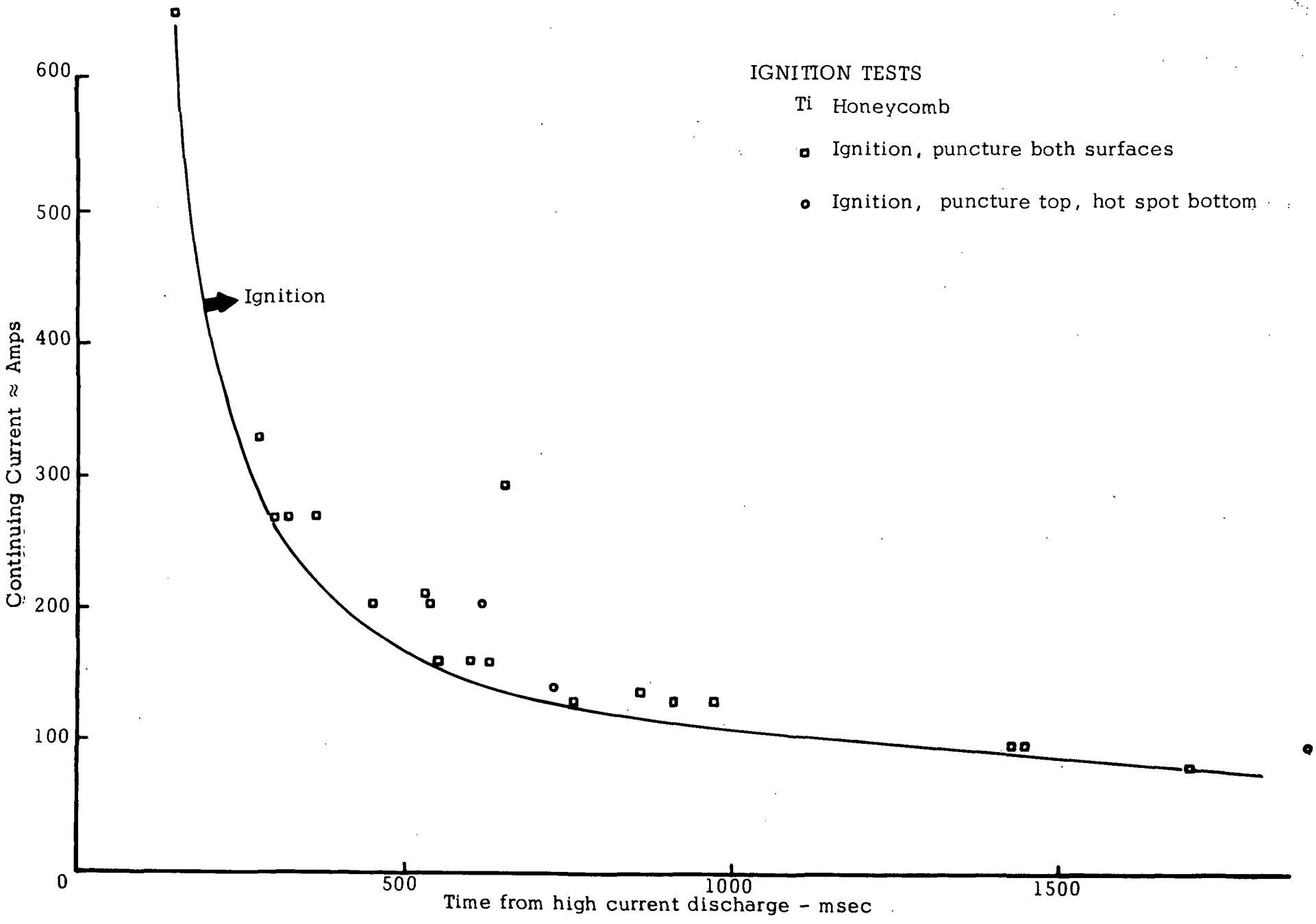

Figure 15. Ignition Tests With Honeycomb Sandwich

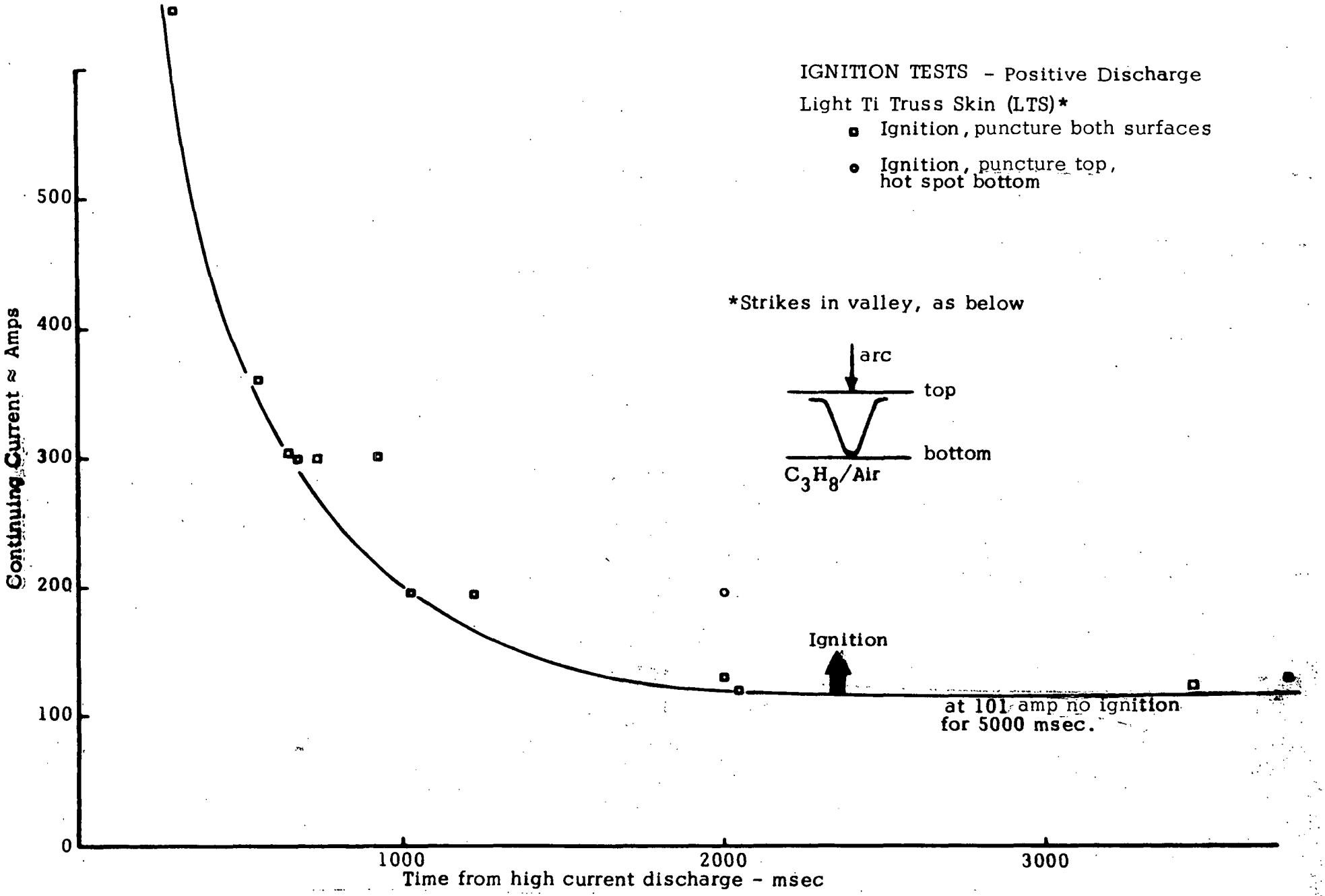

Figure 16. Ignition Tests With Light-Truss Sandwich (Strike at Valley)

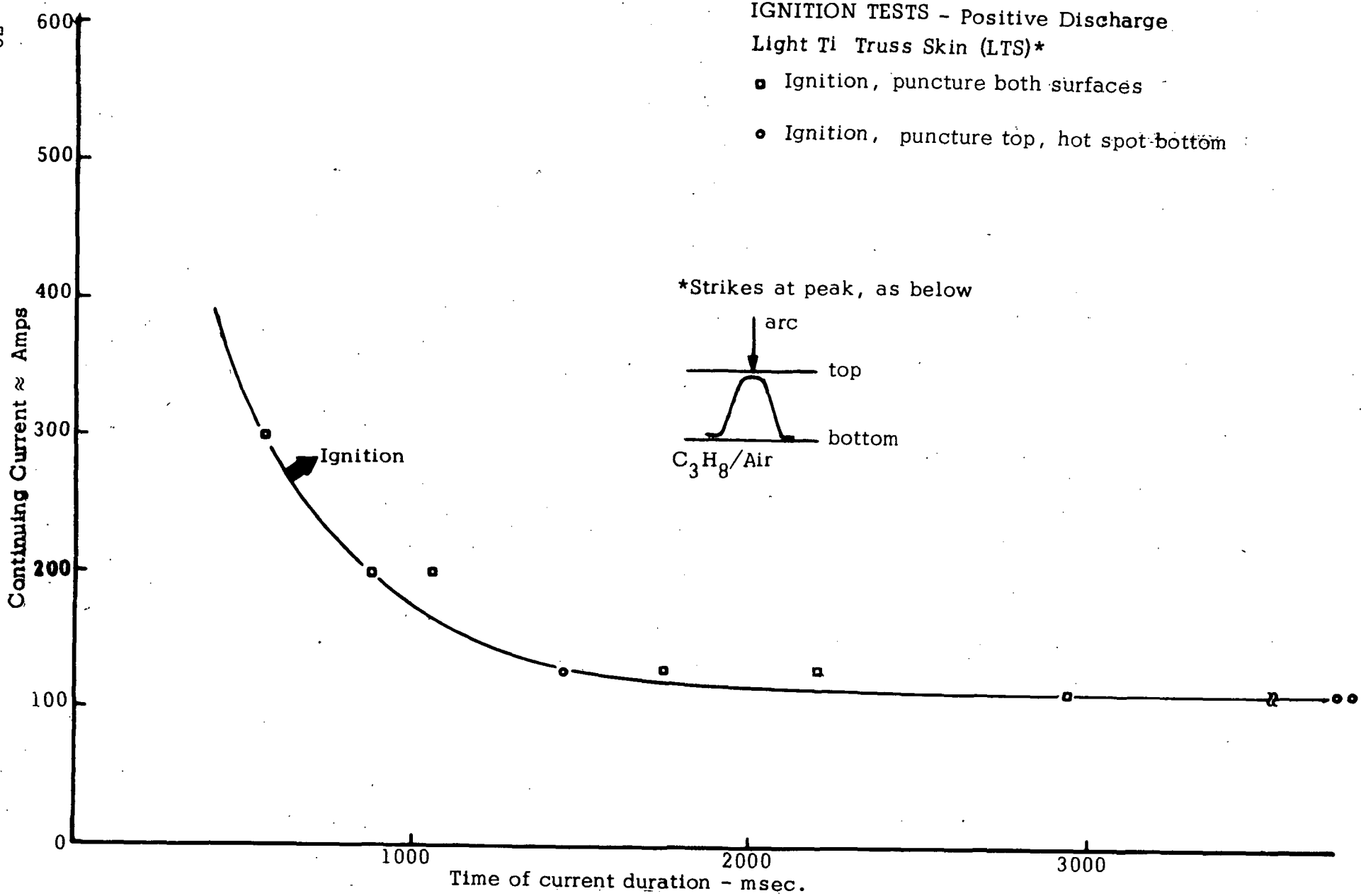

Figure 17. Ignition Tests With Light-Truss Sandwich (Strike at Peak)

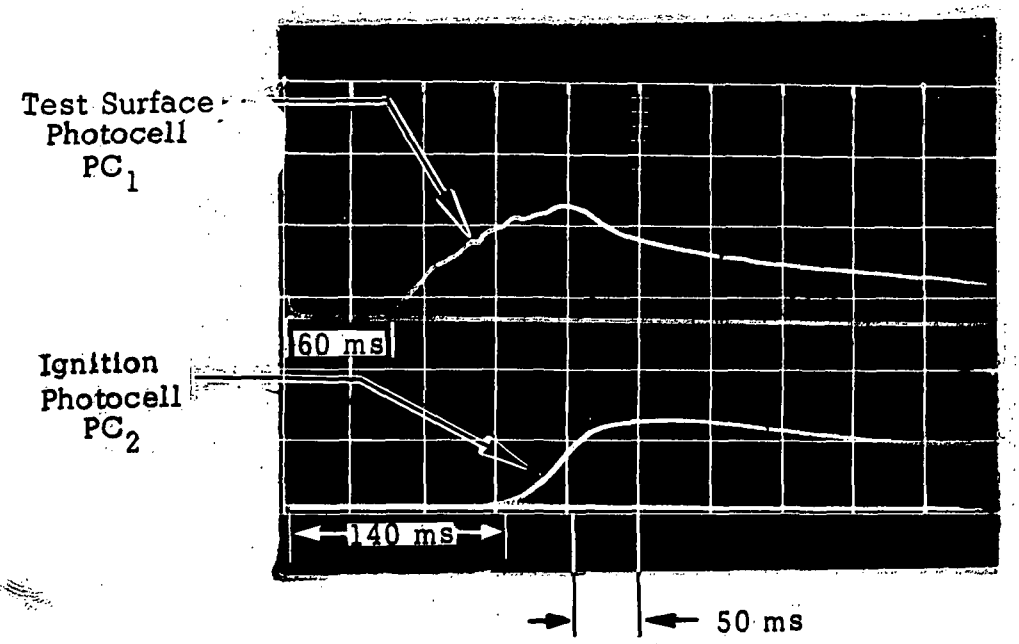

Test #171

I_1 = 40 KAmp

I_2 = 214 Amp

Discharge Dur. = 190 ms

.102 cm (.040 in.) Ti Sheet + Discharge

(a) Hot Spot Ignition

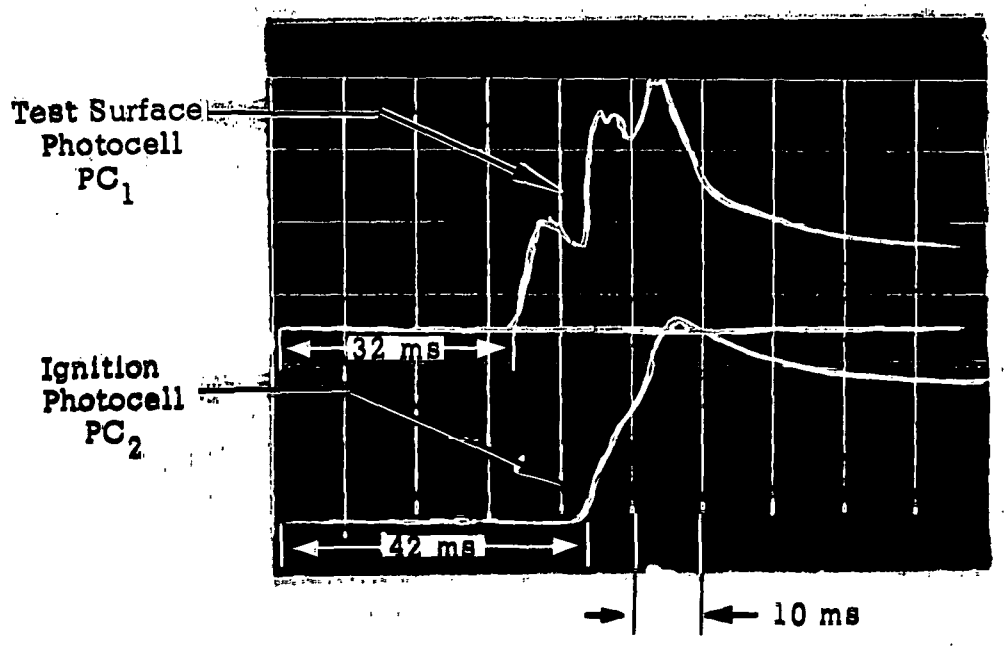

Test #121

I_1 = 40 KAmp

I_2 = 246 Amp

Discharge Dur. = 52 ms

.102 cm (.040 in.) Ti Sheet - Discharge

(b) Burn Through Ignition

Figure 18. Photocell Traces Showing the Difference Between Ignition by Hot-Spot and Puncture

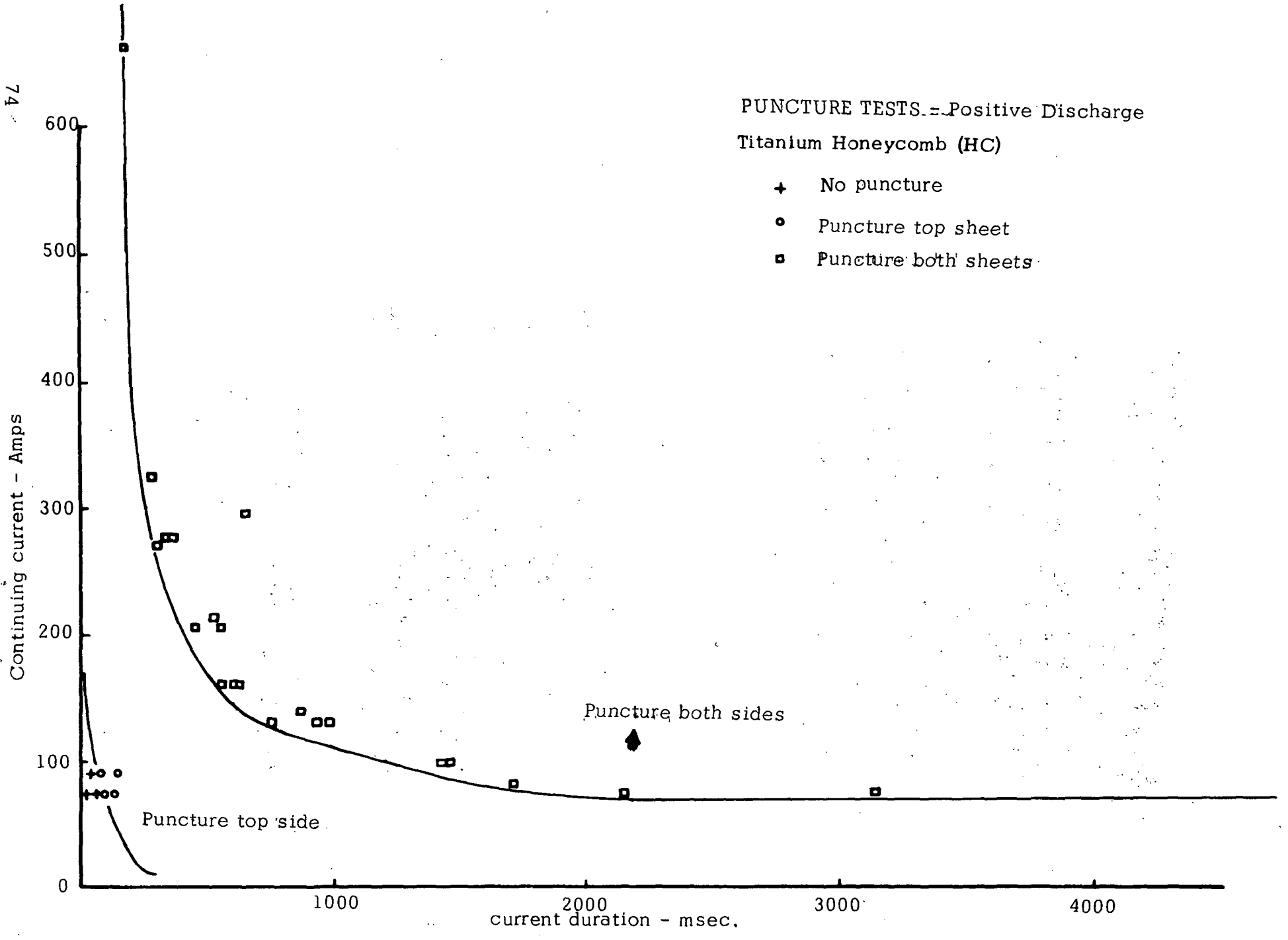

Figure 19. Puncture Tests With Honeycomb Sandwich

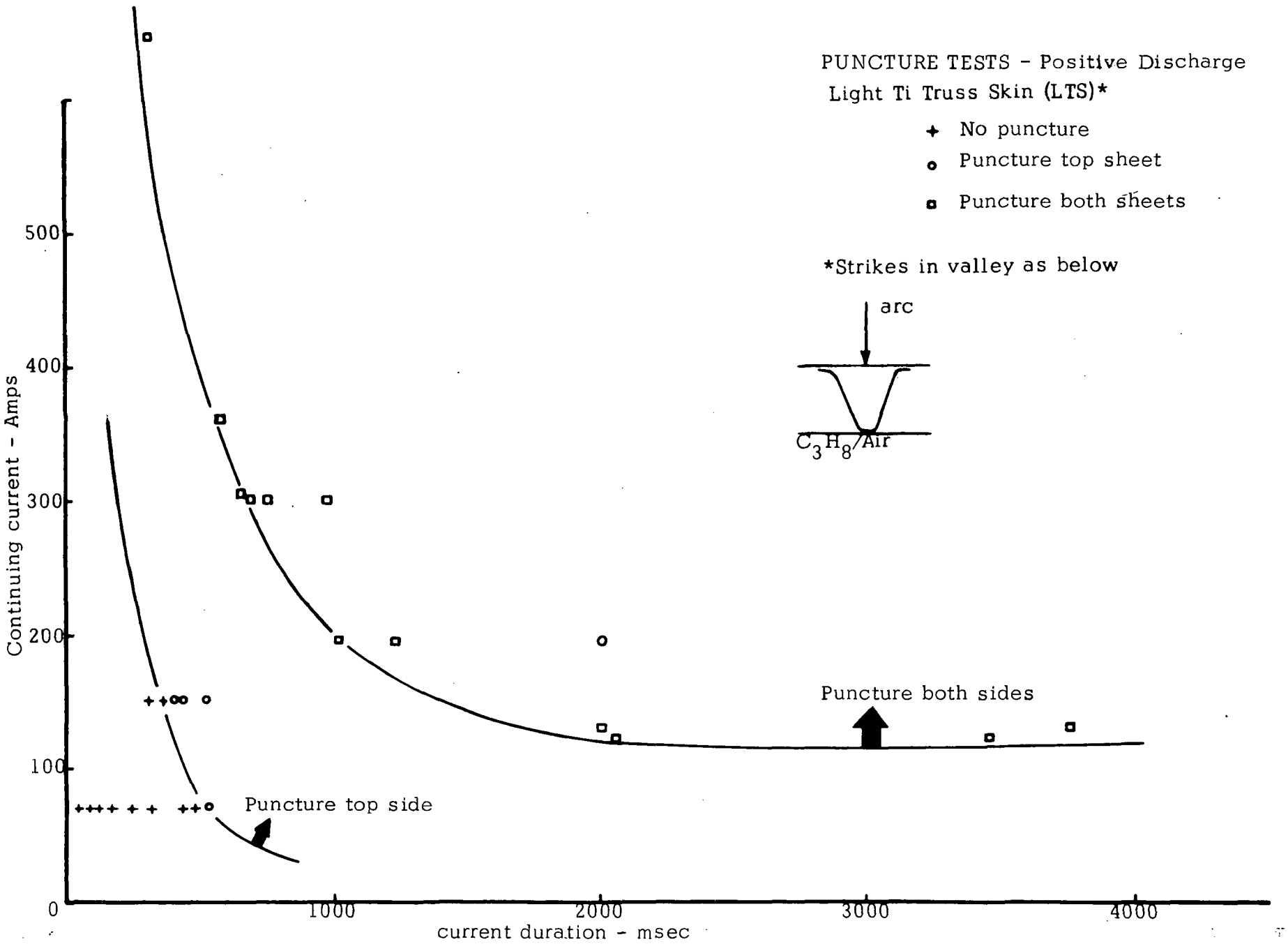

Figure 20. Puncture Tests With Light-Truss Sandwich (Strike at Valley)

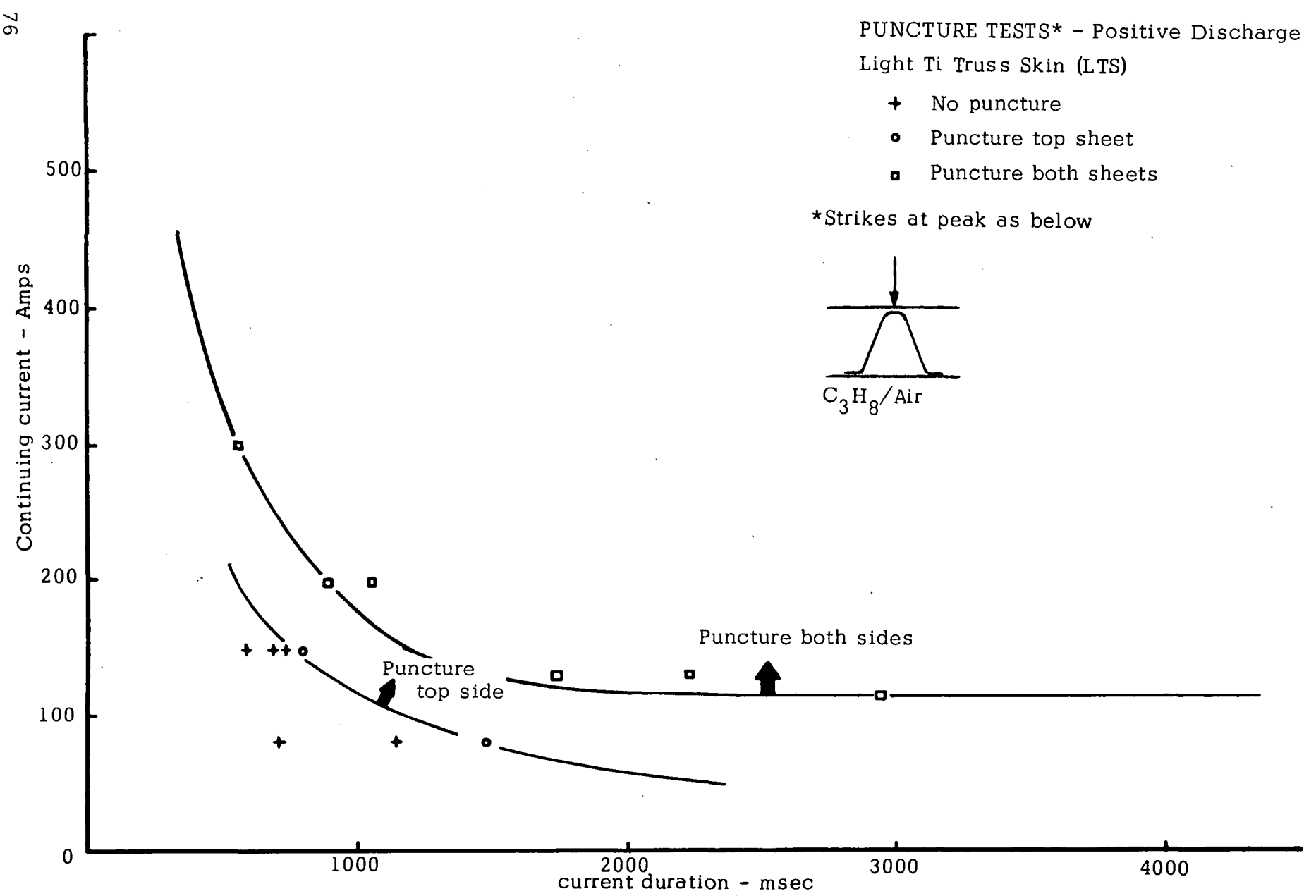

Figure 21. Puncture Tests With Light-Truss Sandwich (Strike at Peak)

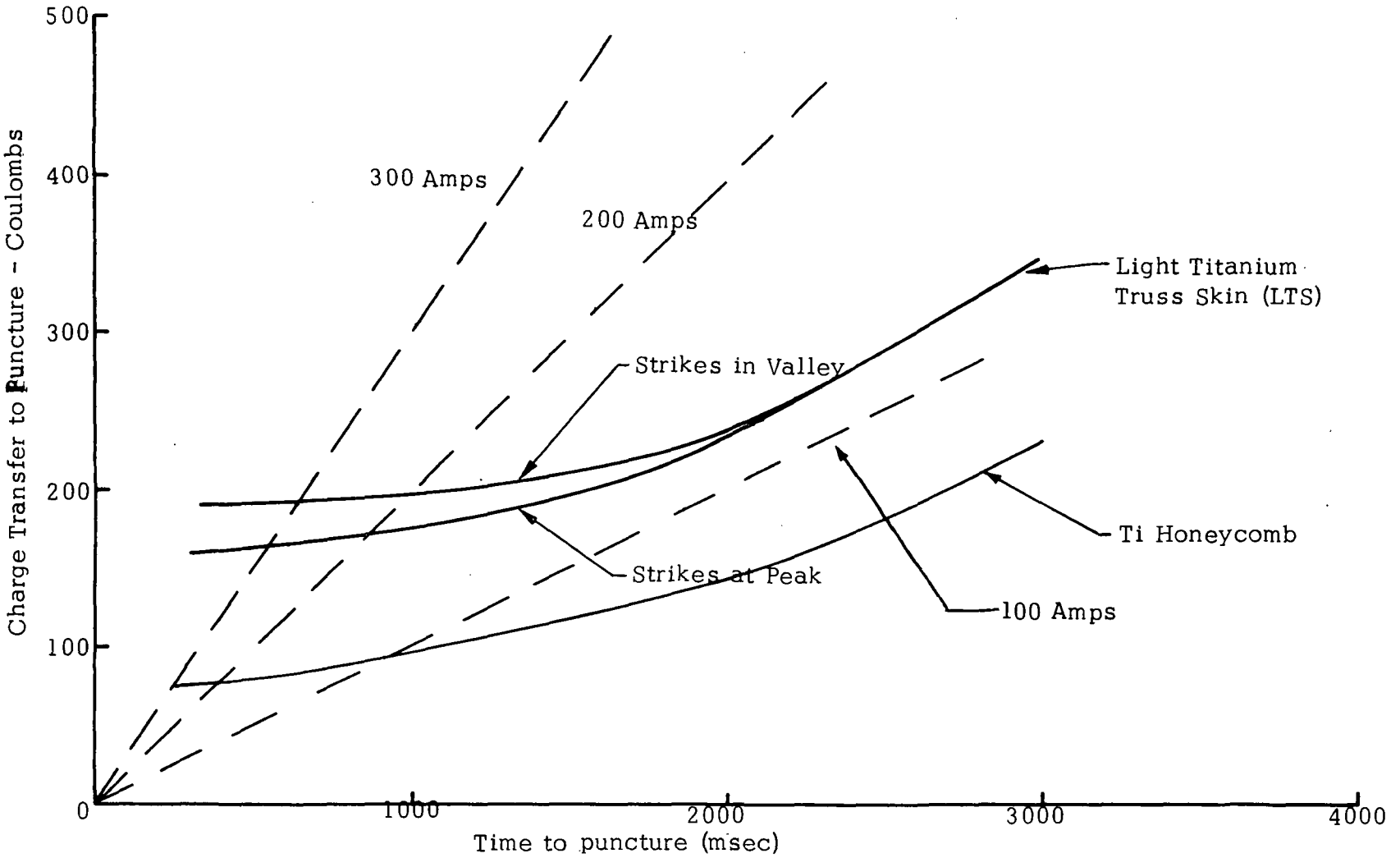

Figure 22. Puncture Threshold for Sandwich Skins

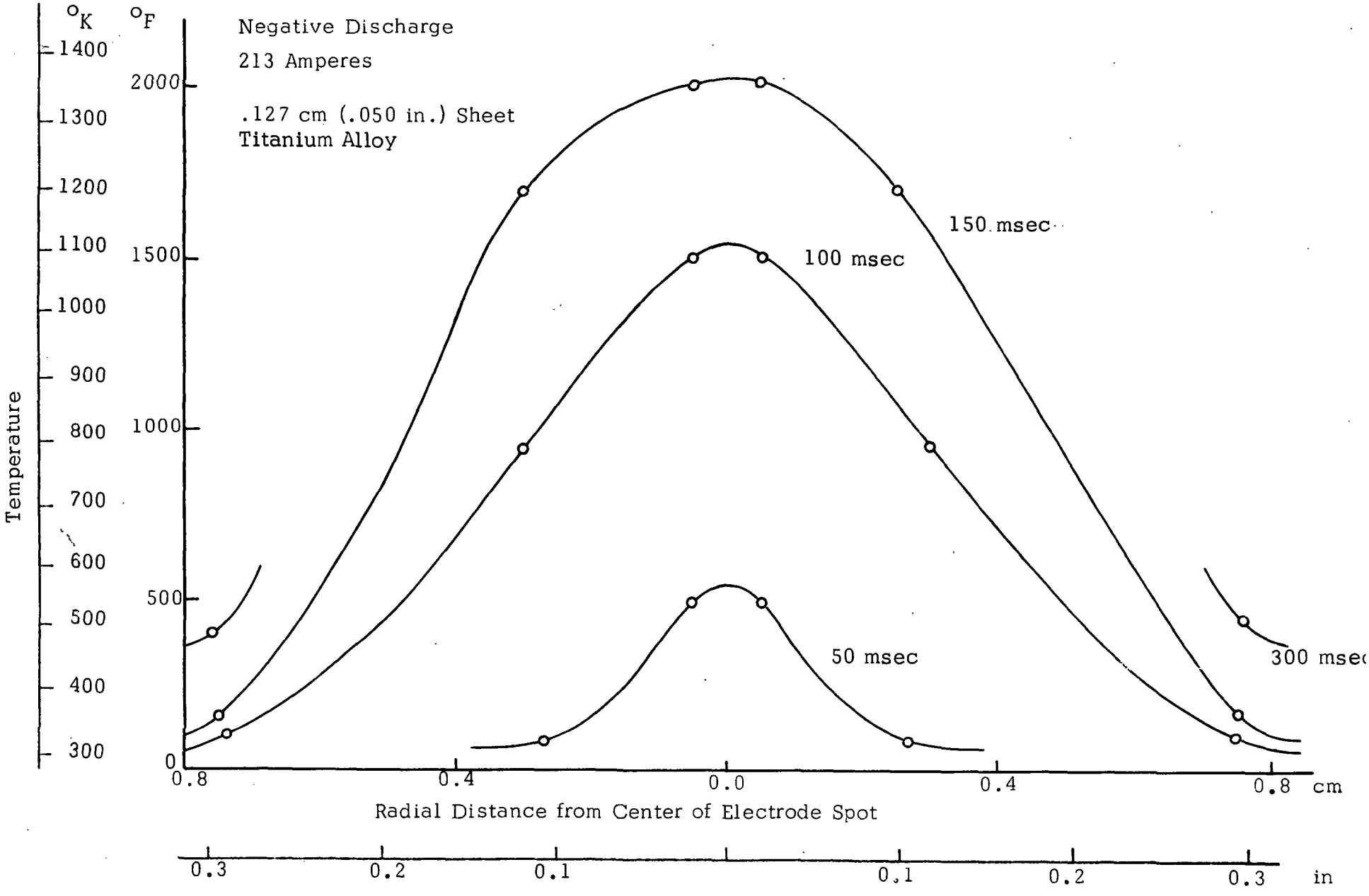

Figure 23. Measured Radial Temperature Profile of the Lower Surface (Negative Discharge, 213 amps)

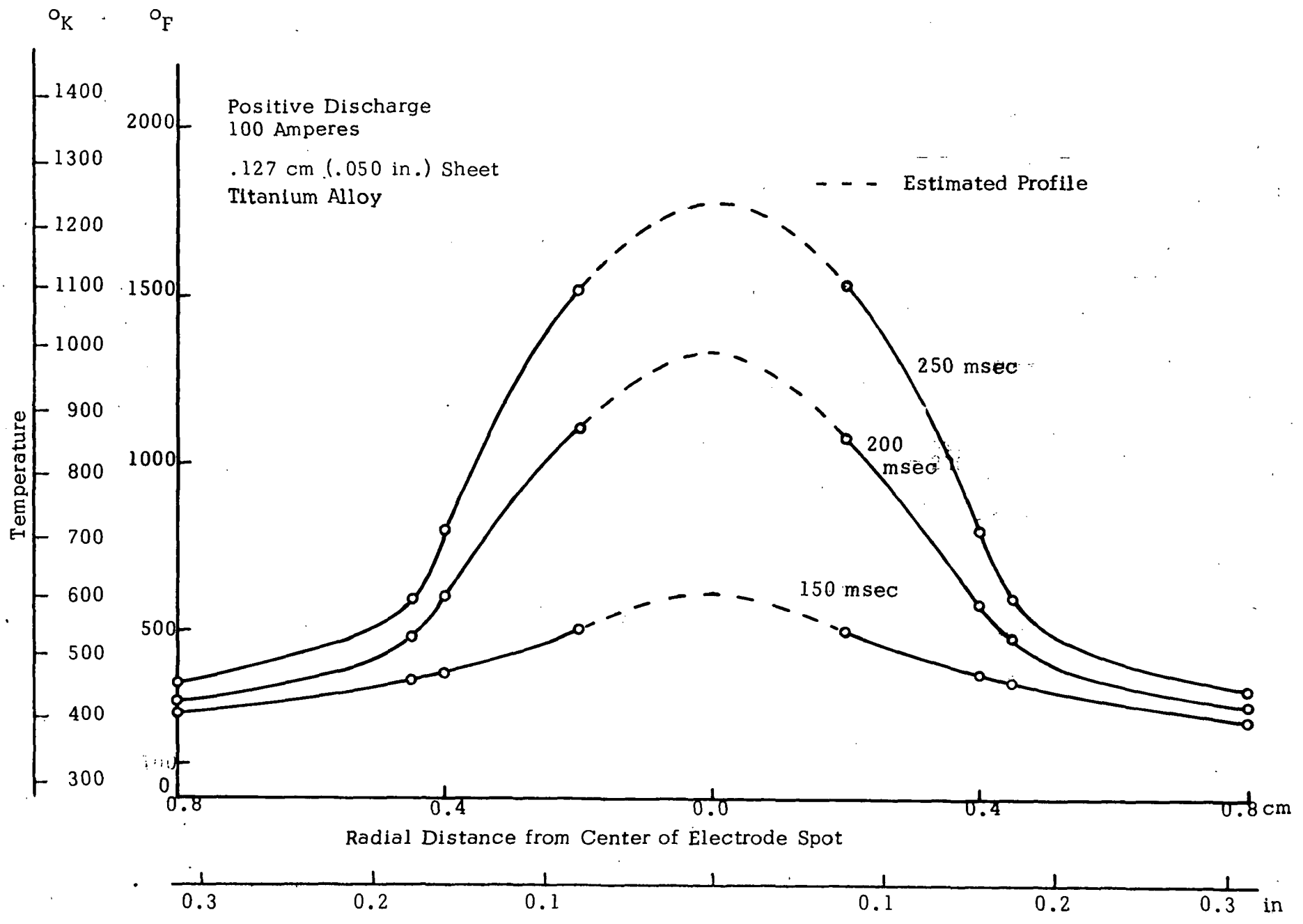

Figure 24. Measured Radial Temperature Profile of the Lower Surface (Positive Discharge, 100 amps)

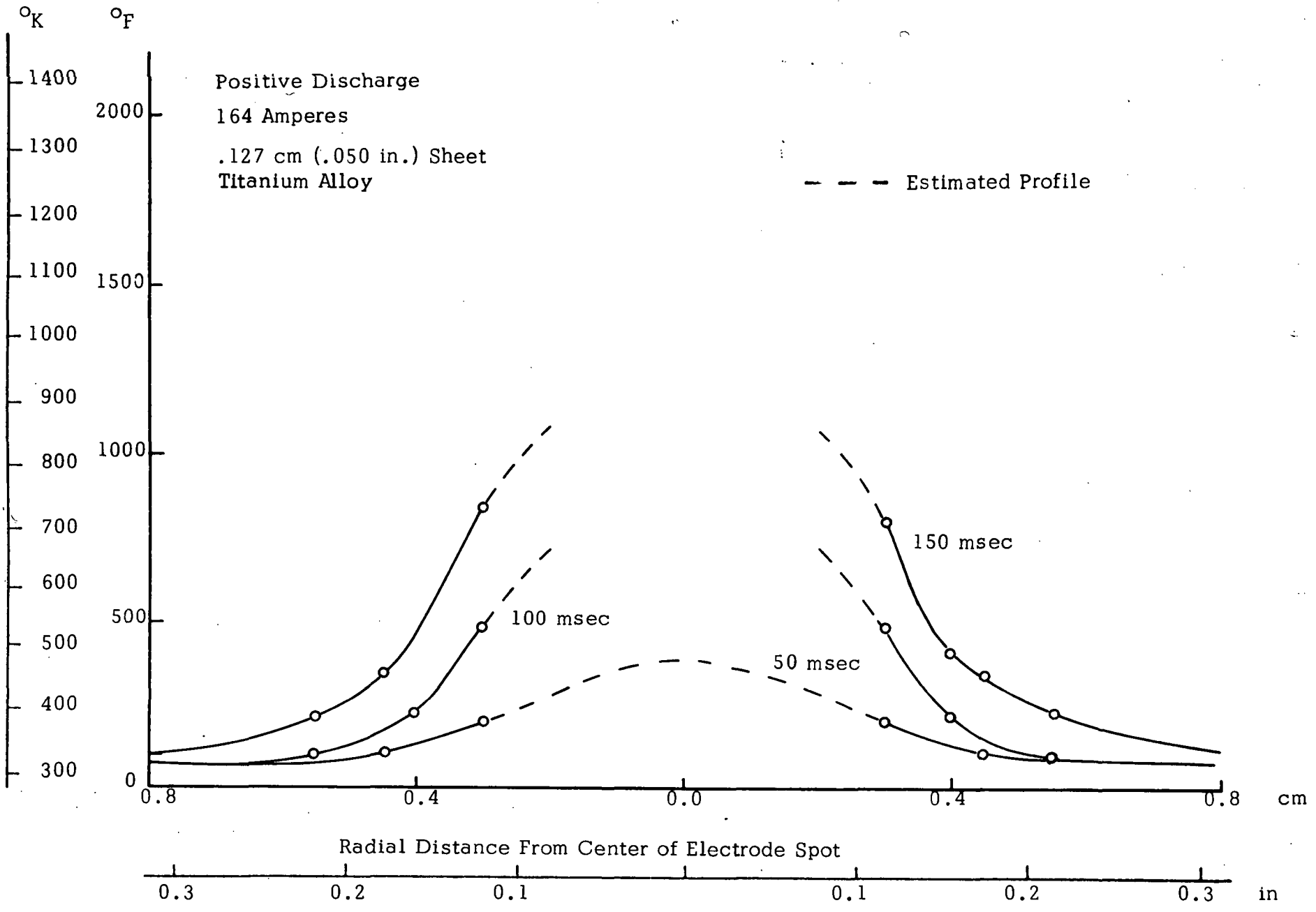

Figure 25. Measured Radial Temperature Profile of the Lower Surface (Positive Discharge, 164 amps)

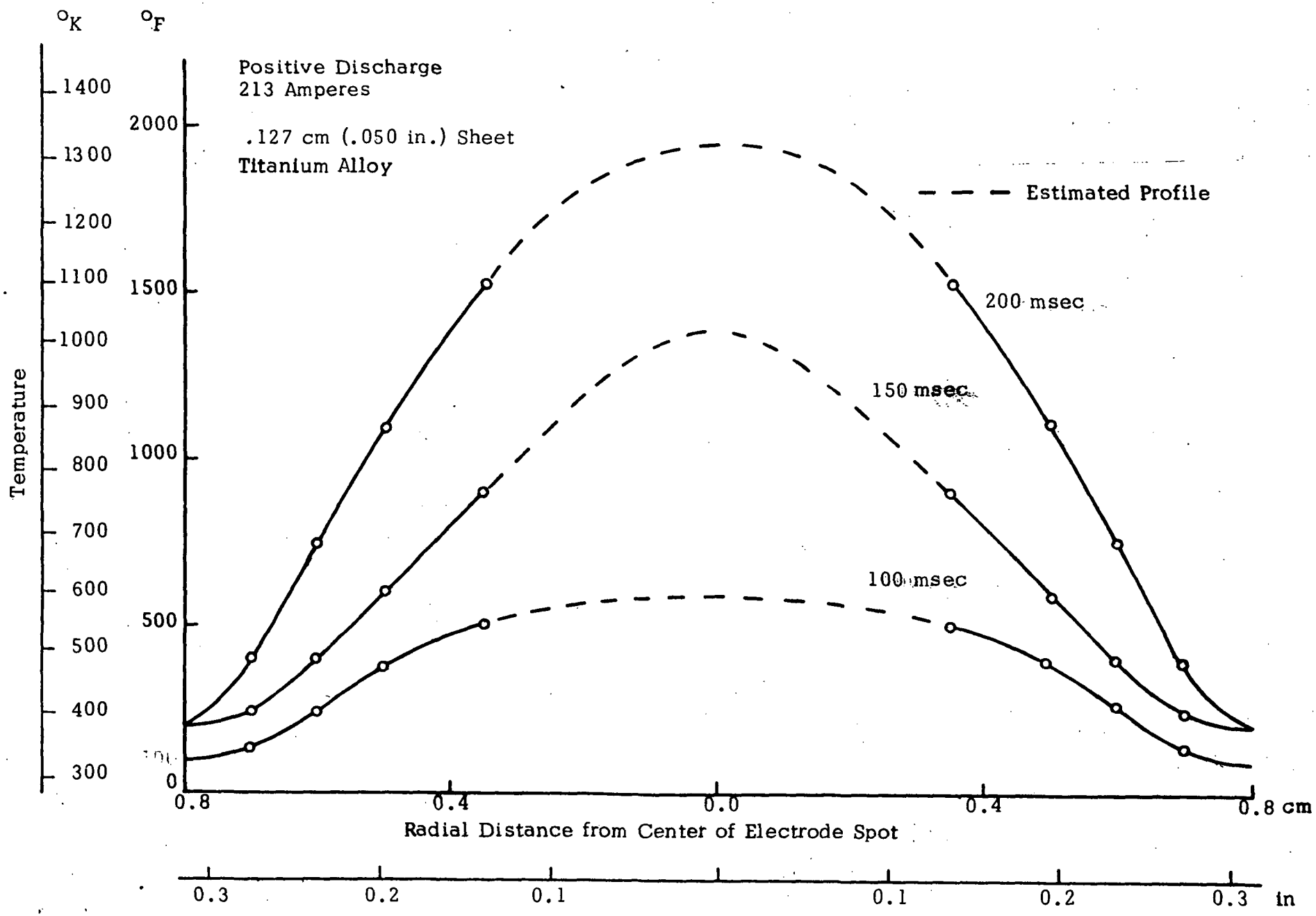

Figure 26. Measured Radial Temperature Profile of the Lower Surface (Positive Discharge, 213 amps)

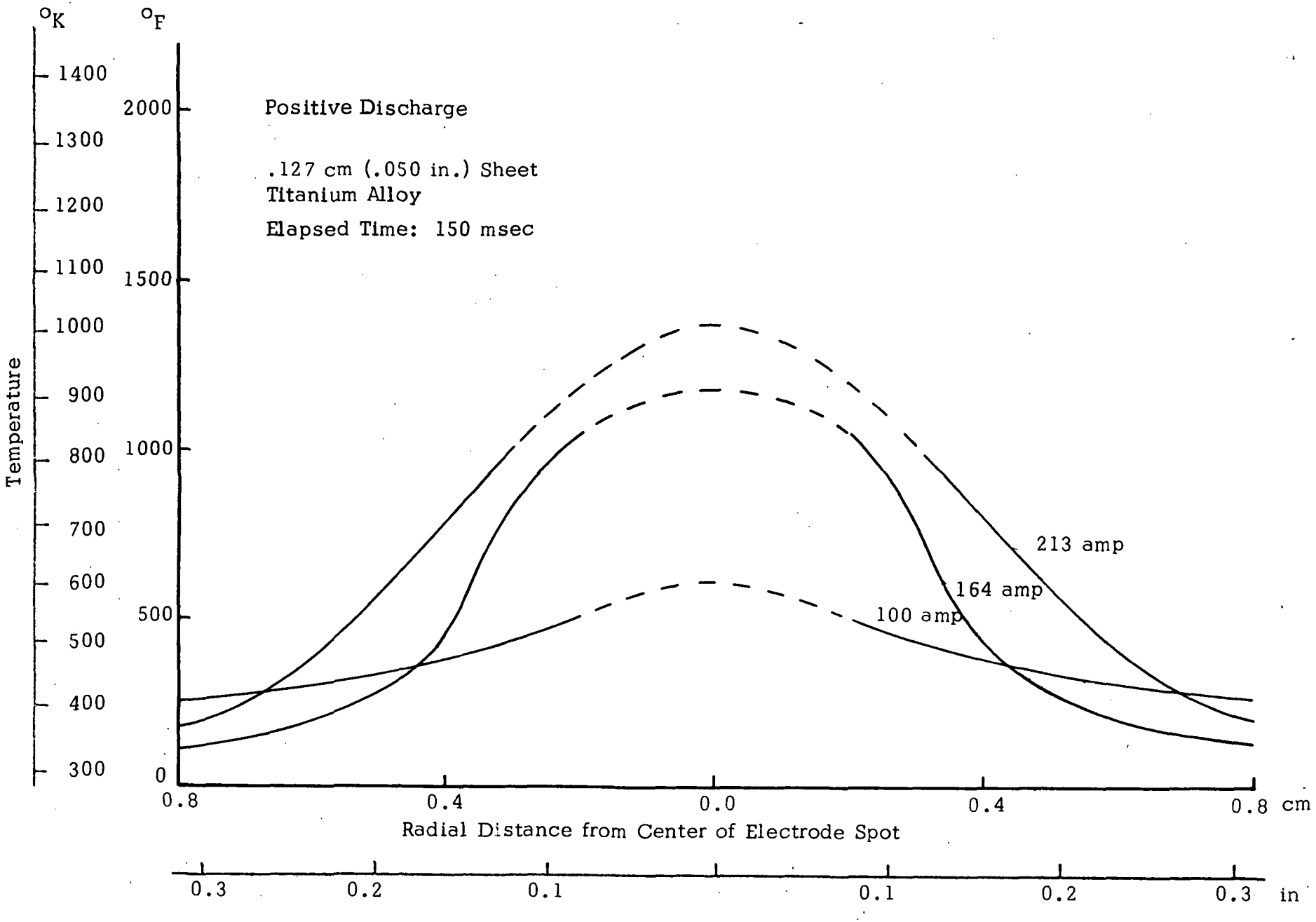

Figure 27. Effect of Current Level on Temperature Rise at Lower Surface (Positive Discharges)

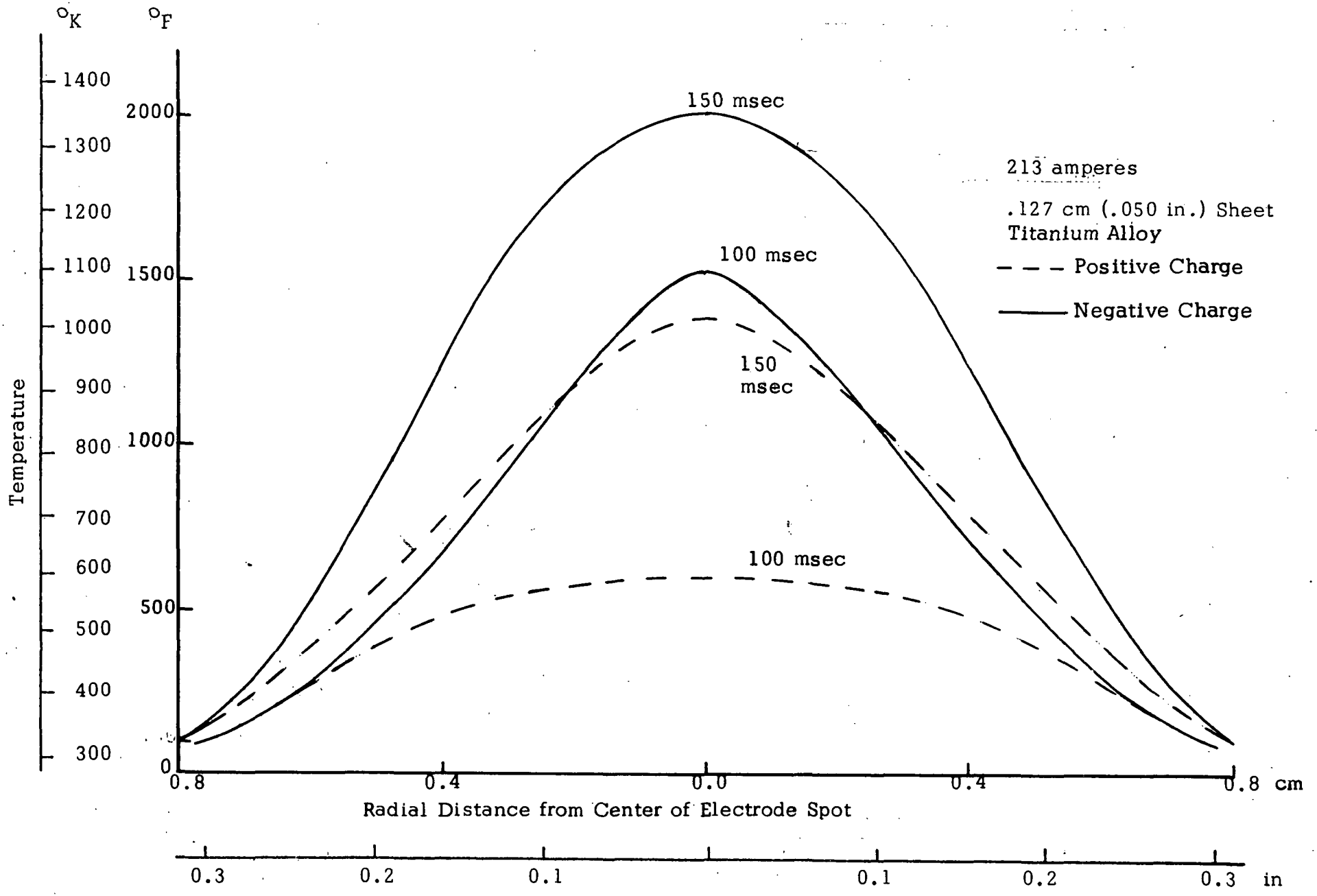

Figure 28. Effect of Polarity on Temperature Rise at Lower Surface

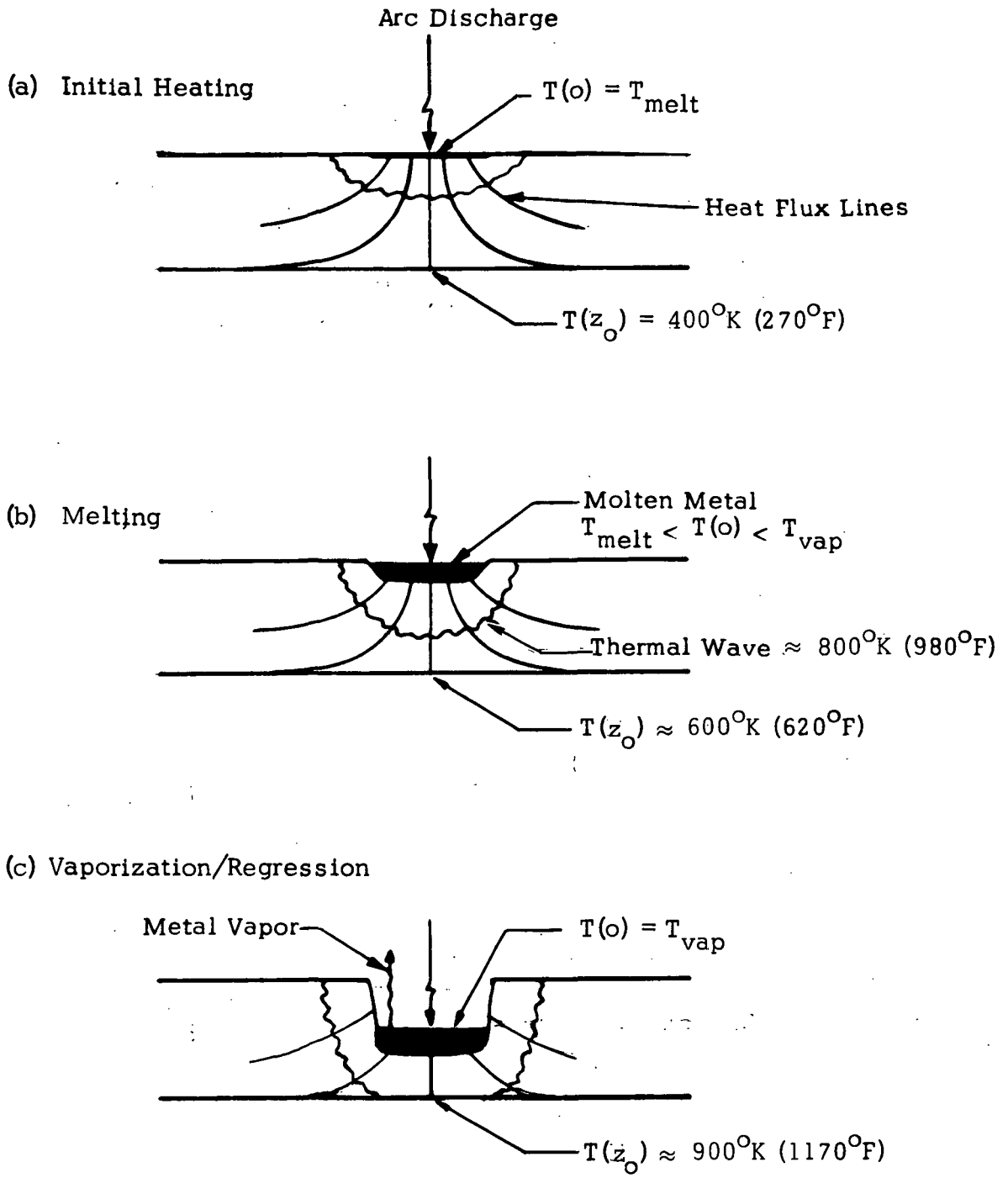

Figure 29. Conceptual Development of Hot-Spot on Undersurface

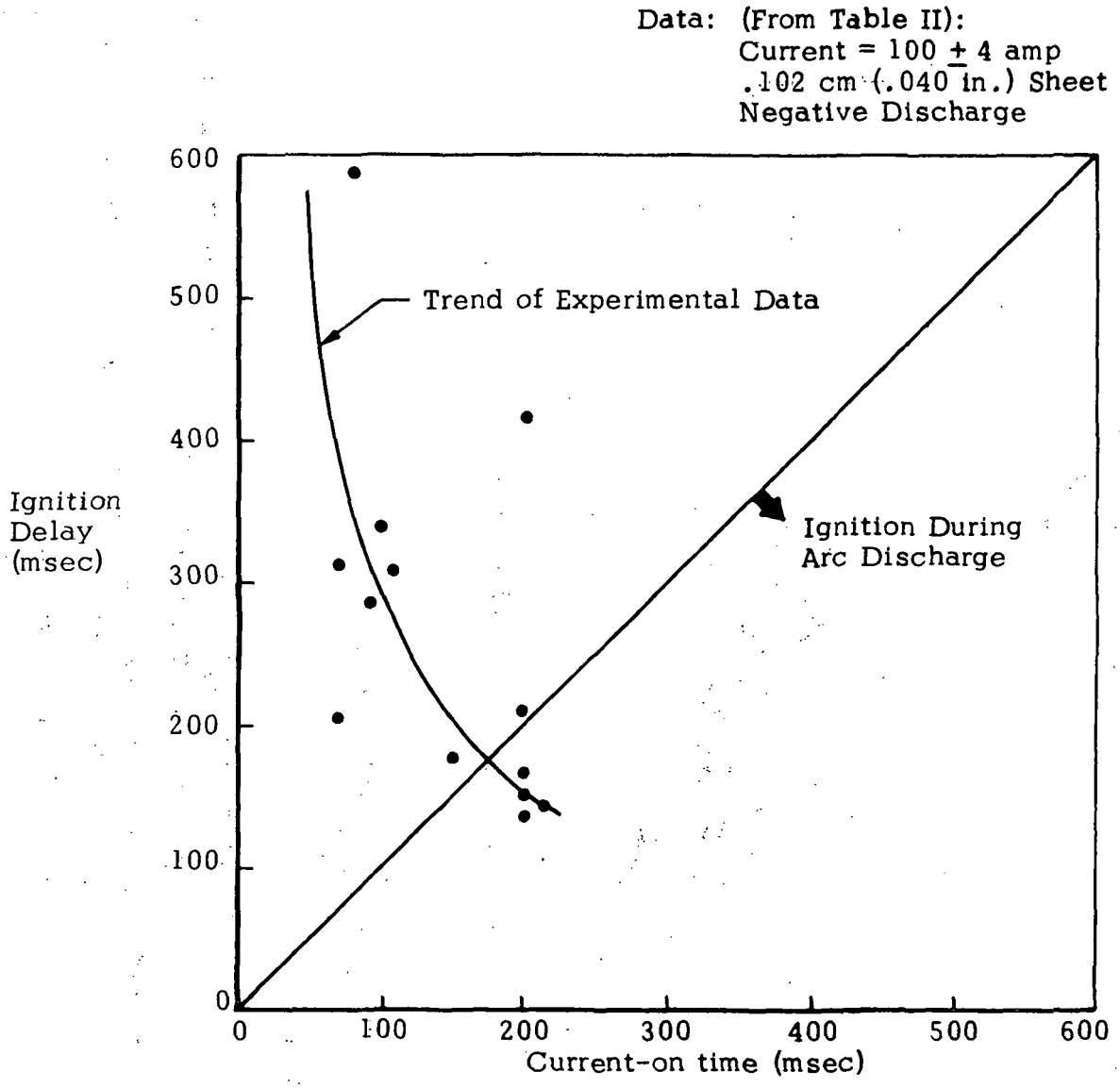

Figure 30. Observed Post-Discharge Ignition, Showing Long Delay at Low Charge Transfer

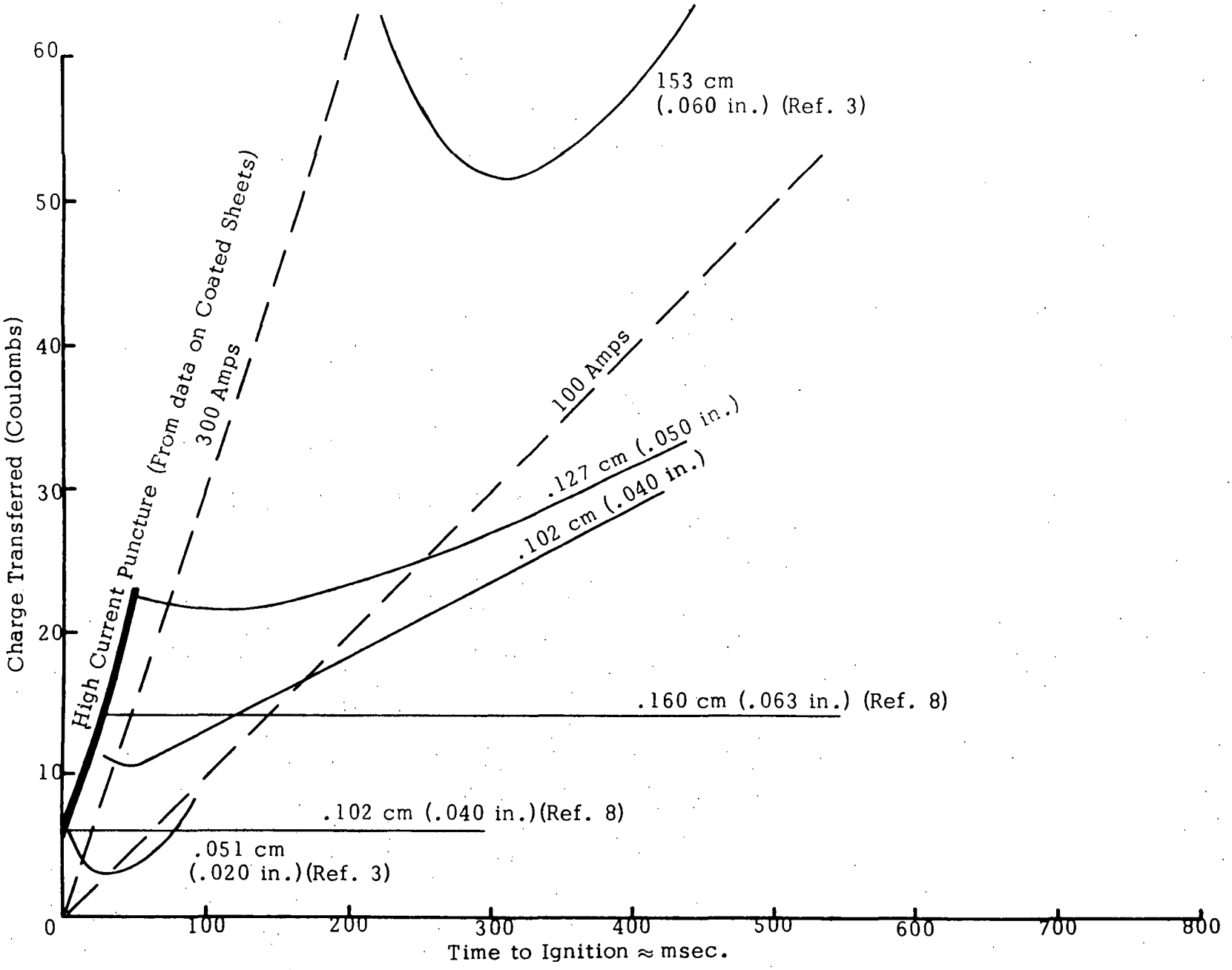

Figure 31. Threshold Charge Transfer for Ignition (Positive Discharge)

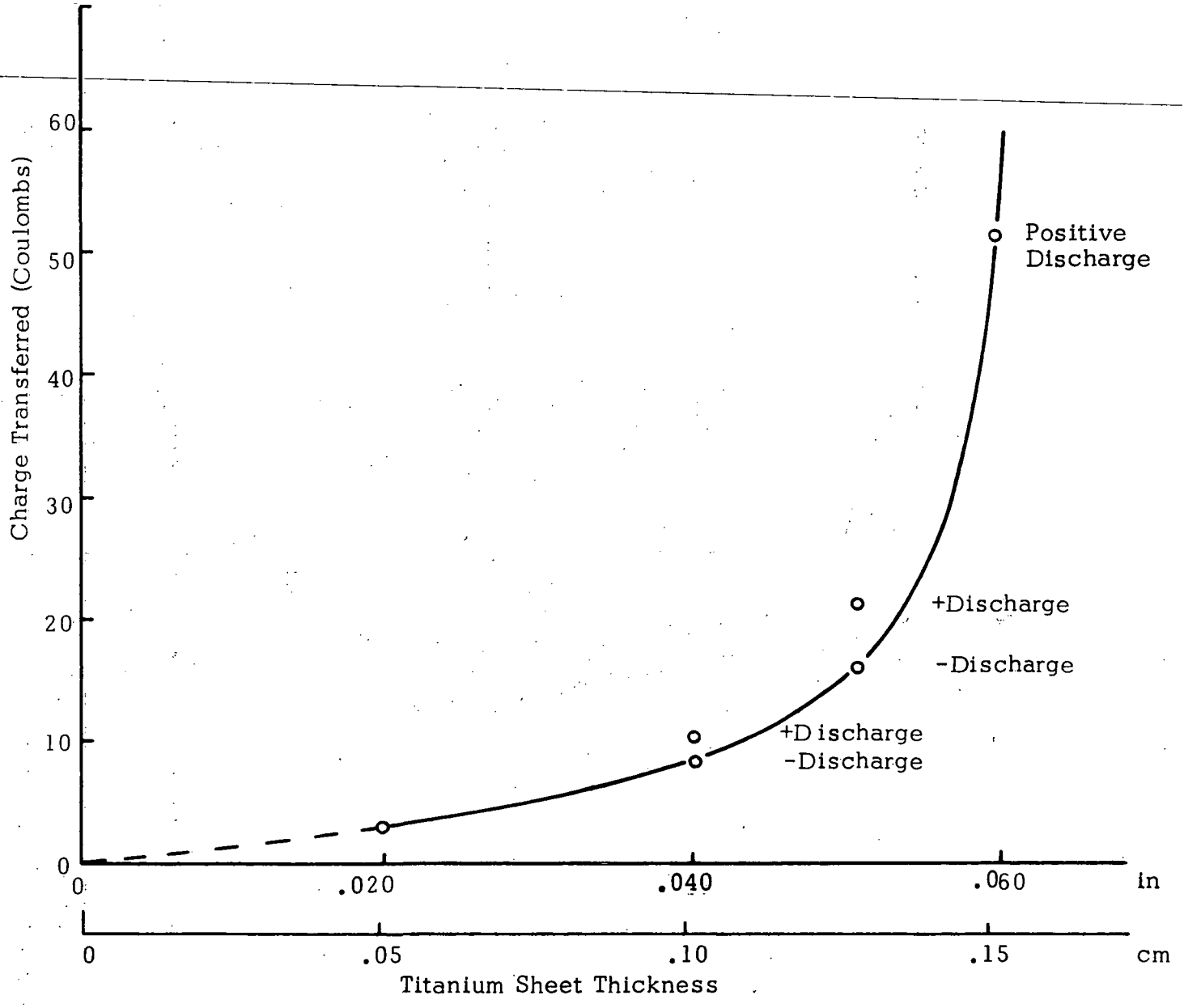

Figure 32. Effect of Skin Thickness on Threshold Charge Transfer for Ignition (at most favorable current).

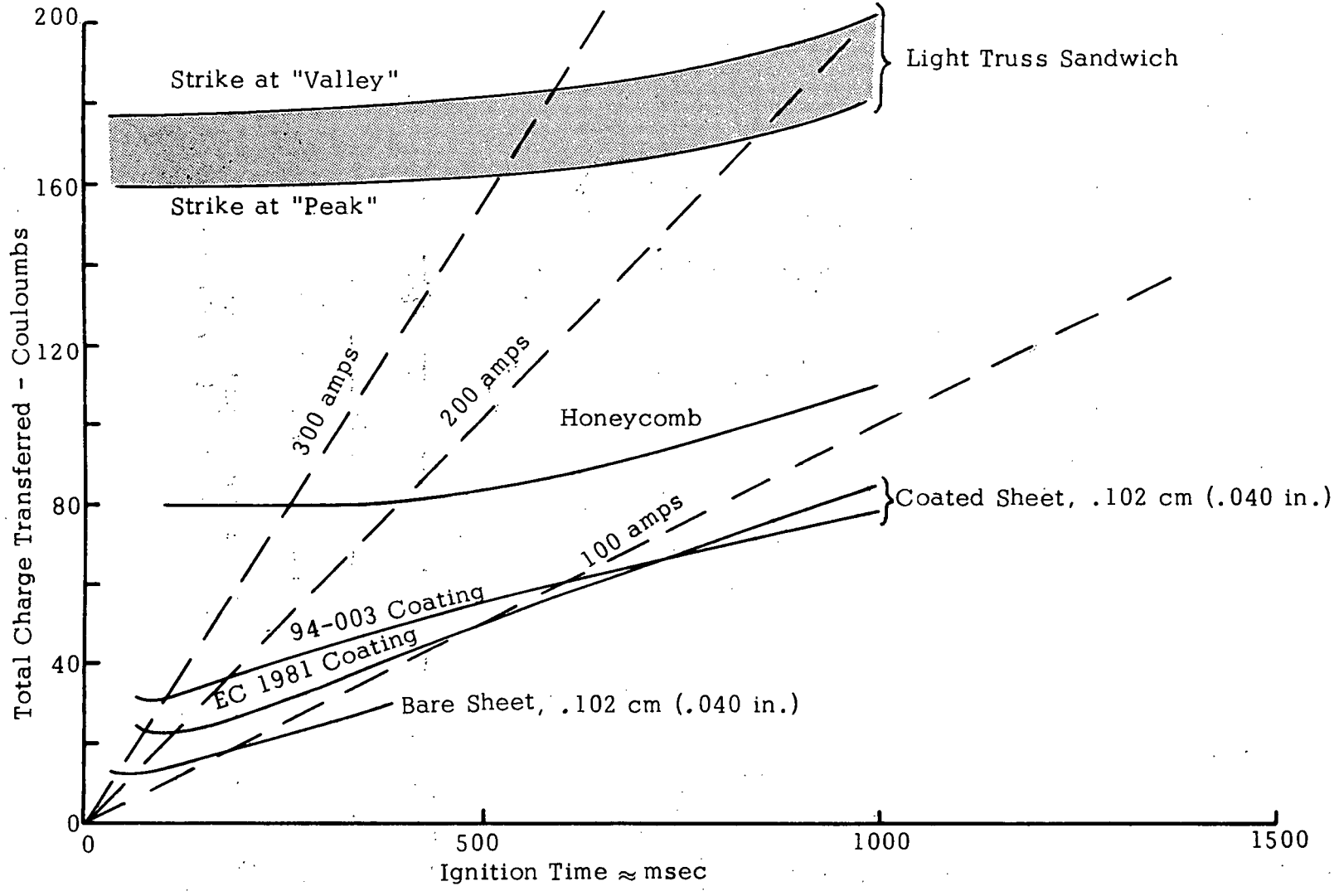

Figure 33. Protectiveness of Candidate Aircraft Skins

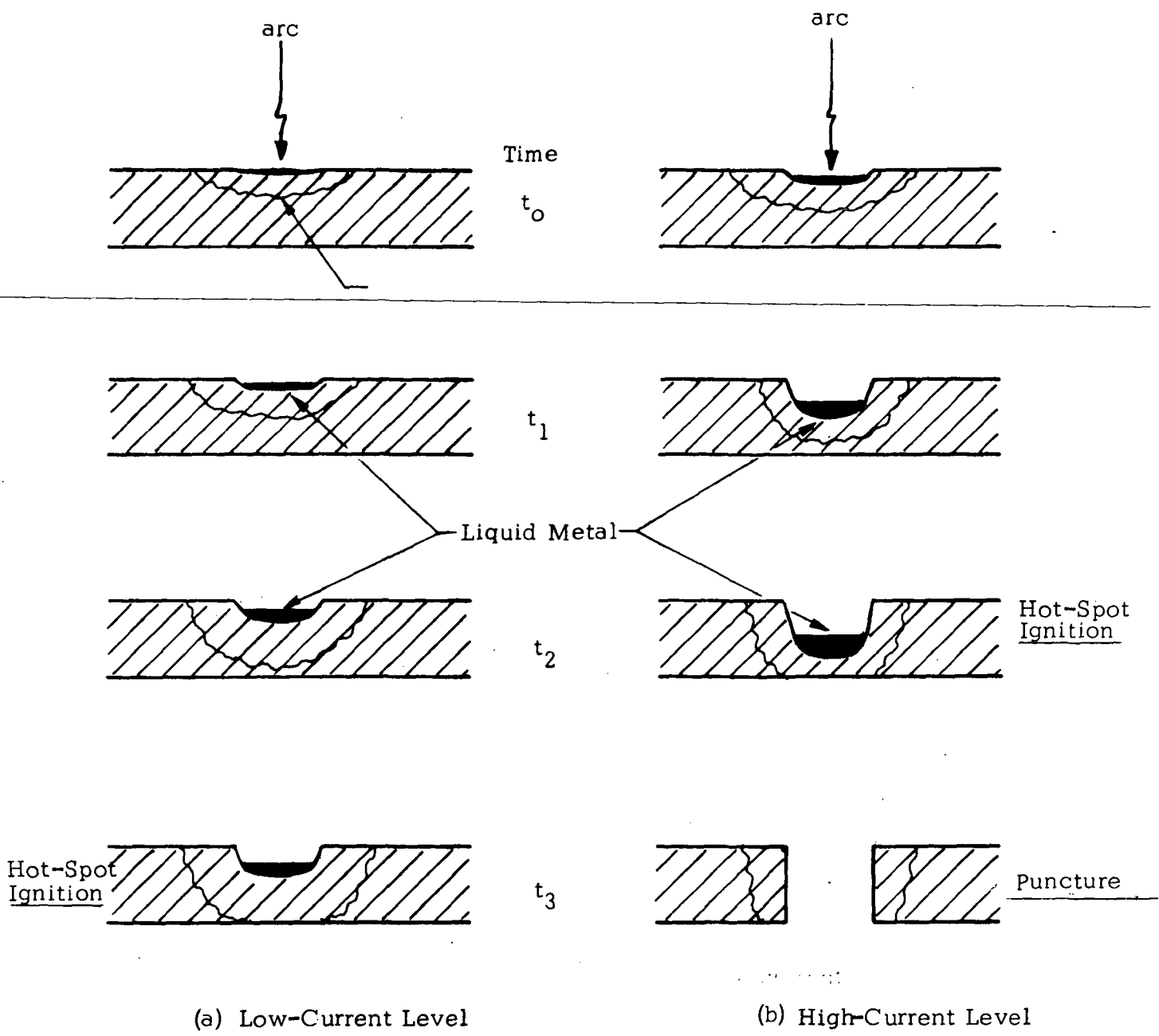

Figure 34. Conceptual Effect of Current Level on Regression Rate, Precursor Lead Time, Hot-Spot Ignition, and Puncture.

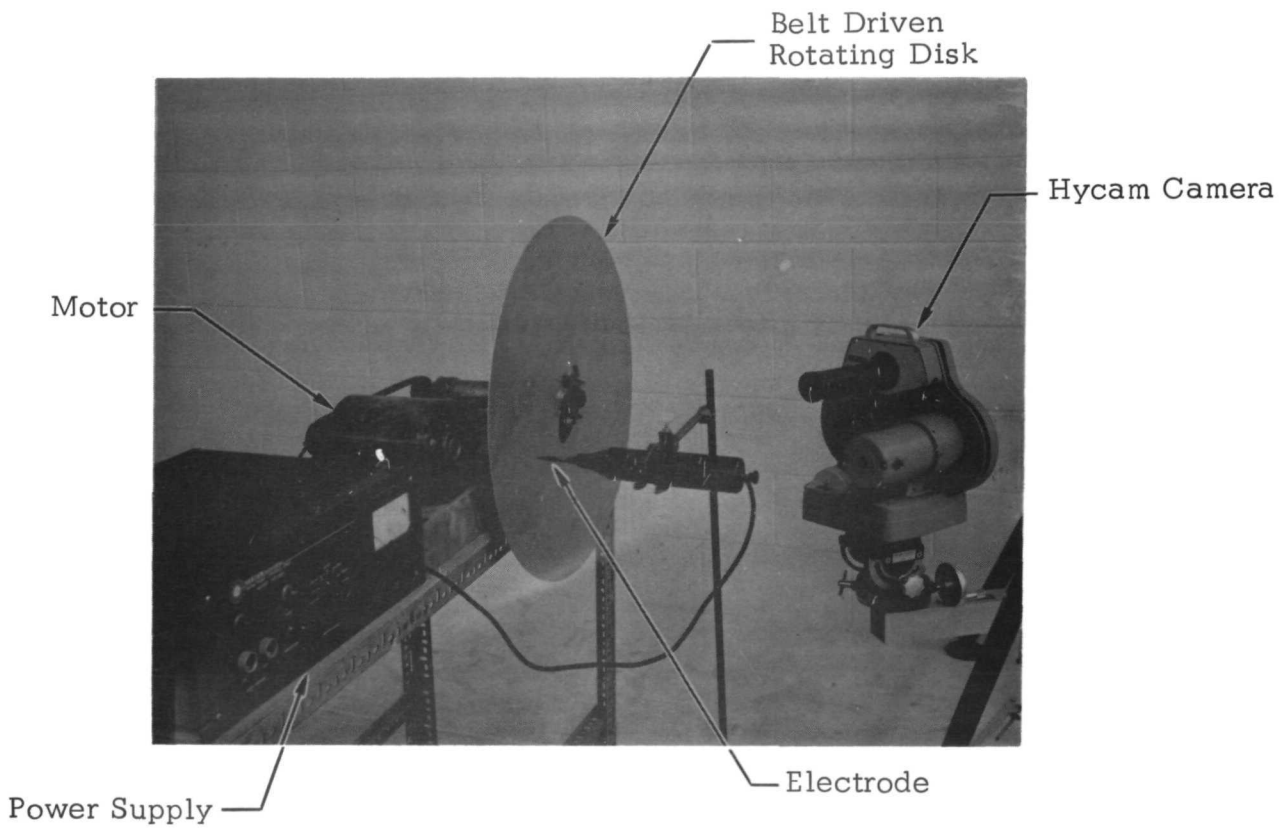

Figure 35. Swept-Stroke Simulator

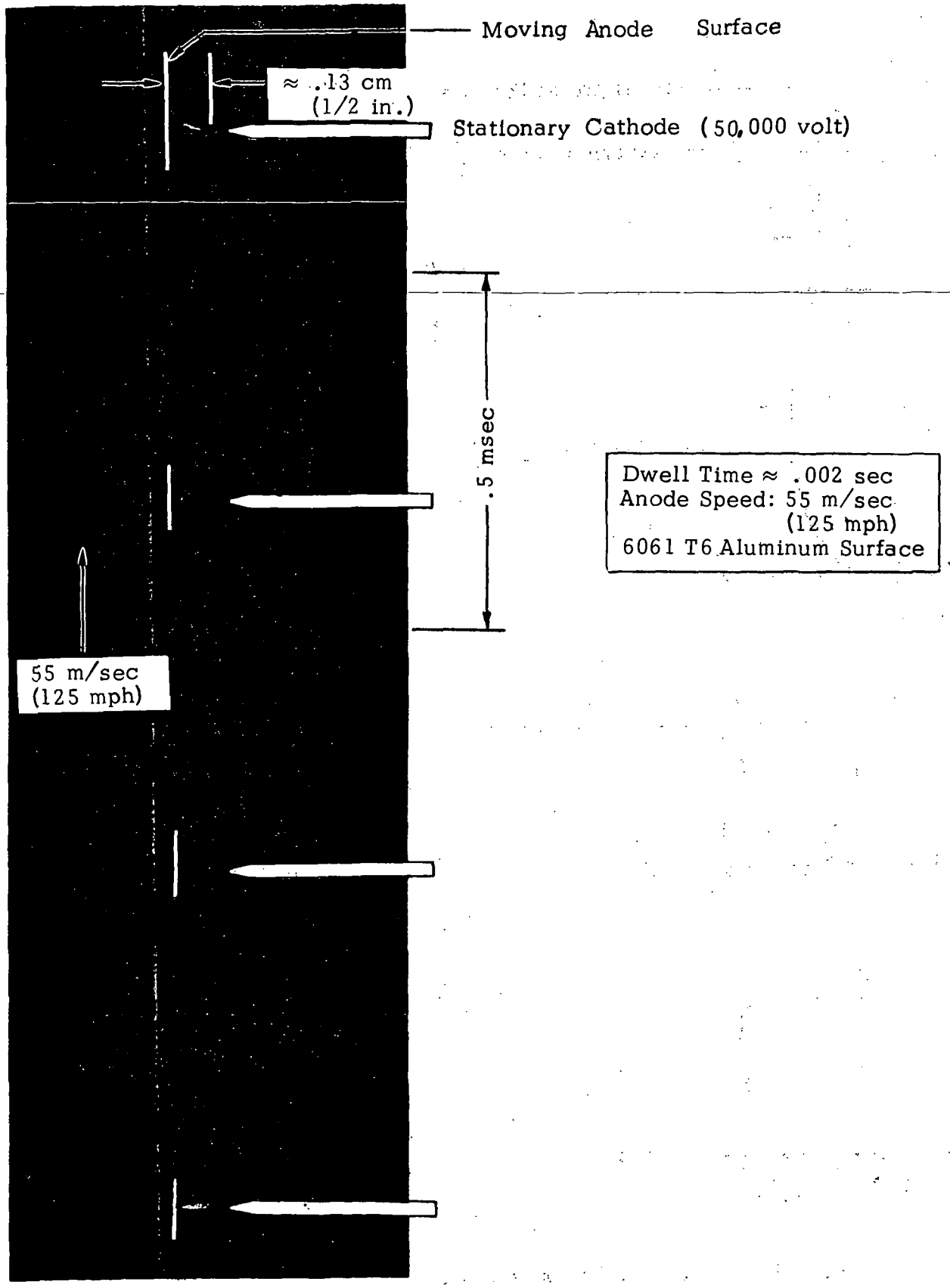

Figure 36. Simulated Swept-Stroke, 55 m/sec (125 mph)

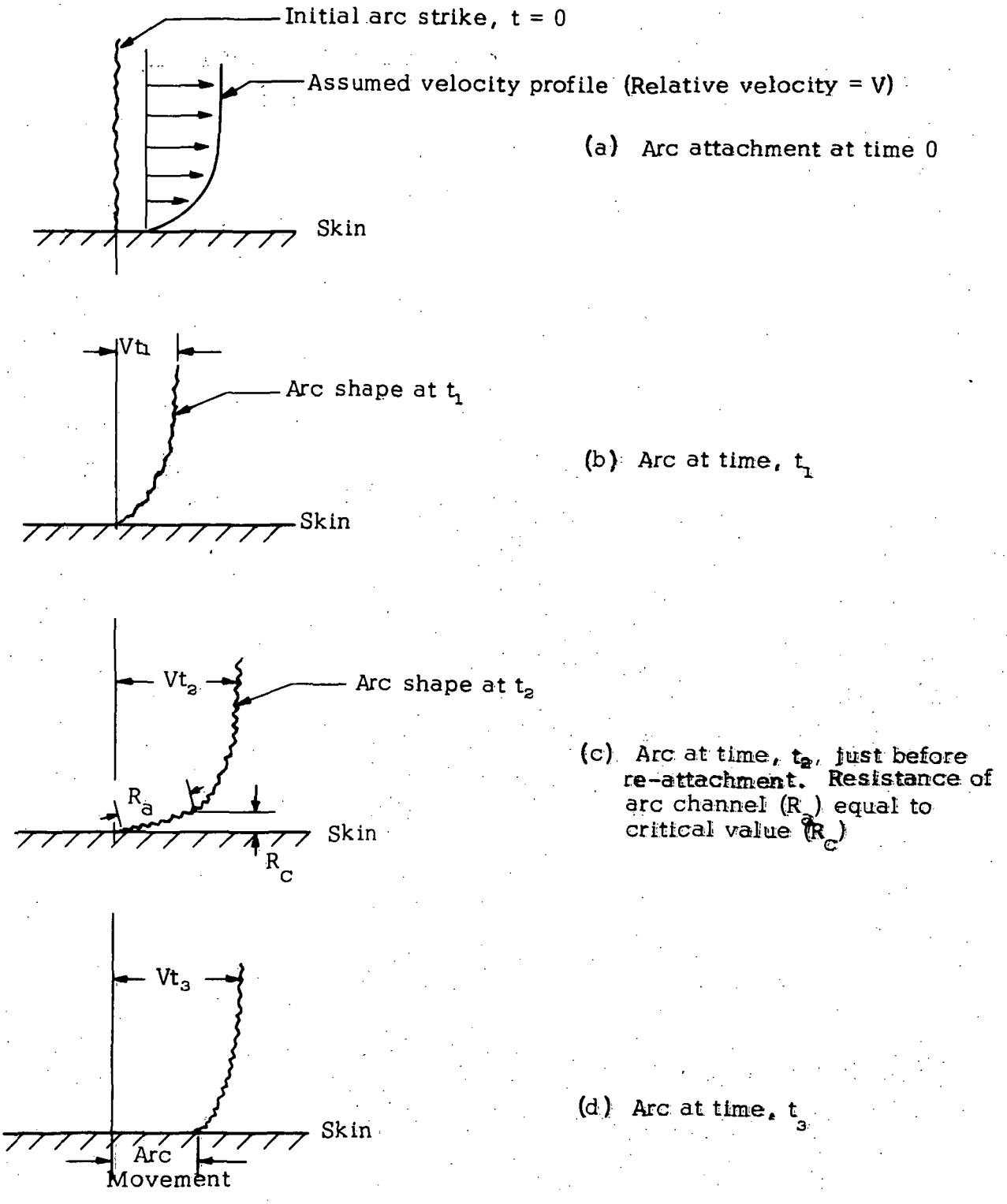

Figure 37. Conceptual Representation of Stroke Stepping

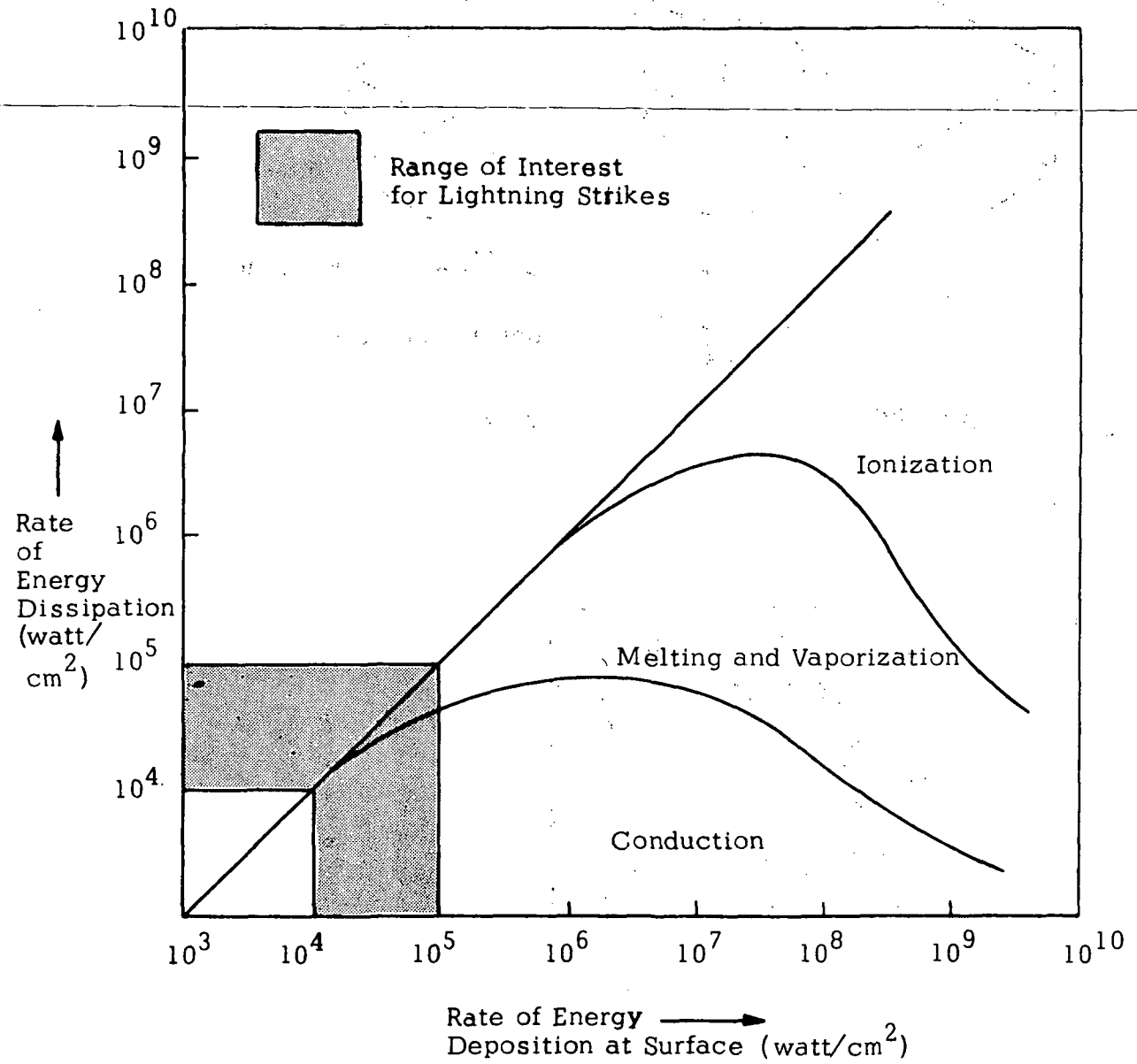

Figure 38. Regimes of Steady-State Thermal Response

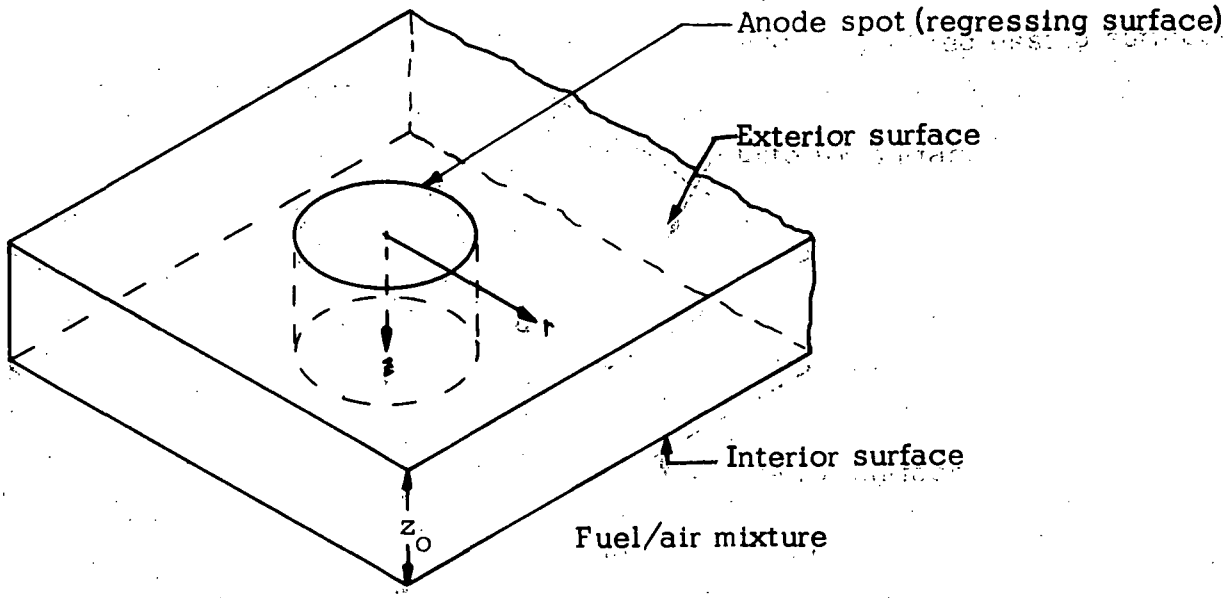

(a) Cylindrical Coordinate System

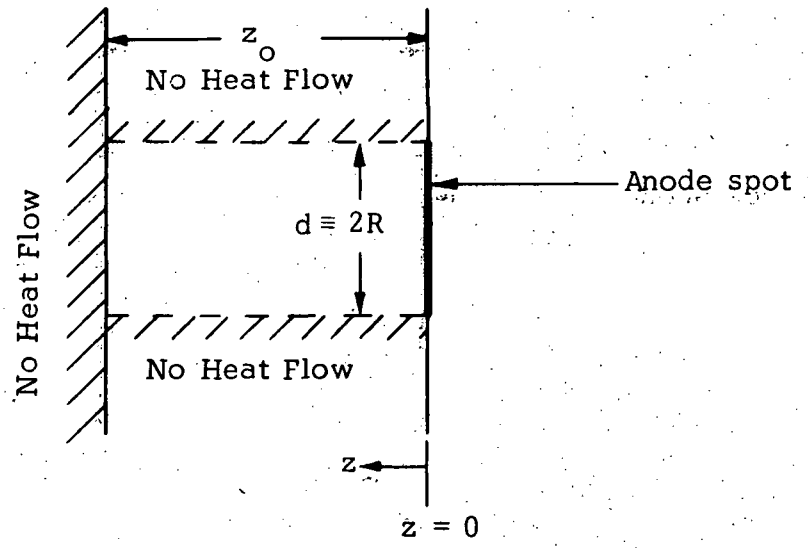

(b) Model for One-dimensional Finite Body

Figure 39. Coordinate Systems for Heat Conduction Analysis

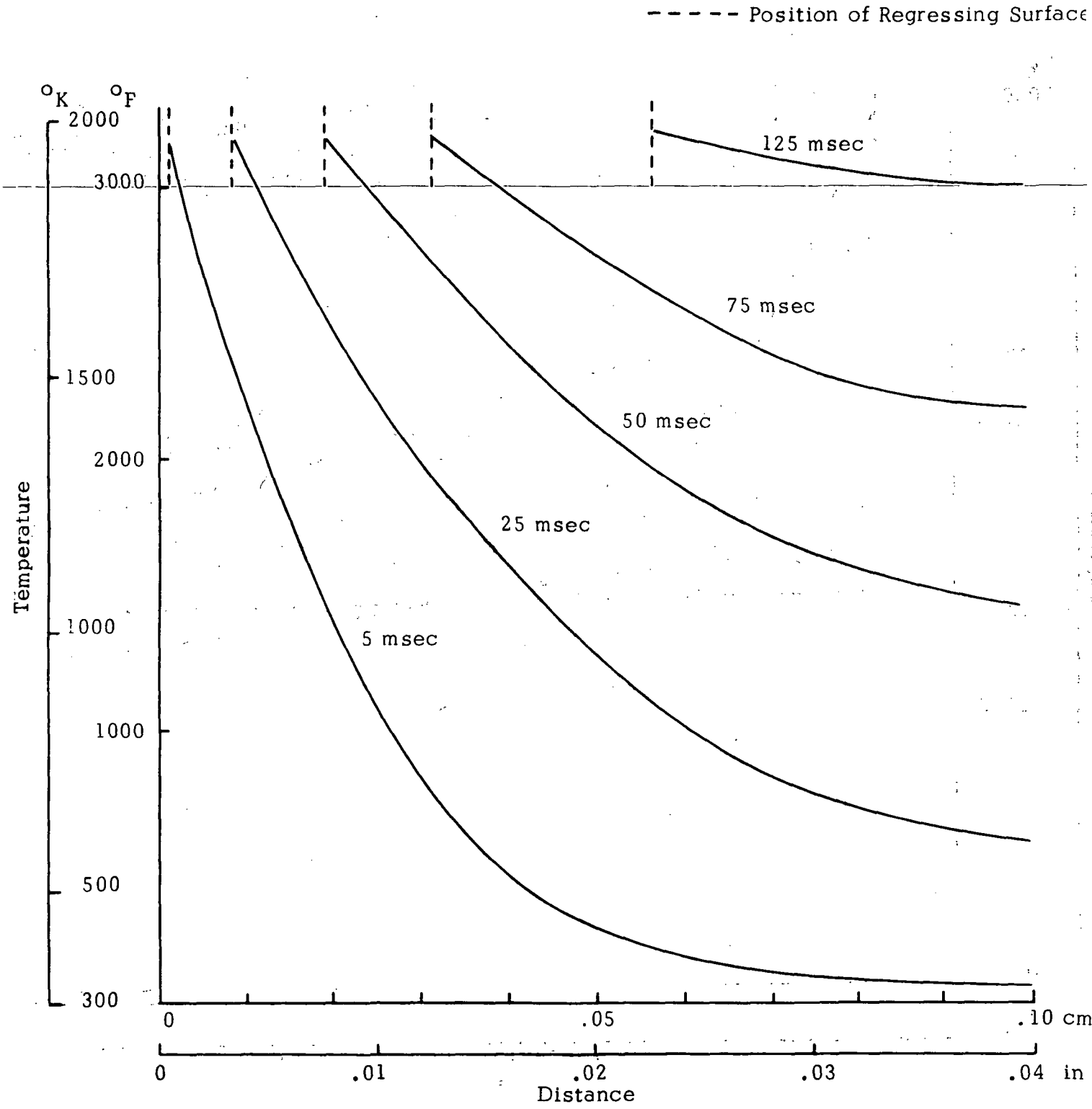

Figure 40. Calculated Regression Rate and Depthwise Temperature Profiles

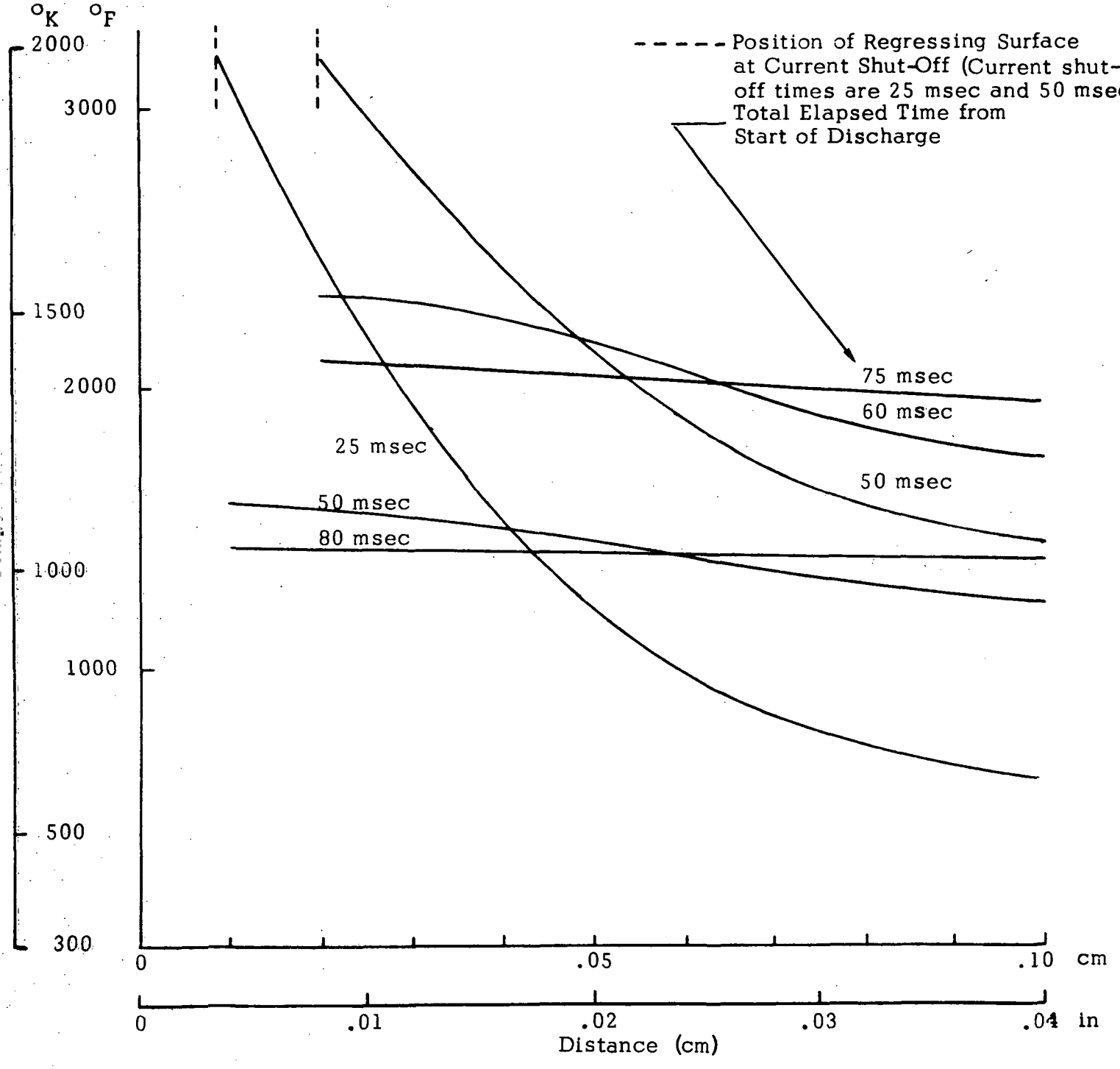

Figure 41. Thermal Equilibration After Current Shut-Off, Showing Rise in Lower Surface Temperature (Without Radial Dissipation).

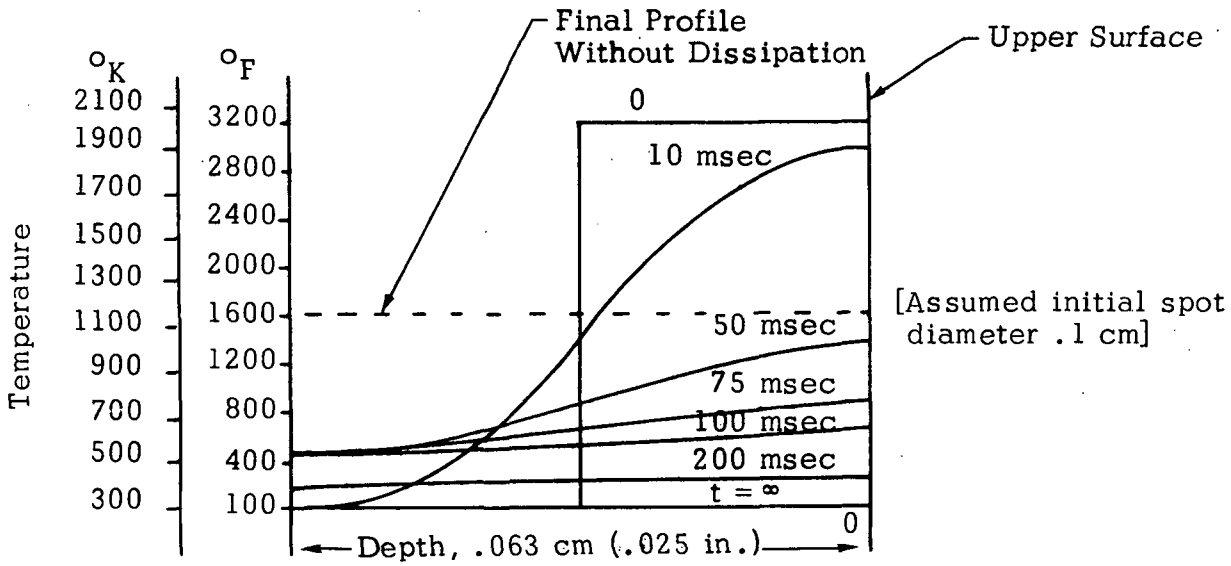

Temperature Profiles through Ti-Skin as Result of Heat Dissipation in Both Axial and Radial Directions (Ref. 18).

Figure 42. Thermal Equilibration With Radial Dissipation, Showing Decreased Ignition Probability

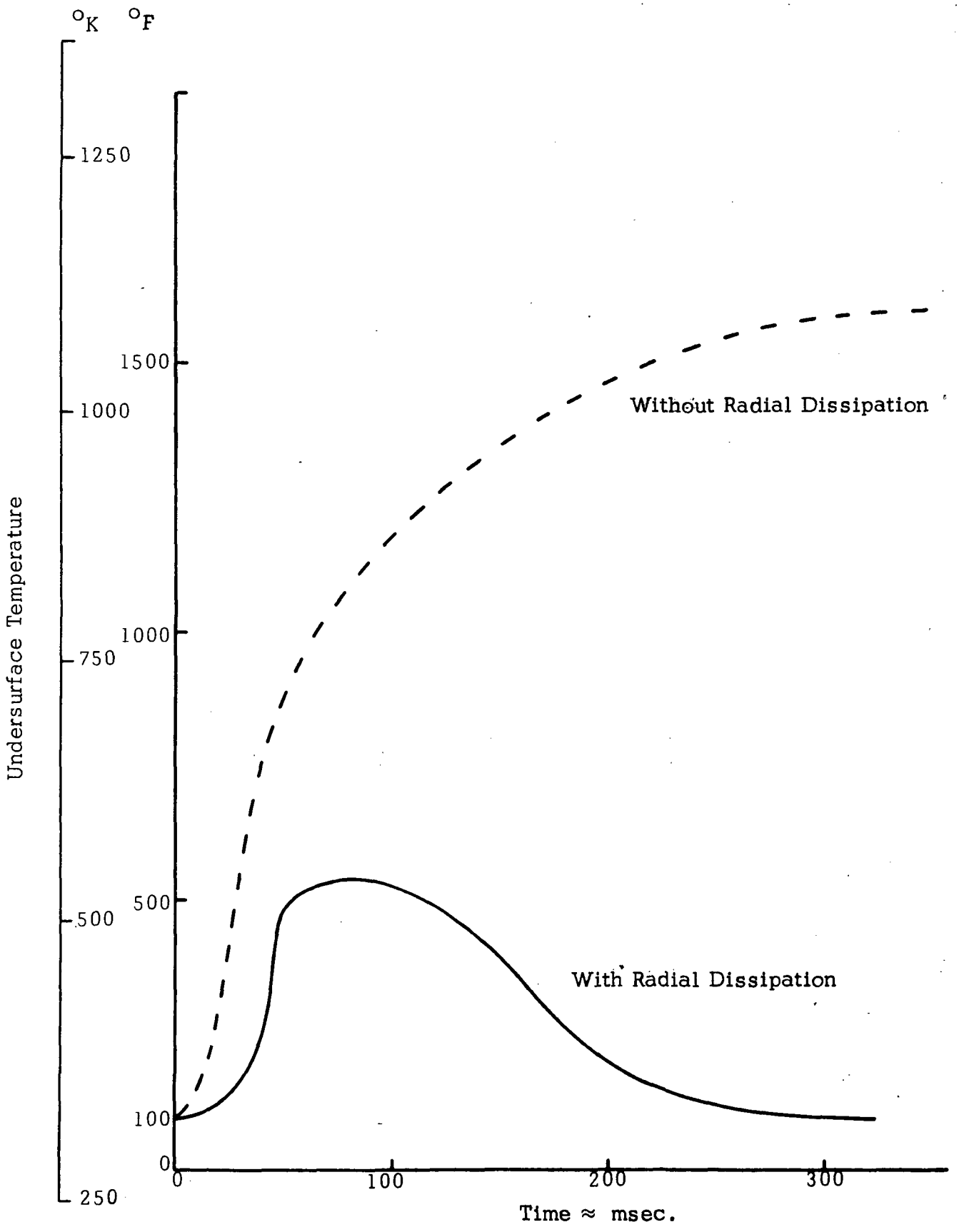

Figure 43. Effect of Radial Dissipation on Undersurface Temperature After Current Shutdown

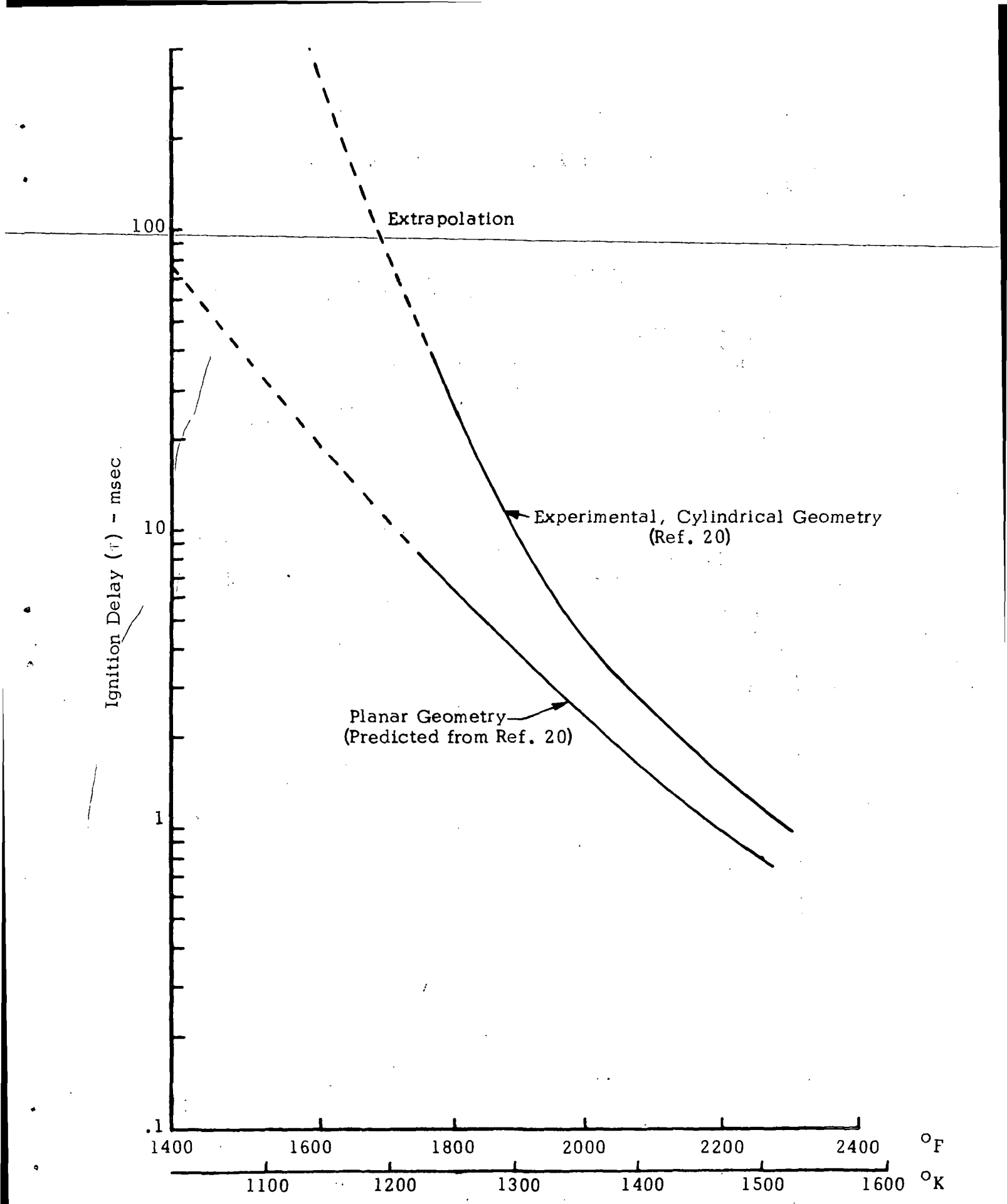

Figure 44. Ignition Delay vs Wall Temperature

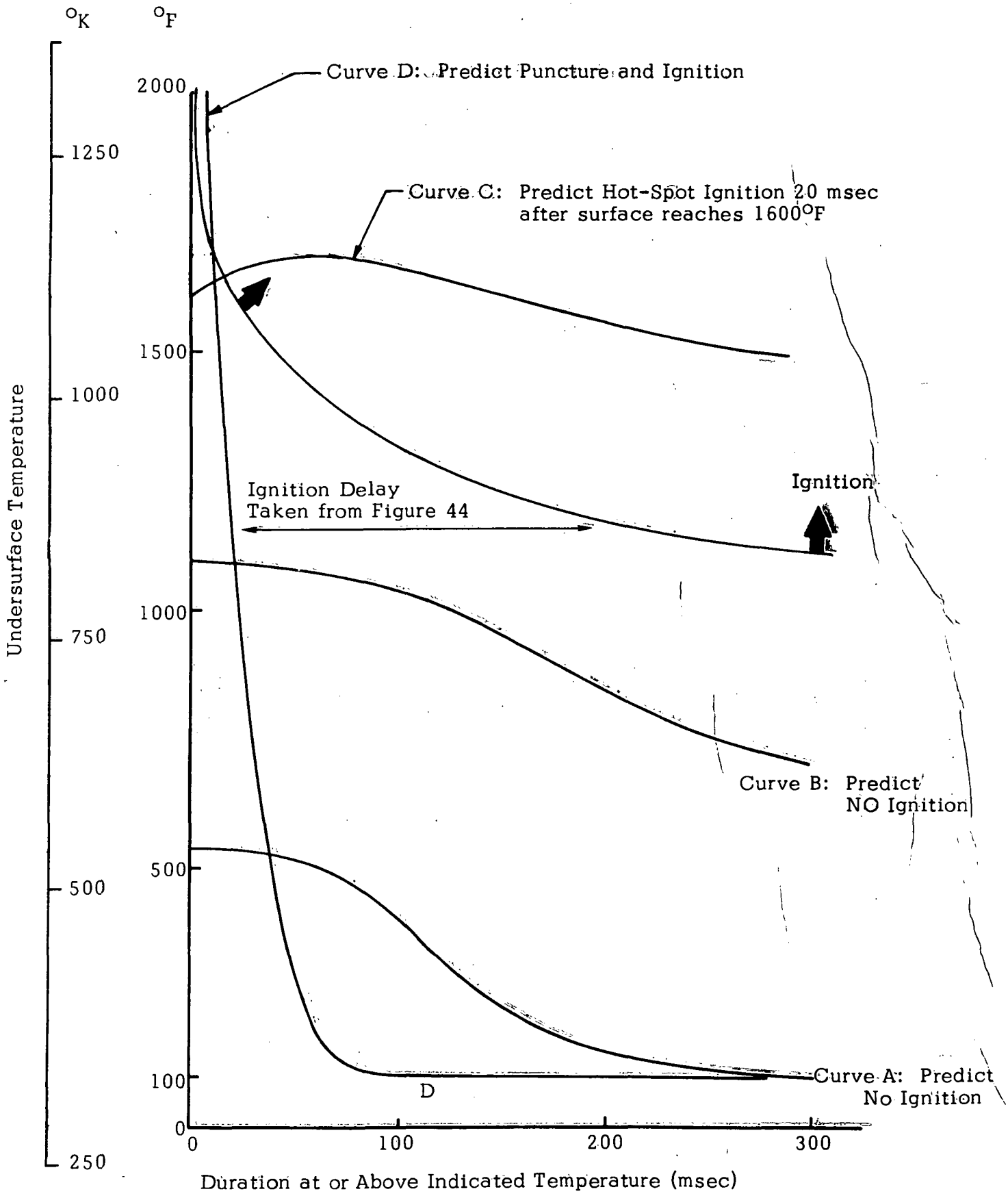

Figure 45. Ignition Criterion in Terms of Undersurface Temperature Histories

REPORT DISTRIBUTION LIST FOR
CONTRACT NO. NAS3-12009

NASA Lewis Research Center
(All undistributed copies)
21000 Brookpark Road
Cleveland, Ohio 44135
Attn: Paul T. Hacker, MS 6-2

NASA Lewis Research Center (1)
21000 Brookpark Road
Cleveland, Ohio 44135
Attn: Myrna K. Borke, MS 500-312

NASA Lewis Research Center (1)
21000 Brookpark Road
Cleveland, Ohio 44135
Attn: Norman T. Musial, MS 500-311

NASA Lewis Research Center (2)
21000 Brookpark Road
Cleveland, Ohio 44135
Attn: Library, MS 60-3

NASA Lewis Research Center (1)
21000 Brookpark Road
Cleveland, Ohio 44135
Attn: Report Control Office, MS 5-5

NASA Scientific and Technical
Information Facility (6)
Box 33
College Park, Maryland 20740
Attn: NASA Representative

NASA Headquarters (2)
Washington, D. C. 20546
Attn: George W. Cherry, RO

NASA Headquarters (1)
Washington, D. C. 20546
Attn: William S. Aiken, Jr., RA

Department of Transportation (1)
Federal Aviation Administration
800 Independence Avenue, S.W.
Washington, D. C. 20590
Attn: Robert J. Auburn, PS-140

Department of Transportation (1)
Federal Aviation Administration
800 Independence Avenue, S.W.
Washington, D. C. 20590
Attn: Thomas G. Horeff, RD-730

Air Force Systems Command (1)
Installation Division
Wright-Patterson Air Force Base
Ohio 45433
Attn: Fred A. Wright, ASD/ENJI

Air Force Systems Command (1)
Aero Propulsion Laboratory
Wright-Patterson Air Force Base
Ohio 45433
Attn: Benito P. Botteri, APFH

The Boeing Company (1)
P. O. Box 3707
Seattle, Washington 98129
Attn: B. A. Hansberger, MS (73-20)

The Boeing Company (1)
Electro-Dynamics Technology Staff
Seattle, Washington 98129
Attn: Stanley Schneider

General Electric Company (2)
Power Transformer Department
High Voltage Laboratory
100 Woodlawn Avenue
Pittsfield, Massachusetts 01201

American Airlines, Inc. (1)
633 Third Avenue
New York, New York 10017
Attn: Franklin W. Kolk

Lockheed California Company (1)
A Division of Lockheed Aircraft Corp.
Flight Sciences Division
Burbank, California
Attn: Edward Versaw

NASA Ames Research Center (1)
Moffett Field, California 94035
Attn: Library

NASA Langley Research Center (1)
Langley Station
Hampton, Virginia 23365
Attn: Library

U. S. Department of Commerce (1)
National Bureau of Standards
Office of Fire Research and Safety
Gaithersburg, Maryland 20760
Attn: Alex F. Robertson